NON-COVALENT INTERACTIONS AND THEIR ROLE IN BIOLOGICAL AND CATALYTIC CHEMISTRY

A Thesis
Presented to
The Academic Faculty

by

Matthew R. Kennedy

In Partial Fulfillment
of the Requirements for the Degree
Doctor of Philosophy in the
School of Chemistry and Biochemistry

Georgia Institute of Technology
December 2014

NON-COVALENT INTERACTIONS AND THEIR ROLE IN BIOLOGICAL AND CATALYTIC CHEMISTRY

Approved by:

Professor Kenneth Brown,
Committee Chair
School of Chemistry and Biochemistry
Georgia Institute of Technology

Professor C. David Sherrill, Advisor
School of Chemistry and Biochemistry
Georgia Institute of Technology

Professor Angelo Bongiorno
School of Chemistry and Biochemistry
Georgia Institute of Technology

Professor Chris Jones
School of Chemical and Biomolecular Engineering
Georgia Institute of Technology

Professor Peter Ludocive
School of Chemical and Biomolecular Engineering
Georgia Institute of Technology

Date Approved: November 2014

This thesis is dedicated to my parents,

William B. Kennedy and Lynn G. Kennedy,

without whose love and support,

none of this would have been possible.

ACKNOWLEDGEMENTS

I would like to thank my thesis adviser Dr. C. David Sherrill for teaching me the skills needed to do well in the area of computational chemistry. His style of interacting with graduate students is unique and is what drew me to join his group. His flexibility with projects for graduate students allowed me to choose projects that interested me enough to motivate me through a project. Allowing his students to find projects that interest and motivate them, has turned his group into one of the top non-covalent interactions research groups in the country. Lastly, I would like him for patience with me as a graduate student and projects that didn't always pan out. The environment he has created at Georgia Tech in his research group is the best work environment I've ever been a part of, and for that, I thank Dr. Sherrill.

I would not have become interested in chemistry without the teaching and guidance from a few past teachers. Mrs. Mary Elizabeth Atwell Davis and Mr. Kurt Haldeman were my chemistry teachers in high school who first introduced me to the subject matter. Mr. Haldeman taught me to learn independently while teaching his AP Chemistry course. I quickly realized that I had a passion to learn independently about chemistry. This motivated me to pursue chemistry as a major when I began at the University of Tennessee. The head of the chemistry department when I began attending was Dr. Craig Barnes. Dr. Barnes was able to pair me with Dr. Robert Hinde as my academic and research adviser. Dr. Hinde was a great teacher and showed me how to work through projects and keep working on them until the end. I then transitioned to begin working with Dr. Robert Harrison at the University of Tennessee as well as at Oak Ridge National Labs. My time at ORNL allowed me to get caught up in the wonder of so many different research projects going on around me. I would like

to deeply thank all the teachers and professors who impacted me and my interest and chemistry and more specifically in computational chemistry. Without them I would have never started down the path that led me to this point.

I would like to thank past and present members of the Sherrill group, many of which are good friends as well as co-workers. I would like to thank Dr. Shawn Marshall specifically, as he was a great man and scientist to bounce ideas off of while working through projects that didn't seem to have any natural way to conclude. I would also like to thank Dr. Lori Burns for being a great co-worker who is always willing to proofread anything for the group. Dr. Burns was also involved with the DOE project which we both worked on during my tenure in graduate school. She was always around to talk about DOE projects which may or may not have ever been destined to be finished. I would like to thank Dr. Eugene DePrince, while he was in the group during his post-doc appointment, he was a great help to keep me sane and happy during my graduate school career. Each day at 3PM when we would go to the atrium and have "apple time", it would remind me that there is plenty of things to talk about other than work. I would also like to thank Dr. Sahan Thanathiriwatte, Dr. Tait Takatani, Dr. John Sears, Rob Parrish, Trent Parker, Vernon Crowell and Dr. Jerome Gonthier.

I would also like to thank my wife, Karen, for helping me acclimate to Atlanta, and helping me to feel comfortable and welcome in a a new city. She was also an amazing supporter while working through my dissertation and job hunt at the end of graduate school which helped ease the pressure of those high stress tasks. Finally, I would like to thank my parents, William and Lynn Kennedy. They have always supported me unconditionally. At a young age, my dad began teaching me math concepts a year or two ahead of my current grade. If I learned addition at school he would teach me multiplication. He also gave me a great love for trivia and word games. My mom taught me how to enjoy life and have a good time, which has greatly allowed me to

not become overwhelmed or stressed when deadlines approach. My parents allowed me to excel in what I preferred and never tried to steer me down a life path which I didn't seem interested in or inspired by. They allowed me to find my own way, and watched happily as I gained opportunities in my career path. I can not imagine having been born into a better home with better parents.

TABLE OF CONTENTS

LIST OF TABLES

LIST OF FIGURES

SUMMARY

The focus of this thesis is the question of how non-covalent interactions affect chemical systems' electronic and structural properties. Non-covalent interactions can exhibit a range of binding strengths, from strong electrostatically-bound salt bridges or multiple hydrogen bonds to weak dispersion-bound complexes such as rare gas dimers or the benzene dimer. To determine the interaction energies (IE) of non-covalent interactions one generally takes the supermolecular approach as described by the equation

$$E_{IE} = E_{AB} - E_A - E_B, \tag{1}$$

where subscripts A and B refer to two monomers and AB indicates the dimer. This interaction energy is the difference in energy between two monomers interacting at a single configuration compared to the completely non-interacting monomers at infinite separation. In this framework, positive interaction energies are repulsive or unfavorable while negative interaction energies signify a favorable interaction. We use prototype systems to understand systems with complex interactions such as π-π stacking in curved aromatic systems, three-body dispersion contributions to lattice energies and transition metal catalysts affect on transition state barrier heights. The current "gold standard" of computational chemistry is coupled-cluster theory with iterative single and double excitation and perturbative triple excitations [CCSD(T)].[94] Using CCSD(T) with large basis sets usually yields results that are in good agreement with experimental data.[140] CCSD(T) being very computational expensive forces us to use methods of a lower overall quality, but also much more tractable for some interesting problems. We must use the available CCSD(T) or experimental data available to benchmark lower quality methods in order to ensure that the low quality methods

are providing and accurate description of the problem of interest.

To investigate the effect of curvature on the nature of π-π interactions, we studied concave-convex dimers of corannulene and coronene in nested configurations. By imposing artificial curvature/planarity we were able to learn about the fundamental physics of π-π stacking in curved systems. To investigate these effects, it was necessary to benchmark low level methods for the interaction of large aromatic hydrocarbons. With the coronene and corannulene dimers being 60 and 72 atoms, respectively, they are outside the limits of tractability for a large number of computations at the level of CCSD(T). Therefore we must determine the most efficient and accurate method of describing the physics of these systems with a few benchmark computations. Using a few benchmark computations published by Janowski et al. (Ref. [76]) we were able to benchmark four functionals (B3LYP, B97, M05-2X and M06-2X) as well as four dispersion corrections (-D2, -D3, -D3(BJ), and -XDM) and we found that B3LYP-D3(BJ) performed best. Using B3LYP-D3(BJ) we found that both corannulene and coronene exhibit stronger interaction energies as more curvature is introduced, except at unnaturally close intermolecular distances or high degrees of curvature. Using symmetry adapted perturbation theory (SAPT)[78, 148], we were able to determine that this stronger interaction comes from stabilizing dispersion, induction and charge penetration interactions with smaller destabilizing interactions from exchange interactions.

For accurate computations on lattice energies one needs to go beyond two-body effects to three-body effects if the cluster expansion is being used. Three-body dispersion is normally a smaller fraction of the lattice energy of a crystal when compared to three-body induction. We investigated the three-body contribution using the counterpoise corrected formula of Hankins *et al.*.[58]

$$\Delta^3 E_{ABC}^{ABC} = E_{ABC}^{ABC} - \sum_i E_i^{ABC} - \sum_{ij} \Delta^2 E_{ij}^{ABC}, \tag{2}$$

where the superscript ABC represents the trimer basis and the E_i denotes the energy

of each monomer, where i counts over the individual molecule of the trimer. The last term is defined as

$$\Delta^2 E_{ij}^{ABC} = E_{ij}^{ABC} - E_i^{ABC} - E_j^{ABC}, \tag{3}$$

where the energies of all dimers and monomers are determined in the trimer basis. Using these formulae we investigated the three-body contribution to the lattice energy of crystalline benzene with CCSD(T). By using CCSD(T) computations we resolved a debate in the literature about the magnitude of the non-additive three-body dispersion contribution to the lattice energy of the benzene crystal. Based on CCSD(T) computations, we report a three-body dispersion contribution of 0.89 kcal mol^{-1}, or 7.2% of the total lattice energy. This estimate is smaller than many previous computational estimates[155, 55, 167, 162] of the three-body dispersion contribution, which fell between 0.92 and 1.67 kcal mol^{-1}. The benchmark data we provide confirm that three-body dispersion effects cannot be neglected in accurate computations of the lattice energy of benzene. Although this study focused on benzene, three-body dispersion effects may also contribute substantially to the lattice energy of other aromatic hydrocarbon materials.

Finally, density functional theory (DFT) was applied to the rate-limiting step of the hydrolytic kinetic resolution (HKR) of terminal epoxides to resolve questions surrounding the mechanism. We find that the catalytic mechanism is cooperative because the barrier height reduction for the bimetallic reaction is greater than the sum of the barrier height reductions for the two monometallic reactions. We were also able to compute barrier heights for multiple counter-ions which react at different rates. Based on experimental reaction profiles, we saw a good correlation between our barrier heights for chloride, acetate, and tosylate with the peak reaction rates reported. We also saw that hydroxide, which is inactive experimentally is inactive because when hydroxide is the only counter-ion present in the system it has a barrier height that is 11-14 kJ mol^{-1} higher than the other three counter-ions which are

extremely active.

CHAPTER I

INTRODUCTION

1.1 Introduction to Electronic Structure Theory

This section is an introduction to the fundamentals of electronic structure theory which will be necessary to understand portions of this thesis. The section uses notation that is consistent with that of Szabo and Ostlund[147].

1.1.1 Schrödinger Equation

The field of electronic structure theory mainly looks for ways to solve the time-independent, non-relativistic Schrödinger equation as shown below,

$$\hat{\mathcal{H}}\Psi = \mathcal{E}\Psi, \tag{4}$$

where $\hat{\mathcal{H}}$ represents the Hamiltonian operator and ψ represents the molecular wavefunction. The Hamiltonian can be defined for a system with N electrons and M atoms as

$$\hat{\mathcal{H}} = -\sum_{i=1}^{N}\frac{1}{2}\nabla_i^2 - \sum_{A=1}^{M}\frac{1}{2M_A}\nabla_A^2 - \sum_{i=1}^{N}\sum_{A=1}^{M}\frac{Z_A}{R_{iA}} + \sum_{A=1}^{M}\sum_{B>A}^{M}\frac{Z_A Z_B}{R_{AB}} + \sum_{i=1}^{N}\sum_{j>i}^{N}\frac{1}{R_{ij}}. \tag{5}$$

The terms represent distinct interactions in the Hamiltonian and are described below. In the first term, $\sum_{i=1}^{N}\frac{1}{2}\nabla_i^2$, the ∇_i^2 represents the Laplacian operator which involves differentiation with respect to all the coordinates of the ith electron. This first term represents the kinetic energy of the N electrons in the system. The second term $\sum_{A=1}^{M}\frac{1}{2M_A}\nabla_A^2$ similarly represents the total kinetic energy of all the nuclei in the system with ∇_A^2 representing the Laplacian operator of the Ath nucleus with mass M_A. The third term in the Hamiltonian, $\sum_{i=1}^{N}\sum_{A=1}^{M}\frac{Z_A}{r_{iA}}$ is the Coulombic attraction between all the nuclei and electrons, with Z_A representing the charge of the Ath

nucleus and R_{iA} as the distance between the ith electron and the Ath nucleus. The fourth term $\sum_{A=1}^{M}\sum_{B>A}^{M}\frac{Z_A Z_B}{R_{AB}}$ is the nuclear-nuclear repulsion between all pairs of nuclei where R_{AB} is the distance between the Ath and Bth nucleus. The final term, $\sum_{i=1}^{N}\sum_{j>i}^{N}\frac{1}{R_{ij}}$ is the electron-electron repulsion term which only involves the R_{ij} distance between the two electrons.

In order to solve the Schrödinger equation, a few approximations must be made to simplify the terms that would otherwise be too difficult to solve. The first approximation to be made is the Born-Oppenheimer approximation. This approximation allows us to consider the nuclei as fixed due to their masses (1.674×10^{-27} kg for hydrogen, the lightest nucleus) being much larger than the mass of an electron (9.109×10^{-31} kilograms). This allows us to consider the movements of the electrons in the electric field of the fixed nuclei. With this approach, we are able to approximate the second term in Equation 5 as zero with respect to the electron motions. Also with this approximation we are able to consider the fourth term in Equation 5 to be a constant value, referred to as the nuclear repulsion energy. The remaining three terms in Equation 5 are the terms in the electronic Hamiltonian (Equation 6) that fully describes the electrons moving in the field of the fixed nuclei.

$$\hat{\mathcal{H}}_{electronic} = -\sum_{i=1}^{N}\frac{1}{2}\nabla_i^2 - \sum_{i=1}^{N}\sum_{A=1}^{M}\frac{Z_A}{R_{iA}} + \sum_{i=1}^{N}\sum_{j>i}^{N}\frac{1}{R_{ij}} \tag{6}$$

Having removed two terms from our operator by employing the Born-Oppenheimer approximation, we still do not have an analytically solvable operator for a system that has greater than one electron. In order to solve the many-body problem, more approximations must be made. Wavefunctions (Ψ) are considered as the product of many one-electron functions. A Slater determinant (Equation 7) is used in order to

utilize these one electron functions as well as inherently enforce anti-symmetry.

$$\Psi(\mathbf{x}_1, \mathbf{x}_2, \cdots, \mathbf{x}_N) = \frac{1}{\sqrt{N!}} \begin{vmatrix} \chi_i(\mathbf{x}_1) & \chi_j(\mathbf{x}_1) & \cdots & \chi_k(\mathbf{x}_1) \\ \chi_i(\mathbf{x}_2) & \chi_j(\mathbf{x}_2) & \cdots & \chi_k(\mathbf{x}_2) \\ \vdots & \vdots & \ddots & \vdots \\ \chi_i(\mathbf{x}_N) & \chi_j(\mathbf{x}_N) & \cdots & \chi_k(\mathbf{x}_N) \end{vmatrix} \tag{7}$$

In Equation 7 $\frac{1}{\sqrt{N!}}$ is the normalization factor for an N-electron determinant. The $\chi(x)$ represent one-electron spin orbitals which are formed from a linear combination of atomic orbitals (LCAOs). Molecular orbitals are formed from the linear combination of orbitals in LCAO-MO approach,

$$\chi_i = \sum_{\mu} C_{\mu}^{i} \phi_{\mu}, \tag{8}$$

with C_{μ}^{i} representing the expansion coefficients with the atomic orbitals ϕ_{μ}. The atomic orbitals ϕ_{μ} are formed from Gaussian-type orbitals (GTOs) which are of the form,

$$\phi_{\mu}^{GTO}(r) = N x^l y^m z^n e^{-\alpha r^2}. \tag{9}$$

These orbitals use integers l, m, n as the orbital angular momentum for various orbitals. By using GTOs as the basis functions for a molecular system, it allows one to utilize the matrix formalism that is necessary for efficiently using CPUs to solve the Schrödinger equation.

1.1.2 Hartree-Fock Theory

The most common approximation to solving the Schrödinger equation in electronic structure theory is the Hartree-Fock (HF) approximation. The HF approximation states that electrons can only interact with the average field of all the other electrons. Within this approximation, remaining terms of Equation 6 is reduced from a two-electron operator $\frac{1}{R_{ij}}$ to a one electron operator, which is referred to as the Fock

operator,

$$\hat{f}(i) = -\frac{1}{2}\nabla_i^2 - \sum_{A=1}^{M} \frac{Z_A}{r_{iA}} + \nu^{HF}(i). \tag{10}$$

Substituting the previous equations into Equation 4 gives the following equation to solve

$$\hat{f}\chi_j(\mathbf{x}) = \varepsilon_j \chi_j(\mathbf{x}). \tag{11}$$

This equation is the result from the approximations listed above that reduces the many-body problem to solving for the eigenvalues of Equation 11. Again, this is only solvable due to the simplification from Hartree-Fock theory that replaces the explicit two-electron interactions with single electrons interacting with the potential, $\nu^{HF}(i)$.

Utilizing the definitions in the previous sections, it can be shown that the the Hartree-Fock energy simplifies to a summation of one- and two-electron integrals, described below

$$E_{HF} = \sum_i \langle i|h|i\rangle + \frac{1}{2}\sum_{ij}[ii|jj] - [ij|ij]. \tag{12}$$

The one- and two-electron integrals are defined as

$$\langle i|h|j\rangle = \int d\mathbf{x}_1 \chi_i^*(\mathbf{x}_1) h(\mathbf{r}_1) \chi_j(\mathbf{x}_1), \tag{13}$$

and

$$[ij|kl] = \int d\mathbf{x}_1 d\mathbf{x}_2 \chi_i^*(\mathbf{x}_1)\chi_j(\mathbf{x}_1)\frac{1}{r_{12}}\chi_k^*(\mathbf{x}_2)\chi_l(\mathbf{x}_2). \tag{14}$$

The above equations show us the basis for solving for the Hartree-Fock energy. Moving forward, we iteratively solve for the coefficients C_μ^i in Equation 8 that minimize the energy of the system. This method is introduced and extensively covered in Szabo and Ostlund[147].

1.1.3 Density Functional Theory

The aim of density functional theory (DFT)[65, 90] is to approximate the electronic Hamiltonian, $\hat{H}_{elec}$ in Equation 6. The main difference between Hartree-Fock computation and DFT is that the DFT method depends on the electron density, $n(r)$,

instead of the many-electron wavefunction from a single Slater determinant. This means that instead of of solving the many-electron system, it is reduced to compute the energy of non-interacting electrons in the external potential, $v(r)$, of all the electrons in the combined with the interacting electrons in a functional form that depends only on the density, $n(r)$[89]. Using $n(r)$ to determine $\hat{H}_{elec}$ is based on the theorem of Hohenberg and Kohn[66] that the ground state density uniquely defines $v(r)$, and the number of electrons can be found by integration. Kohn and Sham derived a Hamiltonian of the form

$$\hat{H}_{elec} = -\frac{1}{2}\nabla^2 + v(r) + \int \frac{n(r')}{|r - r'|} dr' + v_{xc}(r). \tag{15}$$

Solving the Schrödinger equation using this Hamiltonian allows one to compute the orbital coefficients and orbital energies similarly to Hartree-Fock but using only the density. The first, second and third, terms in Equation 15 refer to the electron kinetic energy, electron-nuclear attraction and electron-electron repulsion respectively. These three terms are similar to those expressed in Equation 6. The exchange-correlation term, $v_{xc}(r)$ is the mathematical difference between DFT and HF theory. The exchange-correlation term depends on the exchange-correlation energy, E_{xc},

$$v_{xc}(r) = \delta E_{xc}[n(r)]/\delta n(r). \tag{16}$$

DFT would be an exact theory if an exact $E_{xc}[n]$ was known, except that in practice, the exact functional form of $E_{xc}[n]$ is not known. Many of the first DFT functionals were of local density approximation (LDA) form, which provided a simple functional form of $E_{xc}[n]$,

$$E_{xc}^{LDA} = \int \epsilon_{xc}(n(r))n(r)dr. \tag{17}$$

where ϵ_{xc} is the energy per particle of a uniform electron gas of density n. Within the LDA formalism, the resultant orbitals are very close to HF orbitals of the same system. An incremental improvement over the LDA formalism is the generalized

gradient approximation (GGA) which adds the gradient of the density to the E_{xc} functional form,

$$E_{xc}^{GGA} = \int f(n(r), \nabla n(r)) dr, \tag{18}$$

where $f(n(r), \nabla n(r))$ is a function of both the density and the gradient of the density. This gives functionals one extra degree of freedom when computing the exchange-correlation energy. Functionals can also include some of the Hartree-Fock exchange energy and are called hybrid functionals, of which B3LYP[14] is the most widely known. DFT's ability to compute energies on large systems makes their utility greater than that of many other methods do not have.

1.2 Post Hartree-Fock Methods of Electron Correlation

1.2.1 Møller–Plesset Perturbation Theory

In-depth reviews of Møller–Plesset Perturbation Theory can be found in references [12, 95]. One of the simplest methods that includes electron correlation is Møller–Plesset Perturbation Theory. This theory introduces a small perturbation to the Hamiltonian as,

$$\hat{\mathcal{H}}_{elec} \approx \hat{\mathcal{H}}_0 + \lambda \mathcal{V} \tag{19}$$

where $\hat{\mathcal{H}}_0$ is the unperturbed Hamiltonian from Hartree-Fock theory and $\mathcal{V}$ is the perturbation of electron correlation to the wavefunction. We then expand the ith wavefunction, $|\Psi_i\rangle$, and the energy, $\mathcal{E}_i$, in a Taylor series in λ gives,

$$|\Psi_i\rangle = |\Psi_i^{(0)}\rangle + \lambda|\Psi_i^{(1)}\rangle + \lambda^2|\Psi_i^{(2)}\rangle + \cdots \tag{20}$$

and

$$\mathcal{E}_i = E_i^{(0)} + E_i^{(1)} + E_i^{(2)} + \cdots \tag{21}$$

The energy expressions for a normalized $|\Psi_i^{(0)}\rangle$ up to second-order are

$$E_i^{(0)} = \langle \Psi_i^{(0)} | \mathcal{H}_0 | \Psi_i^{(0)} \rangle \tag{22}$$

$$E_i^{(1)} = \langle \Psi_i^{(0)} | \mathcal{V} | \Psi_i^{(0)} \rangle \tag{23}$$

$$E_i^{(2)} = \langle \Psi_i^{(0)} | \mathcal{V} | \Psi_i^{(1)} \rangle. \tag{24}$$

By defining the operator $\mathcal{V}$ as

$$\mathcal{V} = \sum_{i<j} r_{ij}^{-1} - \mathcal{V}^{HF}, \tag{25}$$

the zero- and first-order energies in the expansion sum to exactly the Hartree-Fock energy, E_{HF}. Obtaining the second-order energy requires the first-order perturbed wavefunction which is constructed as a linear combination of the unperturbed wavefunctions,

$$|\Psi_i^{(1)}\rangle = \sum_{\mu \neq i} \frac{\langle \Psi_\mu^{(0)} | \mathcal{V} | \Psi_i^{(0)} \rangle}{E_i^{(0)} - E_\mu^{(0)}} |\Psi_\mu^{(0)}\rangle. \tag{26}$$

Using the definition of two-electron integrals in Equation 14, the second-order correction to the energy is

$$E^{(2)} = \frac{1}{4} \sum_{ijab} \frac{|[ai|bj] - [aj|bi]|^2}{\epsilon_a + \epsilon_b - \epsilon_i - \epsilon_j} \tag{27}$$

Generally the perturbative expansion is truncated at second-order and referred to as second-order Møller–Plesset perturbation theory (MP2). Corrections after the second-order are generally not considered due to their comparable computational cost with more accurate electron correlation methods which will be discussed below. Perturbation theory provides a better description than HF theory of molecular interactions and energies but there are still cases where it fails. First, it has been shown that including higher order perturbations does not always provide a more accurate answer. Second, due to the denominator of equation of Equation 27, if $\epsilon_a + \epsilon_b$ approaches $\epsilon_i - \epsilon_j$ the energy equation goes to infinity.

1.2.2 Coupled-Cluster Theory

Coupled-cluster (CC) theory has many reviews which the reader is directed to for complete derivations and more information[121, 127, 122, 134, 132, 133]. Coupled-cluster

theory is among the most robust levels of theory to describe electron correlation. It achieves robustness using the exponential ansatz acting on the Hartree-Fock reference $|\Phi_0\rangle$,

$$|\Psi_{CC}\rangle = e^{\hat{\mathbf{T}}}\Phi_0\rangle. \tag{28}$$

where $\hat{\mathbf{T}}$ is the excitation operator that contains all possible excitations,

$$\hat{\mathbf{T}} = \hat{\mathbf{T}}_1 + \hat{\mathbf{T}}_2 + \hat{\mathbf{T}}_3 \cdots + \hat{\mathbf{T}}_N. \tag{29}$$

For example, the $\hat{\mathbf{T}}_1$ will act on the reference wavefunction and form singly-excited determinants Φ_i^a and coefficients t_i^a which are solved for iteratively. Similarly, $\hat{\mathbf{T}}_2$ when acting on the reference produces all doubly excited determinants Φ_{ij}^{ab} with coefficients t_{ij}^{ab}. If $\hat{\mathbf{T}}$ only includes single and double excitations, then the CC wavefunction becomes,

$$|\Psi_{CCSD}\rangle = e^{\hat{\mathbf{T}}_1+\hat{\mathbf{T}}_2}|\Phi_0\rangle. \tag{30}$$

Using $|\Psi_{CCSD}\rangle$, the energy expression can be derived but it is quite long and the reference provided above are excellent resources for that derivation. The energy expression for the correlation energy of coupled-cluster of single and double excitations (CCSD) is

$$E_{CCSD}^{corr} = \sum_{i}^{occ}\sum_{a}^{virt} t_i^a f_i^a + \frac{1}{4}\sum_{ij}^{occ}\sum_{ab}^{virt}(t_{ij}^{ab} + t_i^a t_j^b - t_i^b t_j^a)\langle ij||ab\rangle. \tag{31}$$

Much of the time, truncating CC theory at double excitations provides a very accurate result given its computational cost. For the cases where CCSD does not provide accurate enough an answer, perturbative triples can be added to the CCSD, giving us CCSD(T)[121, 127, 122, 133]. This method is referred to as the "gold-standard" of computational chemistry which is then used to evaluate the performance of other methods.

1.3 Approximations to Two-Electron Integrals

1.3.1 Density Fitting

One of the most common bottlenecks that electronic structure theory faces is the evaluation and storage of the four-index, two-electron integrals represented in Equation 14. A few techniques have been explored to combat this problem, namely Cholesky Decomposition[19, 128, 88, 8, 24, 164, 7, 178, 25, 36], pseudo-spectral techniques[98, 97, 50], and density fitting (DF) or resolution of the identity (RI)[171, 45, 46, 48, 22, 85, 163, 169, 168]. The density-fitting approximation is based on treating the four-index integrals $(\mu\nu|\rho\sigma)$ as two three-index quantities and a metric $[J^{-1}]_{PQ}$ that connects the two in an auxiliary basis set.

$$(\mu\nu|\rho\sigma) \approx \sum_{PQ} (\mu\nu|P)[J^{-1}]_{PQ}(Q|\rho\sigma) \tag{32}$$

$$[J]_{PQ} = \int P(\mathbf{r}_1)\frac{1}{\mathbf{r}_{12}}Q(\mathbf{r}_2)d\mathbf{r}_1 d\mathbf{r}_2 \tag{33}$$

In the DF approximation, the three-index quantity $(\mu\nu|P)$ serves as a way to cast the orbital product ($\mu\nu$ into the auxiliary basis via the Coulomb metric

$$(\mu\nu|P) = \int \mu(\mathbf{r}_1)\nu(\mathbf{r}_1)\frac{1}{\mathbf{r}_{12}}P(\mathbf{r}_2)d\mathbf{r}_1 d\mathbf{r}_2. \tag{34}$$

Density-fitting does not reduce the computational scaling of MP2 or CCSD, but it does reduce the pre-factor in MP2 and eliminates the need for the integral transformation in CCSD. For certain methods like MP2, density-fitting can reduce the cost of the correlation energy computation to a point where the SCF computation becomes the rate-limiting step in the computation.

1.3.2 Frozen Natural Orbitals

One way to accelerate methods which depend on large powers of the number of orbitals is to use eliminate orbitals which do not contribute much to the electron

correlation. One method to do this is using the Frozen Natural Orbital (FNO) approximation which truncates the virtual orbitals according to the MP2 population of those orbitals[144, 87, 152, 153]. This truncation can result in result in a 20%–60% reduction in the number of virtual orbitals while only incurring errors in geometric parameters of a few tenths of a picometer[153]. FNOs allow for a tunable amount of accuracy based on the population used as the cutoff for a virtual orbital being ignored during the correlation portion of the computation. Utilizing this approximation allows one to perform CCSD and CCSD(T) computations on system sizes that are outside the tractability of canonical CCSD and CCSD(T). Also, the FNO approximation makes computation times on an N-mer in an (N+1)-mer basis set effectively free compared to the long time necessary for the (N+1)-mer computation.

1.4 Transition State Searching

Transition states can show us key reaction steps that would allow one to tune the molecules involved to increase reactivity, decrease side reactions or change a number of other properties of a reaction. One could do this by finding a better stabilized transition state structure through non-covalent interactions or by including bulky groups in key areas keep a side reaction from occurring. Transition states are fist-order saddle-points within the Born–Oppenheimer approximation, meaning that the vibrational Hessian will have exactly one negative eigenvalue which represents being at a maximum along a reaction path between two local minima, while being at minimum in all other directions perpendicular to the reaction path. The process by which one finds transition states can be quite complex, but the crucial steps in the process are obtaining a good starting geometry, performing a transition state optimization, verifying the optimized structure is a first-order saddle-point, and ensuring the obtained transition state is along the reaction path between the correct reactants and products.

Obtaining a geometry that approximates the transition state structure may be the most difficult step in the process above. Many algorithms have been developed to help obtain these approximate structures. Of course, one can always attempt to draw the structure in a molecule editor (Avogadro, ChemSketch, Spartan, etc. ...) based on the proposed transition state of the reaction being investigated, but this can sometimes be difficult if there are too many degrees of freedom or too many subtle molecular arrangements in the transition state. If a hand-drawn transition state does not produce successful transition state searches, one can go to the many algorithms developed to assist in generating transition state structures, such as linear synchronous transit or the freezing string method. Linear synchronous transit (LST)[108] requires two input structures, one of the reactants and one of the products. LST then interpolates between the two geometries and produces a guess structure for the transition state. The interpolation can be controlled to interpolate less than 50% of the way between reactants and products if your reaction has an early transition state or greater than 50% if the reaction has a late transition state. For straight-forward reactions, LST produces very good guess geometries for the rest of the transition state searching process. If LST does not produce a structure that is close enough of an approximation to the transition state, one might try a more complex method, the freezing string method. The freezing string method (FSM)[138, 20] also needs input of reactants and products geometries but then produces strings[166] which are grown from the reactants and products until the two fragments meet. Then the points along the string are optimized, and the highest energy point along the string is considered the best guess for the transition state structure. For systems where the transition state is surrounded by a complex chemical environment, sometimes the environment may cause problems in finding the transition state. In those cases, one can simply do a constrained optimization where the atoms involved in the transition state are frozen in place while the rest of the environment is put through a geometry optimization.

This allows the environment to be in a more optimal structure when one then unfreezes the previously frozen atoms and perform a transition state optimization on the entire structure.

Once a transition state has been found, the rest of the effort is put forth towards verification that it is a transition state and it is the transition state that was sought. In order to verify that it is a transition state, one just performs a frequency computation on the transition state structure and verifies that there is only one imaginary vibrational frequency. After the frequency calculation, the last step in the process is to verify that the transition state is the correct one (i.e., it connects the correct reactants and products.) To do this, one must perform an intrinsic reaction coordinate (IRC)[51] computation. IRC computations follow the steepest descent paths going downhill in both directions from the transition state. Because the path between transition state and stationary point is unlikely to be a straight line, the computation takes a series of finite-size steps along the gradient at each point which better simulates the "true" reaction path. If the IRC computation provides structures which are equivalent to the desired reactants and products, then the correct transition state has been found.

1.5 Organization of Thesis

This thesis contains four chapters starting with this introduction to electronic structure theory, Hartree-Fock theory, methods to correlate electrons, and approximations employed by computational chemists to aid in computing larger systems than previously possible. Chapter 2 explores the effect that curvature has on π-π stacking interactions which is normally studied using planar aromatic hydrocarbons. Chapter 3 attempts to reconcile differences in the literature about the magnitude of the three-body non-additive dispersion contribution to the lattice energy of crystalline benzene. Chapter 4 provides mechanistic insights into the proposed rate limiting

step of hydrolytic kinetic resolution (HKR) of terminal epoxides, a reaction that produces extremely enantiopure products by way of selectively opening epoxide rings of one enantiomer but not the other. Chapters 2, 3, and 4 are adapted from previously published or submitted first author publications listed below:

Chapter 2: Kennedy, M. R., Burns, L. A., Sherrill, C. D. "Buckyplates and Buckybowls: Examining the Effects of Curvature on π-π Interactions" *J. Phys. Chem. A*, vol. 116, p. 11920, 2012.

Chapter 3: Kennedy, M. R., Ringer, A. L., DePrince, A. E., Marshall, M. S., Podeszwa, R., Sherrill, C.D. "Communication: Resolving the three-body contribution to the lattice energy of crystalline benzene: Benchmark results from coupled-cluster theory" *J. Chem. Phys.*, vol. 140, p. 121104, 2014

Chapter 4: Kennedy, M. R., Burns, L. A., Sherrill, C. D. "Mechanistic Insight into the Hydrolytic Kinetic Resolution of Epoxides Catalyzed by Co-Salen", *Submitted*

CHAPTER II

BUCKYPLATES AND BUCKYBOWLS: EXAMINING THE EFFECTS OF CURVATURE ON π-π INTERACTIONS

2.1 Abstract

π-π interactions are integral to many areas of chemistry, biochemistry, and materials science. Here we use electronic structure theory to analyze how π-π interactions change as the π-systems are curved in model complexes based on coronene and corannulene dimers. Curvature redistributes electronic charge in the π-cloud and creates a dipole moment in these systems, leading to enhanced intermolecular electrostatic interactions in the concave-convex (nested) geometries that are the focus of this work. Curvature of both monomers also has a geometric effect on the interaction by decreasing the average C–C distance between monomers and by increasing the magnitude of both favorable London dispersion interactions and unfavorable exchange-repulsion interactions. Overall, increasing curvature in nested π-π interactions leads to more favorable interaction energies regardless of the native state of the monomers, except at short distances where the most highly curved systems are less favorable as exchange repulsion terms begin to dominate the interaction.

2.2 Introduction

π-π interactions play a pivotal role in the way proteins fold[100, 32] and drugs bind to targets[130]. They are also critical in determining the crystal packing and charge transport properties of π-conjugated organic materials for organic electronics

applications[40]. In biological contexts and frequently in organic materials, π-π interactions involve planar π-systems, and the fundamental physics of planar π-π interactions has been the focus of significant recent effort[100, 141, 139, 130, 123] π-π. interactions involving prototype molecules such as benzene[157, 142, 74, 113, 139, 170], coronene[73, 75], and linear acenes[69] have been given special consideration. On the other hand, curved π systems including fullerenes and carbon nanotubes are also of significant interest in materials applications. Experimental and theoretical works have examined such curved π systems[31, 41, 82, 49, 38], yet to our knowledge, the effect of curvature on the fundamental physics of π-π interactions has not been systematically explored.

To investigate this issue, we employed as model systems nested dimers of coronene and corannulene, which are among the simplest model systems large enough to exhibit curvature effects. Coronene dimer is naturally flat because its central ring has six sides, and corannulene is naturally curved because its central ring has five sides. High-quality interaction energies for coronene dimer[73], corannulene dimer[76], and coronene-circumcoronene dimer[75] have recently been published by Pulay and coworkers. To probe the effect of curvature directly, we constructed model dimer geometries in which each monomer (coronene and corannulene) was distorted from its natural state (flat and curved, respectively) through to its opposite state (curved and flat). Using these model systems, we are able to examine the interaction between monomers (at fixed monomer geometries) as a function of intermonomer distance and monomer curvature. Curvature can affect the intermolecular interaction through two routes: by modifying the electronic structure of the monomers and by introducing differences in the contact geometries. An example of the former is that as the monomers become curved, a permanent dipole is created within each monomer that interacts with the dipole on the other monomer for an enhanced or reduced electrostatic interaction, depending on the orientation of the two monomers. Here we seek

to quantify such effects to better understand how curvature influences the strength and character of π-π interactions.

Dispersion plays a major role in π-π interactions, and hence we also use these systems to examine possible differences between recently proposed dispersion corrections to density functional theory. The simplest such corrections are damped C_6R^{-6} terms[174], popularized primarily by Grimme[53, 54, 55]. In most such approaches (including Grimme's second-generation -D2 method[54]), the C_6 parameters are tabulated for each element and are not able to respond to their local chemical environment (and thus, for present purposes, not able to adapt to curving monomers). However, of course the C_6 parameters should change with curvature, and here we examine by how much, using two alternative approaches. First, we employ Grimme's third-generation -D3 method[55], which interpolates C_6 terms from tabulated data based on each atom's coordination number. Second, we employ a more theoretically sophisticated approach, Becke and Johnson's exchange-hole dipole moment model (XDM)[15, 16, 17]. Johnson has recently shown that oxidation state, hybridization, charge, and other chemical properties can affect the atomic C_n by as much as 65% for carbon atoms[79].

2.3 Computational Methods

2.3.1 Geometries

To investigate the effect of curvature on π-π interactions, a set of coronene (buckyplate) and corannulene (buckybowl) dimers was constructed by varying the inter-monomer distance and the degree of curvature of the monomers. The labeling of atoms, bonds, and curvature angles for coronene can be seen in Figure 1 and is analogous for corannulene. The curved monomer geometries were constructed such that bond lengths were fixed while bond angles changed in order to relieve the stress of curvature. The formulae for construction of the molecules can be found in the

Figure 1: (a) Side view of coronene dimer geometry with $\tau = 50°$ and R=3.7 Å. (b) Side view of coronene dimer geometry with $\tau = 0°$ and R=3.7 Å. (c) Top down view of coronene dimer geometry where a, b, and c label distinct groups of carbon atoms. The curvature τ and the dihedral τ' are related by $\tau' = 180 - \frac{\tau}{2}$.

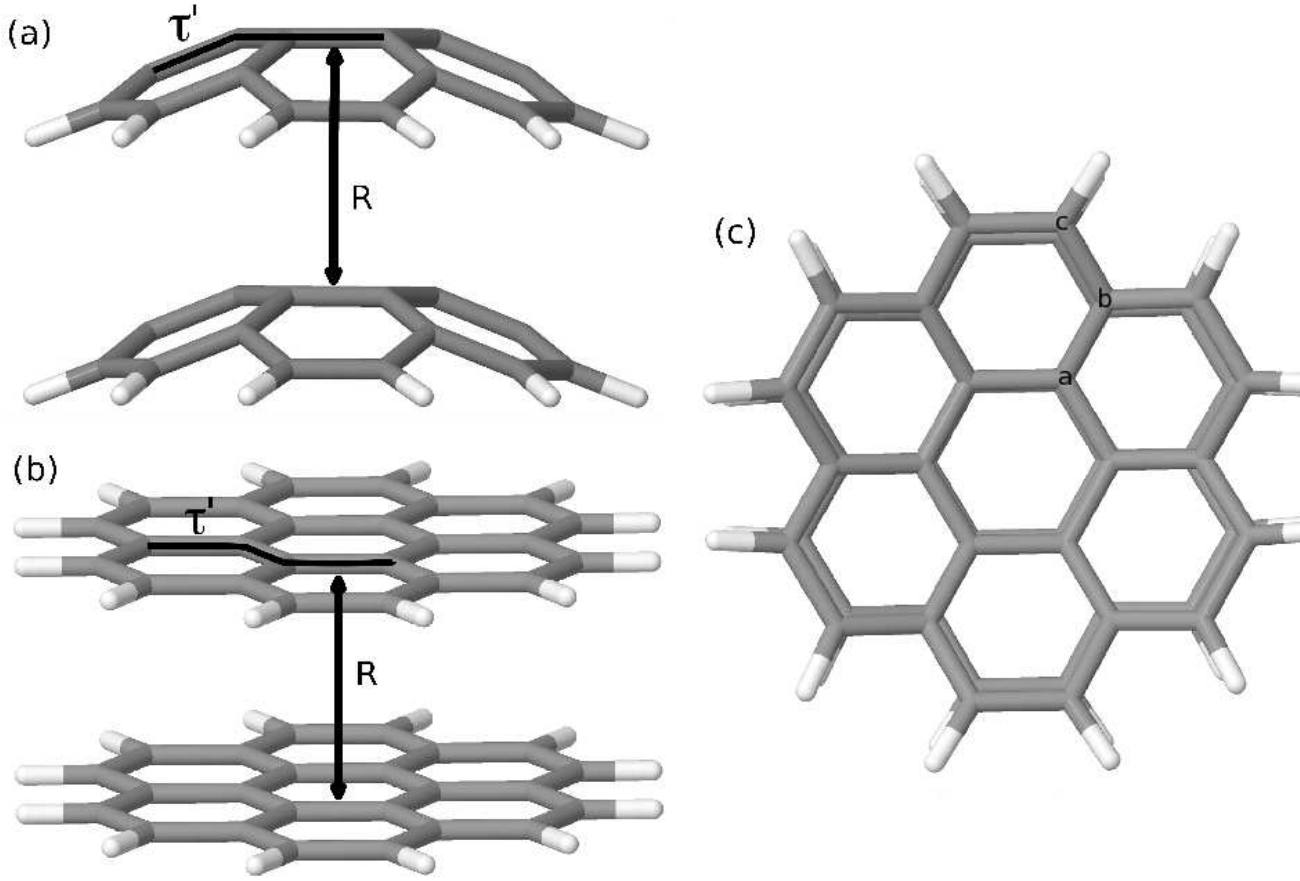

supplementary materials.

In order to find a reliable, computationally tractable methodology for treating these systems, computations using four density functionals and four different dispersion corrections were performed on the geometries of corannulene dimer reported by Janowski *et al.*[76] These structures are nearly identical to those reported by X-ray crystallography[111], with curvature torsion angle (see Figure 1) of $\tau \approx 57.5°$, and were obtained using the PBE1 functional[110] with the 6-31G* basis set [61] using a grid with 99 radial shells and 302 angular points (99,302). Here we employ frozen monomer geometries to simplify the computations. This approximation appears to

be a good one for these systems[76], at least for native monomer curvatures. Of course, there would be large monomer relaxation energies for our artificially curved monomers, but given the artificial nature of the imposed curvature, the associated relaxation energies are not particularly relevant to our study — our focus is on how intermolecular interaction energies (at fixed monomer geometries) are affected by curvature, regardless of how the monomer curvature might have been achieved (the curvature will be natural in our corannulene dimer, or in larger systems like carbon nanotubes or fullerenes).

2.3.2 Dispersion–Corrected DFT

Single-point energy computations were performed using the B3LYP[14], B97-D[54], M05-2X[176], and M06-2X[177] functionals with the heavy-aug-cc-pVDZ (haDZ) basis set (defined as aug-cc-pVDZ[84] for non-hydrogen atoms and cc-pVDZ[47] for hydrogen atoms) to determine which functional most accurately reproduced the estimated triple-ζ quality QCISD(T) interaction energies for concave-convex stacked corannulene dimer recently reported by Janowski *et al.*[76] That work examined the B97-D, M06-2X, and ωB97X-D functionals in conjunction with the cc-pVQZ basis set and noted that B97-D provided an intermonomer distance within 0.06 Å and an interaction energy within 1.1 kcal mol^{-1} of benchmark values.

DFT computations reported in this work utilized NWChem 6.0[160], with the "fine" or (70,590) grid. Grimme's -D2 and -D3 corrections[54, 55] were both applied to all the functionals through the dftd3 program[55]. The computations of XDM dispersion coefficients were performed in Q-Chem 3.2 [137] with the full aug-cc-pVDZ basis and damped into a dispersion correction according to revised parameters[29, 28]. Generally our computations are counterpoise corrected according to the Boys and Bernardi approach[27] to reduce basis set superposition error (BSSE); however the XDM computations are not counterpoise corrected because parameters for the XDM

damping function were optimized using uncorrected interaction energies.

The three dispersion corrections considered here all take slightly different forms. Grimme's DFT-D2 correction [54] is the simplest, employing C_6 only in the dispersion series, and is expressed in Equation (35).

$$E_{disp}^{D2} = -s_6 \sum_{i,j>i}^{N} \frac{C_6^{ij}}{R_{ij}^6} f_{damp}(R_{ij}). \tag{35}$$

The C_6 coefficients are calculated as the geometric average between the two elemental C_6 coefficients C_6^i and C_6^j. The s_6 parameter is optimized for each functional and is usually between 0.5 and 1.5.

Grimme recently released a more refined method[55], DFT-D3, which additionally implements the R^{-8} term in the dispersion correction, changes the method of calculating C_6, and alters the damping functional. Atomic C_6^i coefficients are interpolated from reference values based upon coordination number in the current molecular structure. Thus, the C_6 values are allowed to respond to the molecular environment in -D3, rather than being simply looked-up from a table of elemental values. The DFT-D3 correction has the form:

$$E_{disp}^{D3} = -\sum_{n=6,8} s_n \sum_{i,j>i}^{N} \frac{C_n^{ij}}{R_{ij}^n} f_{damp}(R_{ij}). \tag{36}$$

We investigated two different damping functions for use with the DFT-D3 correction. The first is the original damping function for DFT-D3, which damps the dispersion interaction to zero at short ranges[55], and the other is the damping function suggested by Becke and Johnson[15, 80, 81], and now advocated by Grimme, DFT-D3(BJ). Implementing the latter entailed a reoptimization of the s_n parameters as well as a switch of damping functional form[56].

The last dispersion correction considered is the XDM method of Becke and Johnson[15, 5, 17, 62]. Calculation of the XDM correction is based upon the non-zero dipole

moment of exchange holes[18] on one monomer that can induce a complementary dipole moment on the other monomer, leading to a dispersion interaction between the molecules. This method is quite different from the first two approaches to dispersion corrections because XDM calculates C_n parameters from the electron density instead of using tabulated C_6 data. The computation of the XDM dispersion contribution to the energy in Equation (37) uses a similar functional form as those used for the DFT-D2 and DFT-D3 corrections but involves one term further, C_{10}.

$$E_{disp}^{XDM} = -\sum_{n=6,8,10}\sum_{i,j>i}^{N}\frac{C_n^{ij}}{R_{ij}^n}f_{damp}(R_{ij}). \tag{37}$$

To help illustrate electronic changes due to curvature, electrostatic potentials of coronene and corannulene at different curvatures were produced using the Spartan '08 package[1]; the electrostatic potential [between -80 (red) and +80 (blue) kcal mol^{-1}] was mapped onto the electron density (produced at the B3LYP/6-31G level of theory) with an isovalue of 0.002 e^- bohr^{-3}. Our discussions of the plotted electrostatic potentials is purely qualitative, and we do not expect the figures to change noticeably at higher levels of theory.

2.3.3 SAPT Energy Decomposition

Symmetry adapted perturbation theory (SAPT) is an approach by which individual physical components (electrostatics, induction, dispersion, and exchange) of a non-bonded interaction can be elucidated.[78, 148]. SAPT partitions the Hamiltonian into contributions from the Fock operator of each monomer, the interaction between the two monomers, and the fluctuation potential (electron correlation), as explained in Ref [78]. Examining the components along a potential energy curve allows for insight into how the nature of the interaction changes as the monomers approach each other. These calculations were performed with the jun-cc-pVDZ (jaDZ) basis set[106] (formerly referred to as aug-cc-pVDZ′ by our group) inside a development version of

PSI4[2]. Compared to the aug-cc-pVDZ basis, jun-cc-pVDZ removes diffuse functions from hydrogen atoms and diffuse *d* functions from the non-hydrogen elements. For SAPT0, jun-cc-pVDZ has been shown to yield favorable error cancellation[70].

2.4 Results and Discussion

The performance of density functional methods versus the estimated QCISD(T)/aug-cc-pVTZ benchmarks for corannulene dimer reported by Janowski *et al.*[76] is pre-

Figure 2: Counterpoise-corrected DFT/haDZ interaction energies for corannulene dimer compared to QCISD(T) reference values from Ref. [76] (see text for XDM details).

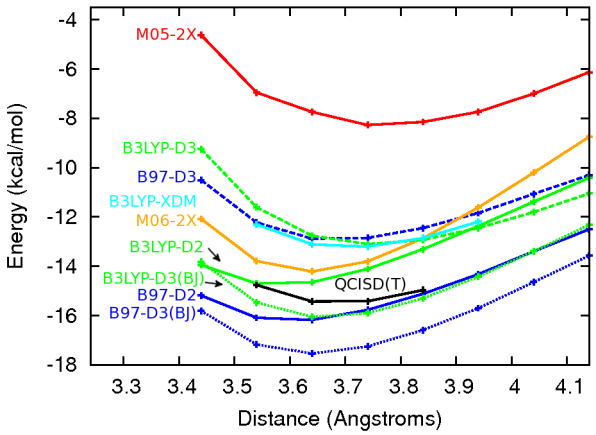

sented in Figure 2 as a function of intermonomer distance. The benchmark curve shows a minimum of 15.43 kcal mol^{-1} at 3.64 Å. It is apparent that M05-2X and M06-2X both underbind (M05-2X by a larger margin) when compared to the reference, with neither curve tracking the shape of the reference curve very closely. The B3LYP-D3 and B97-D3 methods also underbind the reference by 3-4 kcal mol^{-1}. B3LYP-D2 and B97-D2 are closer to the reference data than their respective -D3 curves, but both have the wrong shape, shifting the equilibrium distance to shorter distances. B97-D3(BJ) and B3LYP-D3(BJ) both show good agreement with the shape of the reference curve, and the B3LYP-D3(BJ) curve is rather close to the benchmark curve

(differences of 0.4-0.8 kcal mol^{-1}). The last method investigated is B3LYP-XDM using the parameterization of Burns *et al.*[29, 28], which performs very well in providing a curve with the right shape; the interaction energies are underestimated by 2.0-2.5 kcal mol^{-1} across the potential curve. However, these errors are significantly larger than the errors exhibited by B3LYP-D3(BJ). Hence, we selected the latter method for primary use in this work. We also performed limited tests using XDM with the PBE functional, but the dimers were more underbound using this functional than they were using B3LYP-XDM.

Results for the full two-dimensional scan of intermonomer distance and curvature (R, τ) are displayed in Figure 3. The B3LYP-D3(BJ)/haDZ computations show that as τ is varied from 0° to 50°, minima of the coronene interaction energy curves range from -17.7 to -22.9 kcal mol^{-1} (-13.1 to -16.2 kcal mol^{-1} for corannulene). Coronene and corannulene exhibit the same trend from 0° to 50°: the minima of the interaction energy curves deepen with increasing curvature. This stabilization results from an enhancement in both the dispersion interaction and electrostatic interaction between the two monomers, as seen from the SAPT0 results plotted in Figure 4. Induction also increases with increasing curvature (Figure 4), although this effect is smaller than that for the electrostatic and dispersion terms. Induction accounts for approximately 25% of the interaction energy at the most extreme curvature studied, and 6.5% at τ=0°. Such percentages are higher than those typically observed in other π systems that have been examined to date[68, 126]. The relatively large induction interaction is due to a very strong dependence of the monomer dipole moment on curvature, increasing from 0 at τ=0° to 2.5 Debye at τ=50°. Counterbalancing these increases in attractive components with increasing curvature is an increase in the unfavorable exchange-repulsion term.

Of the two primary contributors to extra stabilization with increasing curvature (electrostatics and London dispersion forces), let us begin with the electrostatic term.

Figure 3: B3LYP-D3(BJ)/haDZ interaction energy curves for various curvatures of coronene dimer (top panel) and corannulene dimer (bottom panel).

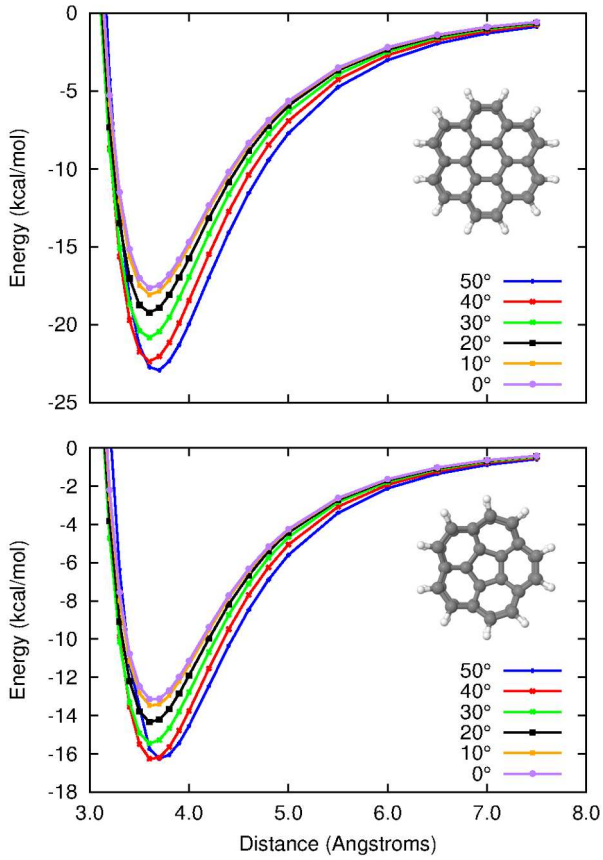

The electrostatic interaction becomes more favorable with curvature in these concave-convex (nested) geometries for two reasons: first, the curvature redistributes the electronic charge leading to more favorable interactions, and second, at a fixed distance between the central rings, greater curvature leads to shorter average intermolecular C–C distances, in turn leading to larger favorable charge penetration terms.

The first effect, that coming from charge redistribution, is illustrated in Figure 5 and Figure 6. For flat monomers, the two sides of the monomer are symmetric, and hence the charge distribution is equivalent on both sides. However, upon curvature, the monomers adopt a positive charge on the outside of the bowl and a negative charge on the inside, leading to an electronic dipole moment. For the nested (concave-convex)

geometries considered here, this means that the two dipoles are aligned in a head-to-tail arrangement, which contributes to a favorable electrostatic interaction. The dipole moment of the monomers is a significant 2.5 Debye when τ=50°.

The second effect, a geometric effect in which average interatomic contact distances get shorter, also enhances the electrostatic interaction. For a fixed distance between the central rings of the two monomers, curvature of both monomers means that the atoms around the periphery of the outer monomer get closer to the atoms of the inner monomer in a concave-convex geometry. As the curvature changes from 0° to 50° at an intermolecular distance of 3.7 Å, this results in a 10% reduction in the sum of interatomic distances between pairs of atoms on separate monomers. Having closer contact between the monomers is favorable electrostatically because it leads to enhanced charge penetration terms. Charge penetration is a favorable contribution to electrostatic interactions due to orbital overlap, and its importance to π-π interactions has been recently emphasized by Hohenstein *et al.*[67] The effect is visible in the SAPT0 electrostatic term plotted in Figure 4, which becomes both exponentially more attractive at short intermonomer distances and more attractive with increasing curvature for a fixed intermonomer distance. A comparison of the more rigorous (charge-penetration including) SAPT electrostatic energy and a (charge-penetration neglecting) distributed multipole analysis[145] (DMA) estimate is presented in Figure 7. The DMA is performed based on Hartree–Fock/6-311G** results and includes terms through quadrupole-quadrupole. The DMA analysis actually shows repulsive electrostatics at short distances, indicating that electrostatics in these systems would not be favorable if not for the charge penetration terms. For dimers 3.3 Å apart, the deviation is upwards of 40 kcal mol^{-1}, whereas for dimers over 5 Å separation (where a multipole description of the monomers becomes more appropriate), the deviation is less than 1 kcal mol^{-1}. Again, the SAPT electrostatics term shows more favorable interactions for more curved monomers at a fixed intermolecular distance.

Figure 4: SAPT0 breakdown of the interaction energy for various values of τ. Top panel: coronene, bottom panel: corannulene.

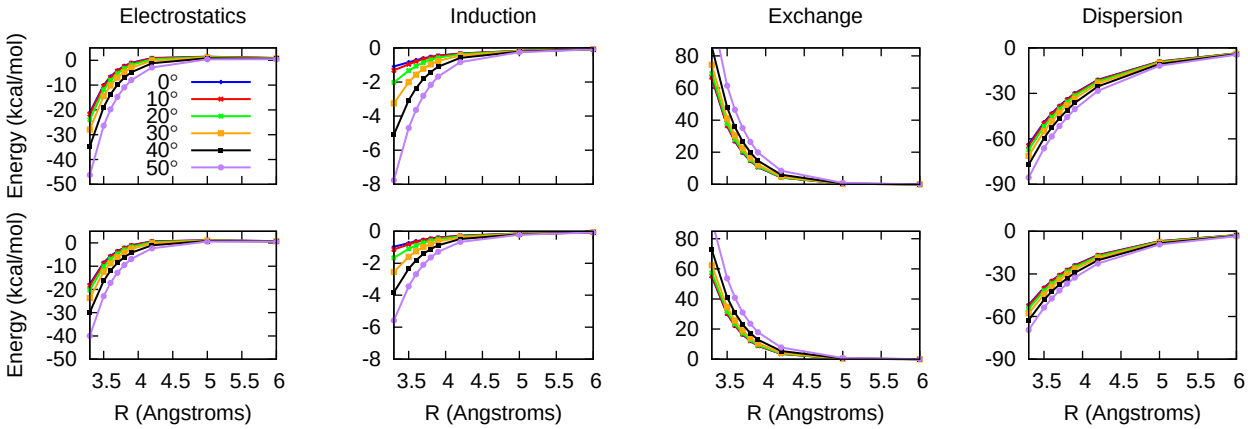

Next, let us consider changes to the dispersion contribution as a function of curvature. Figure 4 indicates that the dispersion term becomes more favorable with increasing curvature at a fixed distance between the central rings of the monomers. Just as for the electrostatic term, there can be two origins of this change: an electronic effect (changes in electron distribution and polarizability) and a geometric effect (closer interatomic contacts with curvature). Because the dispersion interaction depends sensitively on interatomic distances (the leading term being proportional to R^{-6}), the geometric effect on dispersion is easy to understand. The -D2 dispersion contribution to the interaction energy goes from -25.69 to -33.96 kcal mol^{-1} for coronene as the curvature is increased from 0^{o} to 50^{o}, as seen in Table 1. The increase in the magnitude of the dispersion term as computed by -D2 is from geometric effects alone, because the C_6 coefficients in that approximation are fixed for each element and are not dependent on chemical environment. Hence, the geometric contribution to the dispersion term is substantial.

Changes in the electronic distribution with respect to curvature are another possible source of changes to the dispersion term. Grimme's -D3 model allows for some response of the dispersion coefficients to an atom's coordination geometry, and the

Figure 5: Electrostatic potential at the B3LYP/6-31+G* level of theory, using a scale of -80 (red) to +80 (blue) kcal mol^{-1} for (a) coronene with τ=0°, (b) Convex side of coronene with τ=50°, (c) Concave side of coronene with τ=50°.

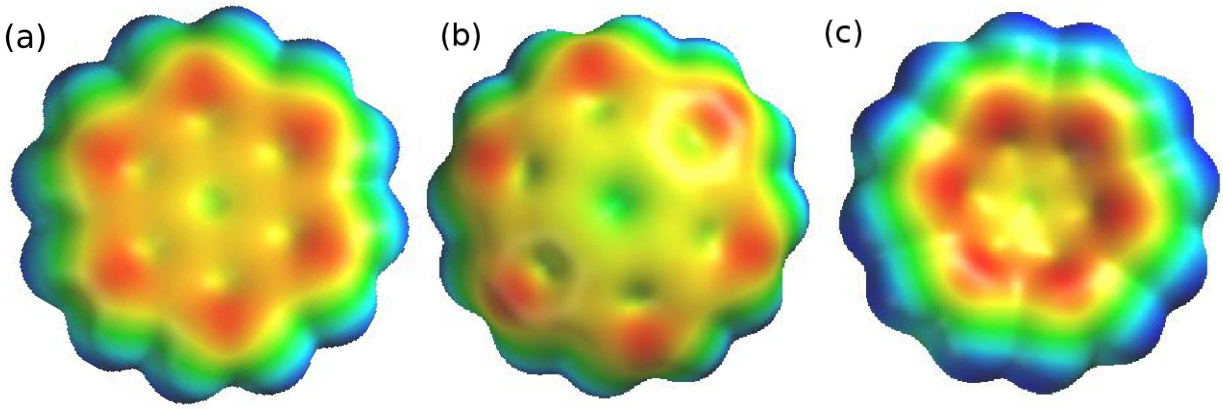

XDM model allows for a full response to the chemical environment because the dispersion coefficients are computed directly from the electron density. To quantify how much the changing chemical environment affects the dispersion contribution, we evaluated -XDM and -D3(BJ) dispersion terms at 0° and 50° curvature, for both coronene dimer and corannulene dimer. Next, we took the computed dispersion coefficients C_n at each geometry, and then applied them at the other geometry to re-evaluate the dispersion contribution. This provides a measure of how much the changing C_n coefficients change the total dispersion contribution in these systems as they progress from flat to curved.

Figure 6: Electrostatic potential at the B3LYP/6-31+G* level of theory, using a scale of -80 (red) to +80 (blue) kcal mol^{-1} for (a) corannulene with τ=0°, (b) Convex side of corannulene with τ=50°, (c) Concave side of corannulene with τ=50°.

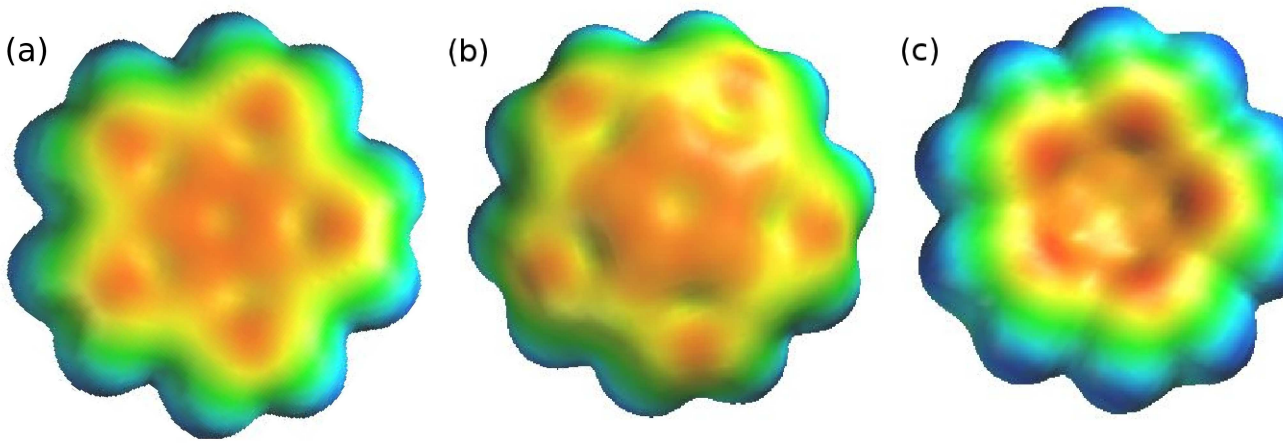

Table 1 shows dispersion interactions for the two dimers, relative to their dispersion interactions at τ=0°. Comparing the first two rows, we see that the C_n coefficients affect the dispersion interaction of corannulene by 0.51 and 0.08 kcal mol^{-1} for -D3(BJ) and -XDM, respectively, when applying the C_n coefficients from τ=50° to the geometry τ=0°. These are modest contributions compared to the overall dispersion contributions of -16 to -29 kcal mol^{-1} (see Table footnote). Comparing the first and third rows of the Table shows that using fixed C_n values on two different geometries changes the dispersion interaction by 5.2 or 4.3 kcal mol^{-1} for -D3(BJ) and -XDM, respectively, for corannulene. This is a much larger change than that observed in the previous comparison. This indicates that the geometric effect is around 10-50 times larger than the electronic effect in determining the changes in dispersion contributions

Figure 7: Comparison of SAPT0 electrostatic contribution (dashed lines) and distributed multipole analysis (DMA) of electrostatics through quadrupole-quadrupole (solid lines) at various τ. Top panel: coronene, bottom panel: corannulene.

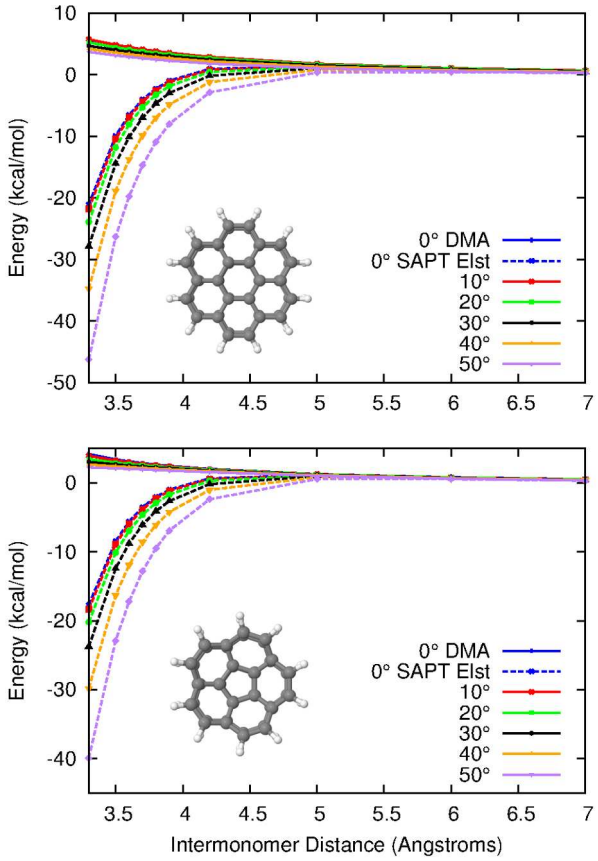

with respect to curvature. Results for coronene in Table 1 show similar trends.

Lastly, in Figure 8 we examine the changes of the C_6 coefficients in both -D3(BJ) and -XDM for various τ. First, the coefficients from -D3(BJ) and -XDM follow the same trends with respect to monomer curvature. Second, both sets of C_6 coefficients change by no more than 5% between τ=0° and τ=50°, consistent with the results from Table 1 discussed above.

Table 1: Dispersion corrections for coronene and corannulene relative to 0° geometry with 0° C_n coefficients at R = 3.7 Å. All values in kcal mol^{-1}.

		Coronene			Corannulene		
Geometry from	**C_6 from**	**-D2**	**-D3(BJ)**	**-XDM**	**-D2**	**-D3(BJ)**	**XDM**
0°	0°	0.00[a]	0.00[b]	0.00[c]	0.00[d]	0.00[e]	0.00[f]
0°	50°	0.00	-0.61	-0.08	0.00	-0.51	-0.08
50°	0°	-8.27	-7.23	-5.64	-6.29	-5.21	-4.31
50°	50°	-8.27	-6.75	-5.34	-6.29	-5.76	-4.22

[a]-D2 dispersion interaction for coronene is -25.69 kcal mol^{-1}; [b]-D3(BJ) dispersion interaction for coronene is -28.85 kcal mol^{-1}; [c]-XDM dispersion interaction for coronene is -20.80 kcal mol^{-1}. [d]-D2 dispersion interaction for corannulene is -20.63 kcal mol^{-1}; [e]-D3(BJ) dispersion interaction for corannulene is -22.28 kcal mol^{-1}; [f]-XDM dispersion interaction for corannulene is -16.89 kcal mol^{-1};

2.5 Conclusions

We have studied concave-convex (nested) dimers of corannulene and coronene at various imposed monomer curvatures to elucidate how curvature affects the fundamental physics of π-π interactions. Both coronene and corannulene dimers exhibit more attractive interaction energies upon curvature, except at short, unnatural intermolecular distances and high degrees of curvature. Curvature in a π system affects all four major components of noncovalent interactions: dispersion, electrostatics, exchange, and induction. Dispersion and exchange are affected most strongly by simple geometric effects because average interatomic distances between monomers decrease with increasing curvature in concave-convex geometries as the peripheral atoms of the outer monomer become closer to the atoms of the inner monomer. This same geometric effect also leads to increased orbital overlap, and hence larger stabilizing charge penetration contributions to the electrostatic interaction. On the other hand, curvature creates a charge redistribution within the monomers that also affects the nature of the interaction. XDM and DFT-D computations suggest that this electronic effect is much less important than the geometric effect when examining the dispersion term. On the other hand, this charge redistribution has a significant electrostatic effect because it creates a dipole on each curved monomer, which leads to a favorable

Figure 8: C_6 coefficients from -D3(BJ) (solid lines, left axis) and -XDM (dashed lines, right axis) at various τ for the three distinct carbon atoms defined in Figure 1. Top panel: coronene, bottom panel: corannulene.

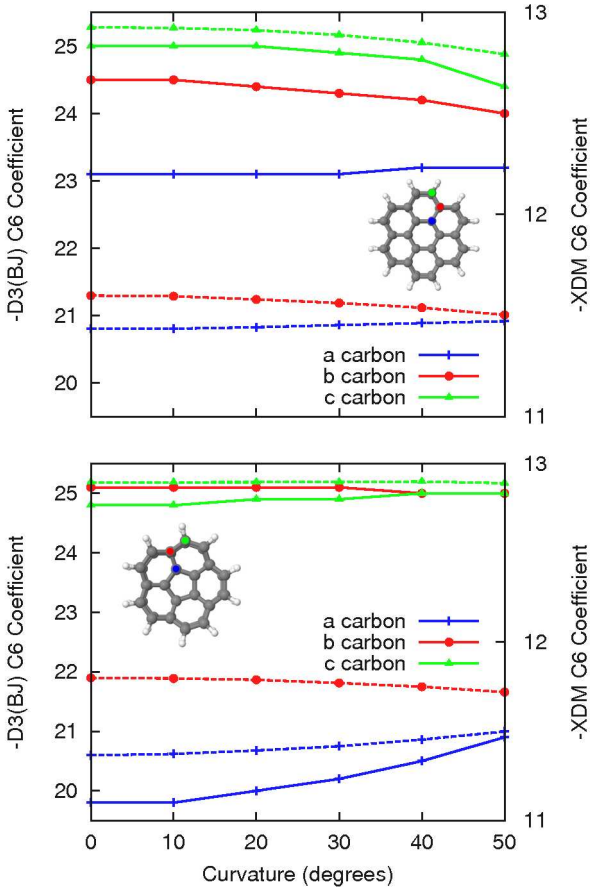

head-to-tail alignment of dipoles in concave-convex geometries. We expect that the careful elucidation of these various factors determining how π-π interactions vary with curvature will aid future studies that explore diverse chemical systems featuring such interactions.

CHAPTER III

RESOLVING THE THREE-BODY CONTRIBUTION TO THE LATTICE ENERGY OF CRYSTALLINE BENZENE: BENCHMARK RESULTS FROM COUPLED-CLUSTER THEORY

3.1 Abstract

Coupled-cluster theory including single, double, and

perturbative triple excitations [CCSD(T)] has been applied to trimers that appear in crystalline benzene in order to resolve discrepancies in the literature about the magnitude of non-additive three-body contributions to the lattice energy. The present results indicate a non-additive three-body contribution of 0.89 kcal mol^{-1}, or 7.2% of the revised lattice energy of -12.3 kcal mol^{-1}. For the trimers for which we were able to compute CCSD(T) energies, we obtain a sizable difference of 0.63 kcal mol^{-1} between the CCSD(T) and MP2 three-body contributions to the lattice energy, confirming that three-body dispersion dominates over three-body induction. Taking this difference as an estimate of three-body dispersion for the closer trimers, and adding an Axilrod-Teller-Muto estimate of 0.13 kcal mol^{-1} for long-range contributions yields an overall value of 0.76 kcal mol^{-1} for three-body dispersion, a significantly smaller value than in several recent studies.

3.2 Introduction

In 2008, we reported coupled-cluster computations aimed at obtaining an accurate theoretical value for the lattice energy of crystalline benzene[125]. Because benzene lacks any permanent charge or dipole moment that could lead to strong polarization

effects, a simple additive scheme was used to determine the total cohesive energy of the crystal from interaction energies of individual dimers. Based on previous work [154] showing good agreement between second-order perturbation theory (MP2) and coupled-cluster through triple excitations [122] [CCSD(T)] for three-body effects in a few prototypical benzene trimer configurations, the three-body effects were examined using MP2 and estimated to contribute only a minor amount.

Although MP2 will capture certain three-body effects, such as three-body induction, it cannot capture any three-body correlation effects, such as three-body dispersion, which can be significant in crystals for some trimer orientations[115]. Further, estimates of three-body lattice energy contributions using symmetry-adapted perturbation theory based on density-functional descriptions of the monomers [SAPT(DFT)] [172, 77, 63, 101, 119, 64, 116, 120] for crystalline benzene indicated that three-body effects contribute around 1.6 kcal mol^{-1} (or about 14% of the total lattice energy)[117]. More recent studies [167, 162] suggest that the majority of the three-body effects in crystalline benzene are due to three-body dispersion interactions, estimated to contribute 1.1 or 1.7 kcal mol^{-1} using the Axilrod-Teller-Muto expression (below).

Given increasing recent interest in high-accuracy computations of lattice energies (see, for example, Refs. [118, 21, 102, 39]), it would be valuable to have reliable estimates of three-body effects in systems like crystalline benzene. For this reason, we have performed counterpoise-corrected CCSD(T) computations to obtain accurate values for this contribution. We use the -135 °C crystal structure of Bacon, Curry, and Wilson[11], the same as that used in previous studies[125, 117].

3.3 Theoretical Methods

Three-body, triple-dipole dispersion between atoms A, B, and C may be modeled by the Axilrod-Teller-Muto expression [10, 103] as

$$V_{ABC} = D\frac{3\cos\gamma_{BAC}\cos\gamma_{ABC}\cos\gamma_{ACB}+1}{R_{AB}^3 R_{BC}^3 R_{AC}^3}, \tag{38}$$

where D is a positive constant proportional to the ionization energy of the atoms and the cube of their polarizability. Assuming a qualitatively similar behavior for the three-body dispersion between molecules, the R^{-9} decay behavior suggests that only closely interacting trimers can exhibit a non-negligible three-body dispersion term. To generate the relevant trimers in crystalline benzene, we first extracted a cube 30 Å on a side from the crystal lattice (coordinates provided in the ancillary materials). From this cube, we then selected all monomers whose centers of mass were within 15 Å of the central benzene, and then formed trimers by adding to the central benzene all unique pairs of selected monomers. The trimers were then sorted by increasing values of $R_{AB}^3 R_{BC}^3 R_{AC}^3$, where A, B, and C denote the three monomers. This first pass yielded 7750 (non-symmetry-unique) trimers. Fortunately, as discussed below, the difference in three-body energies computed by CCSD(T) and MP2 diminishes rapidly with increasing distance between the monomers; this suggests that for the more distant trimers, three-body interaction energies can be estimated using MP2 plus the Axilrod-Teller-Muto expression for the three-body dispersion terms neglected by MP2.

To determine the counterpoise corrected three-body interaction energies a modified Boys-Bernardi counterpoise correction developed by Hankins *et al.* was employed[58]. The non-additive three-body interaction is given by

$$\Delta^3 E_{ABC}^{ABC} = E_{ABC}^{ABC} - \sum_i E_i^{ABC} - \sum_{ij} \Delta^2 E_{ij}^{ABC}, \tag{39}$$

where the superscript ABC denotes a computation in the trimer basis (the basis of all molecules A, B, and C). E_i denotes the energy of each monomer, where i counts over the individual molecules in the trimer. The last term is determined by the equation

$$\Delta^2 E_{ij}^{ABC} = E_{ij}^{ABC} - E_i^{ABC} - E_j^{ABC}, \tag{40}$$

where the energies of all dimers and monomers are determined in the trimer (ABC) basis. The individual three-body interaction energies for individual trimers are all

computed according to this approach. When they are summed to obtain lattice energy contributions, the sum is divided by three to obtain a lattice energy in kcal per mole of benzene monomers (bearing in mind that in crystalline benzene, all the monomers are symmetry-equivalent).

To reduce computational cost, the aug-cc-pVDZ basis set [47, 84] is used. Previous results indicate that three-body effects require smaller basis sets for convergence than two-body terms[52]. To verify that three-body interaction energies can be accurately computed with this basis set, for one representative cyclic trimer we also employed the large aug-cc-pVTZ basis. The CCSD(T) benzene trimer computations (with no spatial symmetry) were difficult to perform, particularly for the one computation where we used an aug-cc-pVTZ basis set (1242 contracted basis functions). We utilized the Cray XT4 "Jaguar" supercomputer at Oak Ridge National Laboratory, running NWChem 5.1 on 6000 cores[30, 83]. While the *overall* trimer interaction energy cannot be accurately determined with the smaller aug-cc-pVDZ basis, excellent basis set convergence was observed for the non-additive three-body contribution (the focus of the present work), with a value of 0.0278 kcal mol^{-1} for aug-cc-pVDZ and 0.0274 for aug-cc-pVTZ, a difference of 1.5%.

Density fitting (DF)[171, 46, 48, 159, 124, 163, 143, 169] and Cholesky decomposition (CD)[19, 128, 88, 8] were used to reduce computational costs. These approaches reduce disk and memory requirements, and CPU costs in certain terms, by expressing the 4-index two-electron integrals as contractions of 3-index quantities. The aug-cc-pVDZ-JKFIT[163] was used for the DF-SCF procedure, and the aug-cc-pVDZ-MP2FIT[165] basis was used for the DF-MP2 computations. CCSD(T) computations utilized CD[107, 112, 9, 26, 43] with a tolerance of 10^{-4}, and they were also accelerated with Frozen Natural Orbitals[144, 87, 152, 153, 93, 44] (FNOs), truncating at a very conservative [44] natural orbital occupation of 10^{-7}. With this cutoff, the FNO approximation led to errors on the order of 10^{-4} kcal mol^{-1} for the

trimers with the largest three-body contributions. The combined FNO CD-CCSD(T) approach has been carefully benchmarked previously for non-covalent interactions, including three-body interactions in selected benzene trimers[43]. The MP2 and DF-MP2 computations were performed in Molpro 2010[3]. The FNO CD-CCSD(T) computations were performed with a development version of the PSI4 program[158] using a recently developed, multi-core FNO DF/CD-CCSD(T) module[43, 44]. We also obtained SCS-CCSD[149] and SCS(MI)-CCSD[114] values [as a byproduct of the CCSD(T) computations] to see how well these methods match CCSD(T) three-body energies, as recent work [42] suggests that they should be rather accurate for this purpose.

3.4 Results and Discussion

Previous work [154] has shown that cyclic trimers have significantly greater three-body contributions than alternating T-shaped configurations or multiply-stacked sandwich configurations. Therefore, one might expect that the cyclic, all-nearest-neighbor

Figure 9: Two configurations of the benzene trimer extracted from the crystal structure. The trimers shown above have three-body interaction energies of -0.0340 and 0.1339 kcal mol^{-1} for configurations (a) and (b) respectively.

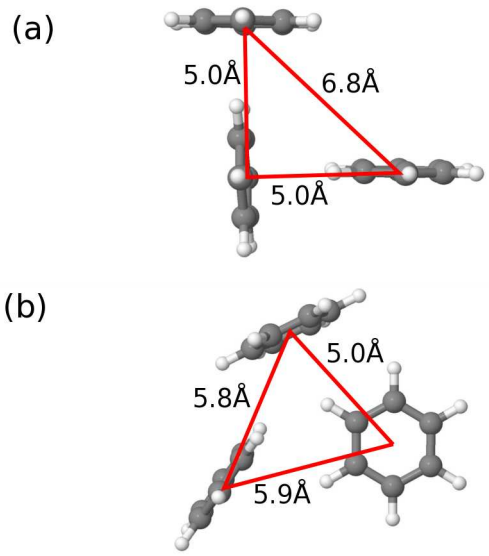

trimers in crystalline benzene would make the largest three-body contributions. Figure 9 shows two orientations of the benzene trimer from the crystal lattice. Trimer (a) in Figure 9 is the trimer with the smallest product $R^3_{AB}R^3_{BC}R^3_{AC}$ in the crystal lattice and trimer (b) has the largest magnitude for the three-body interaction (0.1339 kcal mol^{-1}).

Figure 10: Three-body interaction energy (left axis) of trimers in crystalline benzene using MP2, DF-MP2 and CCSD(T) with an aug-cc-pVDZ basis set (red, blue, and black lines). On the right axis is the error of DF-MP2 relative to CCSD(T) (green line). Horizontal line segments denote degenerate trimers in the crystal.

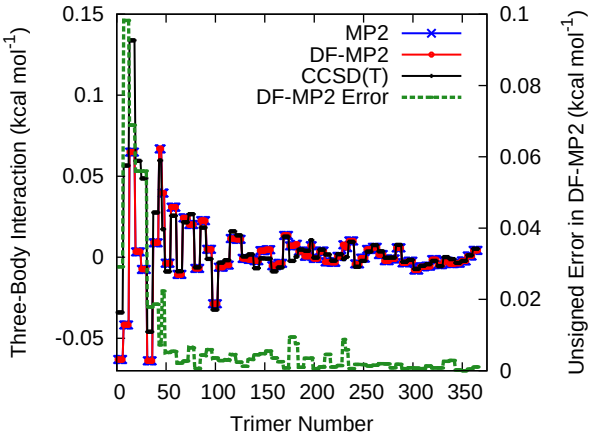

Figure 10 shows the individual trimer three-body interactions for MP2, DF-MP2, and CCSD(T) on the left axis, and the difference between CCSD(T) and DF-MP2 on the right axis. For the 366 closest trimers (including degeneracies), there is no difference between MP2 and DF-MP2 three-body interaction energies that is greater than 0.0002 kcal mol^{-1}, justifying the use of the DF approximation.

The difference between MP2 and CCSD(T) is as large as 0.1 kcal mol^{-1} for the first few trimers, but it decays very quickly. For trimers 51-366, the maximum unsigned error, mean unsigned error, and mean signed error are 0.0094, 0.0026, -0.0002 kcal mol^{-1}, respectively. Figure 11 presents analogous results for SCS-CCSD and SCS(MI)-CCSD. For the first 366 trimers, SCS-CCSD and SCS(MI)-CCSD perform very well, with mean unsigned errors of 0.0008 and 0.0007 kcal mol^{-1} respectively.

Neither method incurs an error of more than 0.006 kcal mol^{-1} error for a single trimer interaction. Unlike MP2, the errors for SCS-CCSD and SCS(MI)-CCSD occur in mostly the same direction, as the mean signed errors (-0.0005 and -0.0006 kcal mol^{-1}) are almost as large in magnitude as the mean unsigned errors.

The small maximum and mean errors of MP2 vs. CCSD(T) beyond the first 50 trimers are not necessarily indicative that three-body dispersion terms have become negligible at the intermolecular distances seen in these trimers. Indeed, if one compares CCSD(T) and MP2 three-body energies for individual trimers in this range, they often exhibit large relative errors. The absolute errors are small primarily because the three-body interaction energies themselves are quite small in this range; the average CCSD(T) three-body energy for trimers 51-366 is just 0.0063 kcal mol^{-1}. In addition, it seems fortuitous that the MP2 errors are mostly random for trimers 51-366 (as evidenced by the much smaller magnitude of the mean error compared

Figure 11: Three-body interaction energy (left axis) of benzene trimers in crystalline benzene using SCS-CCSD, SCS(MI)-CCSD, and CCSD(T) with an aug-cc-pVDZ basis set (solid blue, green, and black lines; differences are so small that the lines are nearly coincident). On the right axis is the error of SCS-CCSD and SCS(MI)-CCSD relative to CCSD(T) (dashed lines). Horizontal line segments denote degenerate trimers in the crystal.

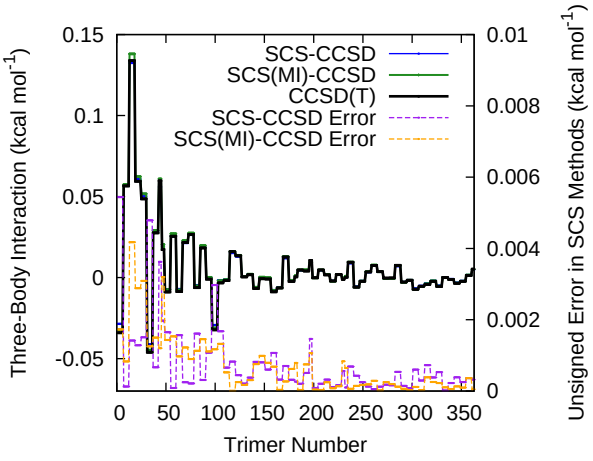

to the mean unsigned error). Unfortunately such good error cancellation will not necessarily hold for further trimers.

Figure 12: Cumulative contribution of the three-body interaction energy to the lattice energy of crystalline benzene, summed through trimer N. Results for SCS-CCSD, SCS(MI)-CCSD, and CCSD(T) beyond trimer 366 are approximated by DF-MP2 values (see text).

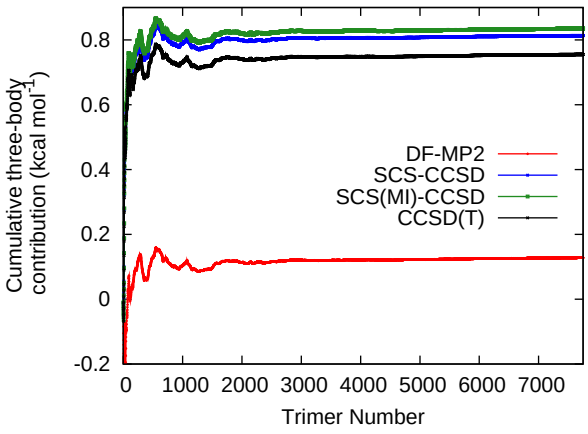

Figure 12 displays the cumulative three-body contribution to the lattice energy computed using DF-MP2 for all 7750 trimers considered. The overall cumulative DF-MP2 three-body lattice energy seems well converged at 0.13 kcal mol^{-1} by the time 3,000 trimers have been included. This represents a rather small correction of 0.06 kcal mol^{-1} to the DF-MP2 result using the first 366 trimers. If we use the more computationally tractable DF-MP2 results in lieu of the much more costly coupled-cluster results for trimers beyond 366, we obtain the estimated SCS-CCSD, SCS(MI)-CCSD, and CCSD(T) curves shown. The CCSD(T) result converges to approximately 0.76 kcal mol^{-1}, a difference of 0.63 kcal mol^{-1} from the DF-MP2 result. Although SCS-CCSD and SCS(MI)-CCSD perform very well for the three-body interaction energy of any particular trimer, the small systematic errors (see above) eventually add up, and the overall SCS-CCSD and SCS(MI)-CCSD three-body contributions (again using DF-MP2 beyond the first 366 trimers) converge to approximately 0.81 and 0.83 kcal mol^{-1}, respectively, slightly above the 0.76 kcal mol^{-1} CCSD(T) result.

Of course, using DF-MP2 for the more distant trimers means we will still be missing an estimate of long-range three-body dispersion. The data above clearly

indicate that the three-body dispersion per trimer is quite small by the time we reach trimer 366, the last trimer for which we have explicit CCSD(T) values. On the other hand, there are a large number of remaining trimers, so the residual three-body dispersion could be significant. We estimate this contribution using the Axilrod-Teller-Muto expression in Eq. (38), using a D coefficient of 82657.65 a.u. from previous estimations using SAPT(DFT)[117]. This value converges asymptotically to 0.13 kcal mol^{-1} once the three-body dispersion from trimers 1-366, already accounted for by CCSD(T), is subtracted. Although the Axilrod-Teller-Muto formula may not be reliable for the closer trimers [where we are using CCSD(T) values instead] it should be reliable for the purposes of this asymptotic estimate. As a check of its suitability, we computed the Axilrod-Teller-Muto three-body dispersion for the most distant 50 trimers for which we have CCSD(T) data. Assuming the difference between CCSD(T) and MP2 is primarily three-body dispersion, we obtain a lattice energy contribution of 0.0125 kcal mol^{-1} from the Axilrod-Teller-Muto expression and 0.0127 kcal mol^{-1} from [CCSD(T)-MP2], a very satisfactory agreement. We also examined asymptotic induction estimates for trimers beyond the 7750 treated by DF-MP2, but the magnitude of this contribution was below 0.005 kcal mol^{-1}.

Our previous work[125] reported a two-body lattice energy of -56.4 kJ mol^{-1} but contained an error in the degeneracy of dimers G and H. Both dimers G and H should have been classified to have a degeneracy of 4. They were mistakenly labeled with a degeneracy of 8 due to there being two dimers with matching center of mass distances but with different orientations. Two-body interaction energies for the additional dimers are -0.25 kJ mol^{-1} (G$'$) and -0.17 kJ mol^{-1} (H$'$). Correcting for this error gives us a lattice energy of -55.3 kJ mol^{-1}. If we add the present estimate of 0.89 kcal mol^{-1} (3.7 kJ mol^{-1}) for the three-body contribution, we obtain a total revised lattice energy of -51.6 kJ mol^{-1}. If we use our earlier estimate of 7.0 kJ mol^{-1} for the enthalpy correction to go from a lattice energy to an experimentally measured sublimation

energy[125], we obtain a sublimation energy of -44.6 kJ mol^{-1}. This remains in the -43 to -47 kJ mol^{-1} experimental range which we favored in our earlier publication [125] due to several values being reported in this range[34, 4]. The lattice energy of -51.6 kJ mol^{-1} also compares well to Beran's analysis [21] of the experimental data, deducing lattice energies of -52 $\pm$ 3 kJ mol^{-1} based on the experimental sublimation energies. Nevertheless, we expect the magnitude of the lattice energy to be slightly underestimated due to the neglect of two-body interactions beyond 9.4 Å in our earlier study[125].

The present estimate of 0.89 kcal mol^{-1} for the three-body contribution is 7.2% of the total revised lattice energy of -12.33 kcal mol^{-1}. We may estimate the total three-body dispersion contribution as 0.63 kcal mol^{-1} [the difference between CCSD(T) and MP2 for the first 366 trimers] plus 0.13 kcal mol^{-1} for the Axilrod-Teller-Muto estimate of the long-range contribution, yielding a total of 0.76 kcal mol^{-1}, or 6.2% of the total lattice energy.

Several groups have recently estimated the three-body dispersion in the benzene crystal using various approximations. Wen and Beran estimated that three-body dispersion contributes 0.92 kcal mol^{-1} using an *ab initio* force field (AIFF)[167]. Using SAPT(DFT) Podeszwa *et al.*[117] estimated the three-body dispersion contribution to be 1.56 kcal mol^{-1} (the total three-body contribution was 1.64 kcal mol^{-1}). Von Lilienfeld *et al.*[162] have also estimated the three-body dispersion in the benzene crystal to be 1.67 kcal mol^{-1} using frequency-dependent polarizabilities to obtain C_9 coefficients. These studies all overestimate the three-body dispersion compared to our value of 0.76 kcal mol^{-1} for three-body dispersion (or 0.89 kcal mol^{-1} for the overall three-body contribution). In the case of the SAPT(DFT) results, the authors were aware their approach tended to overestimate three-body contributions[117]. However, their estimate of the error in the three-body term (about 1 kJ mol^{-1} or 0.24 kcal mol^{-1}) is low compared to the 0.75 kcal mol^{-1} difference between their three-body

value and the present one.

3.5 Conclusions

Our coupled-cluster results confirm that three-body dispersion effects cannot be neglected in accurate computations of the lattice energy of benzene[115, 167, 162]. Three-body dispersion effects may also contribute substantially to the lattice energy of other aromatic hydrocarbons or π-conjugated materials. As these effects are not commonly included in widely-used density functional theory (DFT) methods, it seems important to further explore ways of capturing them using models that can be added to DFT such as the many-body dispersion model of Tkatchenko *et al.*[155], or atom-based triple dipole Axilrod-Teller-Muto terms using C_9 coefficients obtained by geometric means of C_6 coefficients[55], or Casimir-Polder integration of frequency-dependent polarizabilities[167, 162]. However, these contributions must be evaluated with care, as existing results from the literature appear to overestimate three-body dispersion in crystalline benzene by as much as a factor of 2.

CHAPTER IV

COUNTER-ION AND SUBSTRATE EFFECTS ON BARRIER HEIGHTS OF THE HYDROLYTIC KINETIC RESOLUTION OF TERMINAL EPOXIDES CATALYZED BY CO(III)-SALEN

4.1 Abstract

Density functional theory (DFT) has been applied to the proposed rate-limiting step of the hydrolytic kinetic resolution (HKR) of terminal epoxides as catalyzed by Co-salen-X (X = counter-ion) in order to resolve some questions surrounding the mechanism. The present results indicate that the bimetallic mechanism proposed by Jacobsen shows non-additive, cooperative catalysis with a larger reduction in barrier height than the sum of the barrier height reductions from the two monometallic reaction pathways. We computed barrier heights for the reaction using several counter-ions (chloride, acetate, tosylate, and hydroxide). For the three counter-ions that are experimentally active (chloride, acetate, and tosylate) the barrier heights are 35, 38, and 34 kJ mol^{-1}, respectively, while for hydroxide it is 48 kJ mol^{-1}. The similarity of the barrier heights for chloride, acetate and tosylate is in agreement with their similar peak reaction rates. Based on these findings, the fact that Co-salen-X with counter-ions leads to rather different overall reaction profiles suggests that they have quite different rates of reaction with epoxide to form the activated Co-salen-OH required for the bimetallic mechanism. Co-salen-OH is inactive as the sole catalyst for HKR, and this inactivity is ascribed to its larger barrier height for the ring-opening

step, rather than to any inability to activate epoxide. Barrier heights were also computed using 1-hexene oxide, propylene oxide and epichlorohydrin; propylene oxide and 1-hexene oxide have similar barrier heights, 35.5 and 33.2 kJ mol^{-1} respectively, and epichlorohydrin has a significantly lower barrier height of 18.8 kJ mol^{-1}, which is qualitatively consistent with experiments showing faster reactions for epichlorohydrin than propylene oxide when catalyzed by Co-salen-OAc.

4.2 Introduction

Metal-salen catalysts are widely used in enantioselective reactions including epoxide ring-opening[156, 175, 161], nitroaldol reactions[92], and conjugate additions[96]. The hydrolytic kinetic resolution (HKR)[86] of terminal epoxides has garnered much attention due to the production of useful chiral epoxide and diol building blocks for numerous reactions[131, 91, 129]. First developed by Jacobsen, HKR of epoxides catalyzed by Co-salen-X (X = nucleophilic counter-ion like Cl^-, OAc^-, etc.) was shown to follow a second-order, cooperative bimetallic pathway[156, 104, 71, 37, 72] which agrees with experiments on other metal-salen complexes utilized for ring-opening reactions[99, 57, 59]. In the reaction mechanism proposed[104], one Co-salen initially undergoes a counter-ion exchange, trading its X for OH^-. A second Co-salen (with the initial counter-ion, X) activates an epoxide. The two Co-salen complexes then react (the -OH of one attacking the epoxide on the other), and the HKR of epoxides proceeds quickly and in great enantiomeric excess, as shown in Figure 13. Ring opening via the bimetallic transition state is proposed to be the rate limiting step of the HKR reaction of terminal epoxides with water/hydroxide[104]. This reaction can proceed through an attack at either the secondary or tertiary carbon in the terminal epoxide ring, as seen in Figure 13.

There remain numerous unanswered questions about these reactions, including the origin of rate differences among substrates, the source of enantioselectivity, the

Figure 13: Reaction Mechanism of HKR of terminal epoxides using Co-salen catalysts

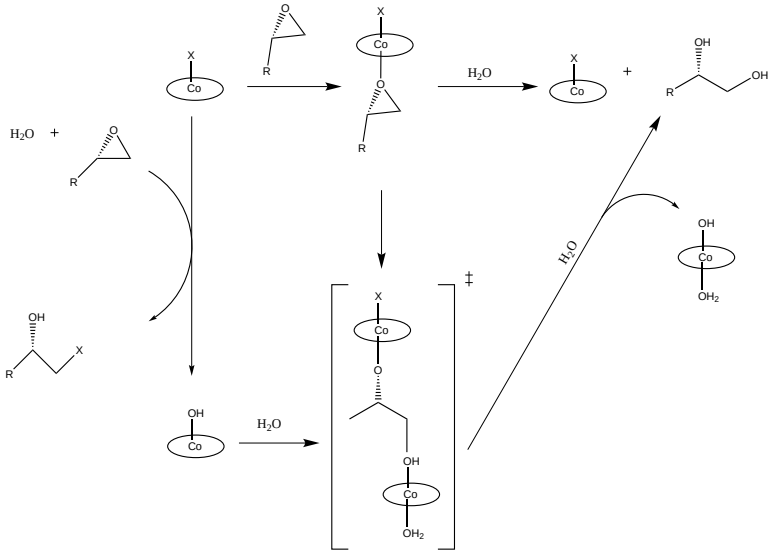

inactivity of Co-salen-OH without the presence of another Co-salen molecule with a different counter-ion, and the effect of different counter-ions on reactivity. A previous investigation[146] using Density Functional Theory (DFT) examined the rate-determining step and showed how the reaction barrier is lowered through the use of two catalysts, one to activate the epoxide and one to activate the nucleophile. The previous study[146] used only a single density functional (B3LYP)[14], and given prior work showing substantial sensitivity of metal salens to the choice of functional[135, 136, 150, 151], it is not clear if the results would change dramatically if another functional was employed. Here we perform a comparison of three density functionals for barrier heights using 0, 1, or 2 catalysts in the transition state; comparing the three functionals allows us to approximately gauge the error bars for DFT energetics of this reaction. We also include a treatment of long-range London dispersion forces using DFT-D; these corrections can be important in larger systems such as those studied here[82, 6]. We then use these methods to investigate counter-ion and substrate effects on Co-salen catalysis of HKR.

4.3 Computational Methods

All DFT computations were performed in the Q-CHEM package[137]. The B3LYP (Ref. [14]), BP86 (Refs. [13] and [109]), and M05-2X (Ref. [176]) density functionals were used for computations of the transition state barriers and geometries. Long-range dispersion interactions were computed using the DFTD3 program[55] of Grimme; both the -D2 and -D3 schemes were tested, but these corrections had little effect on computed barriers (see below). Atomic charges were derived in Jaguar[23] from a fit of the molecular electrostatic potential (ESP)[173, 35] that has been constrained to reproduce the total charge and quantum mechanical dipole moment.

To investigate the epoxide ring opening reaction, DFT transition state optimizations were performed to obtain the transition state geometry, followed by frequency and intrinsic reaction coordinate (IRC)[51] computations. The frequency computation is used to verify that a transition state was found (by having only one imaginary vibrational frequency) and also as a necessary initial step for the IRC computation. The IRC computation uses the computed Hessian and performs a steepest descent optimization along the imaginary mode to move the computed transition state towards the reactants and products along the minimum-energy path, verifying that the transition state connects the correct reactants (epoxide and water/hydroxide) to the diol product. Lastly, the reactants' end of the IRC computation is optimized to obtain the pre-reactive complex needed to obtain the barrier height of the reaction. The Los Alamos National Laboratory 2 double-ζ (LANL2DZ)[60] basis set and corresponding effective core potentials (ECPs) were used in conjunction with a grid of 100 radial shells and 302 angular points.

4.4 Results and Discussion

4.4.1 Transition State Geometry and Barriers

Figure 14 shows reaction barriers for the rate-limiting step of epoxide HKR computed by B3LYP, BP86, and M05-2X with the LANL2DZ basis set and corresponding ECPs. The first row (a) shows the uncatalyzed reaction, rows (b), (c), and (e) show different ways that the reaction can be catalyzed by a single Co-salen, and rows (d) and (f) show the bicatalyzed reaction. The top three reactions have a non-activated epoxide, while the bottom three show barriers for epoxides activated by a Co-salen. The left and right sides of Figure 14 show attack at the tertiary versus the secondary carbon in the epoxide ring. The Co-salen entity is represented in the figure as Co with an oval around it. The representative oval always includes the counter-ion, which is chloride for Co-salen when binding a water or epoxide molecule. Alternatively, when Co-salen is shown bound to -OH there is an implied water molecule for the sixth coordination spot in the Co-salen structure. Our B3LYP results for the reactions in Figure 14 are in agreement with those reported by Sun et al.[146]

First, we examine how the choice of functional affects the barrier heights. Differences in barrier height energies between the the functionals considered can be substantial, with typical differences of several tens of kJ mol^{-1}. Differences tend to be larger when the barrier heights are larger, and reaction a(right) exhibits the maximum difference observed between density functionals, 64 kJ mol^{-1} between BP86 and M05-2X. The differences in barrier heights between functionals tend to be in the range of 15-35%, so we expect roughly this level of accuracy in the barrier heights.

Fortunately, the three functionals studied studied show similar trends in the energetic ordering of the barrier heights for the different reactions considered. For example, B3LYP and BP86 both show that for rows (a)-(c) the left transition state barrier is always lower than that of the right transition state, implying that for rows (a)-(c) attack at the tertiary carbon is favored compared to attack at the secondary

Figure 14: Transition state barrier heights for HKR of terminal epoxides using 0, 1, or 2 Co-salen catalysts reported as B3LYP/LANL2DZ, BP86/LANL2DZ, M05-2X/LANL2DZ under each arrow in kJ mol^{-1}. Reactions are labeled (a)–(f) in accordance with Sun et al. (Ref. [146].

)

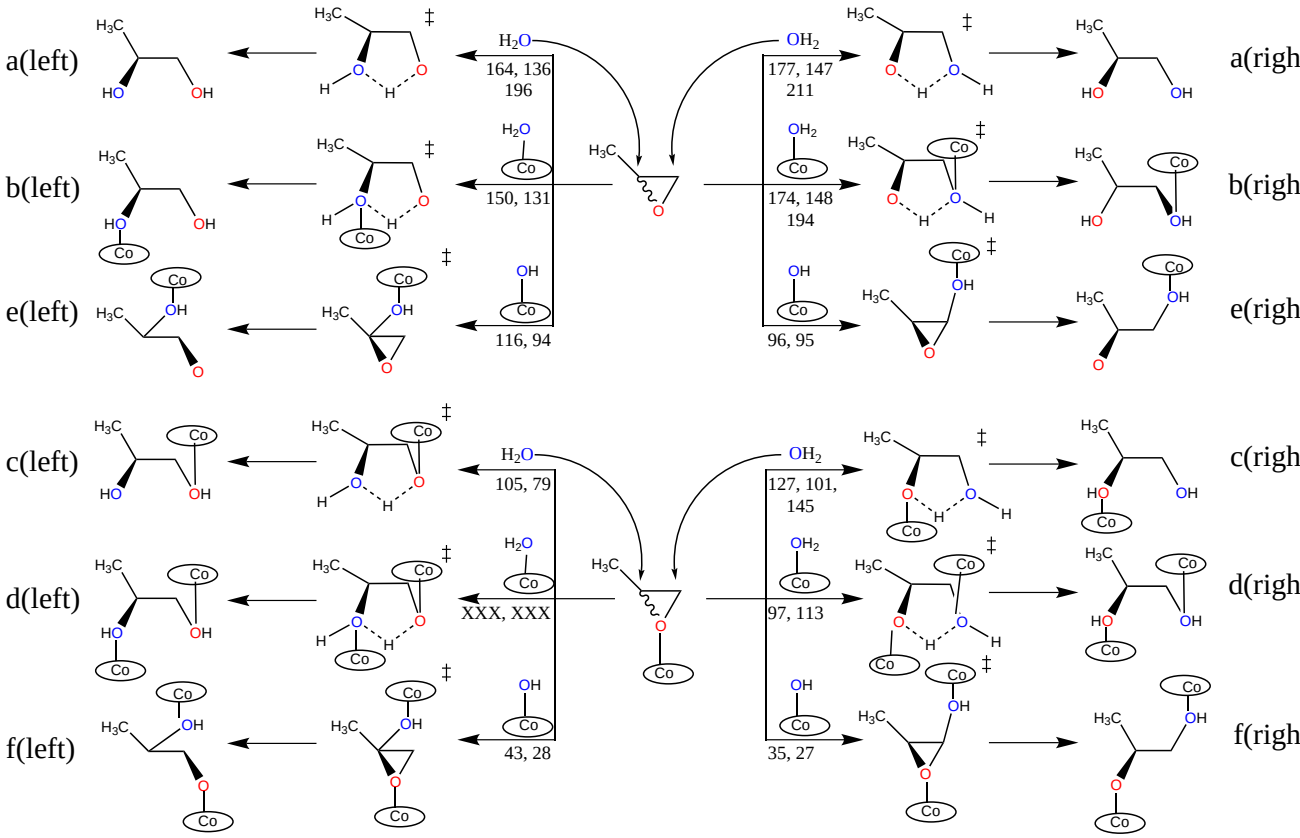

carbon. Similarly, for rows (e) and (f) we see that attack at the secondary carbon is favored in both B3LYP and BP86. We also see that there seem to be three clusters of barrier heights regardless of the functional chosen: rows (a) and (b) have the highest barrier heights, and rows (c), (d), and (e) have barrier heights that are below rows (a) and (b) but are much greater than the barrier heights in row (f). Due to substantial computational expense we did not obtain barrier heights for all of the reactions using M05-2X, but where available the M05-2X barrier heights follow the general trends discussed above. All the barrier heights for M05-2X are greater than those found with B3LYP. Similarly, all but one of the barrier heights [d(right)] for B3LYP are

greater in magnitude than those found with BP86.

Row (a) in Figure 14 shows the uncatalyzed HKR reaction. The barriers for attack at the secondary carbon are 177, 147, and 211 kJ mol^{-1} for B3LYP, BP86, and M05-2X. The corresponding barriers for attack at the tertiary carbon are each lower at 164, 136, and 196 kJ mol^{-1}, respectively. BP86 gives lower barrier heights than B3LYP, which gives lower barrier heights than M05-2X. This trend continues for almost all barriers reported throughout the discussion, with the exception of d(right) which has a BP86 barrier of 113 kJ mol^{-1} versus 97 kJ mol^{-1} for B3LYP.

Rows (b) and (e) depict HKR with an activated nucleophile. Row (b) shows water coordinated by Co-salen as the activated nucleophile while row (e) has a hydroxide coordinated to Co-salen as the activated nucleophile. The reaction barriers for b(right) are 174, 148, and 194 kJ mol^{-1} for B3LYP, BP86, and M05-2X, which are about the same or slightly lower than the uncatalyzed reaction a(right). Similarly, b(left) shows barriers of 150 and 131 kJ mol^{-1} for B3LYP and BP86, which are 5–10 kJ mol^{-1} lower than the uncatalyzed reaction. Also consistent with the uncatalyzed reaction, row (b) shows that attack at the tertiary carbon in the epoxide is favored. Row (e) shows HKR with -OH as the nucleophile instead of water. In this case, the Co-salen complex has a water in the sixth coordination spot which is on the opposite side of the Co-salen complex from the -OH group. Reaction e(right) has Co-salen-OH attacking the secondary carbon in the epoxide ring, with barriers of 96 and 95 kJ mol^{-1} for B3LYP and BP86, respectively. Similarly, e(left) features transition state barriers of 116 and 94 kJ mol^{-1} for B3LYP and BP86, all of which are 42–81 kJ mol^{-1} lower than the uncatalyzed reaction, showing that hydroxide is a much better nucleophile for HKR of epoxides than water. Rows (a), (b), and (c), which have water as the nucleophile, show that attack at the tertiary carbon is favored while rows (e) and (f) with a hydroxide nucleophile show attack at the secondary carbon is favored.

Row (c) shows HKR with an activated epoxide and an unactivated nucleophile.

Activating the epoxide by coordination to Co-salen-Cl reduces the barrier height for both c(left) and c(right) when compared to the uncatalyzed a(left) and a(right) reactions by 46–59 kJ mol^{-1}. This is a much larger effect than just activating water as a nucleophile (through coordination with Co-salen-Cl), which only provided reductions of 5–10 kJ mol^{-1}, and it is similar to the 42–81 kJ mol^{-1} lowering discussed above when using Co-salen activated OH^- as the nucleophile.

Rows (d) and (f) show the HKR of epoxides where both the epoxide and nucleophile are each activated by a Co-salen molecule. Row (d) represents a combination of rows (b) and (c) as it has an activated epoxide from row (c) and activated water molecule from row (b). This combination of two catalysts brings the reaction barrier down to 97 kJ mol^{-1} for d(right) from 177 kJ mol^{-1} for the uncatalyzed reaction a(right). It is also lower than either rows (b) or (c) which were 174 and 127 kJ mol^{-1} respectively. The activation of the water nucleophile lowers the barrier by 2 kJ mol^{-1} and the activation of the epoxide lowers the barrier by 50 kJ mol^{-1} which when combined is less than the 80 kJ mol^{-1} reduction in barrier height observed when both are activated (d). This shows that having the two catalysts working in cooperation leads to non-additive effects in lowering the barrier height. Unfortunately we were unable to find the d(left) transition state despite numerous attempts.

Row (f) is a combination of rows (c) and (e) which contains activated epoxide and an activated hydroxide ion as the nucleophile. For the bimetallic transition state proposed by Jacobsen, we see that the reaction barriers drop to 35–43 kJ mol^{-1} for B3LYP, compared to 96–174 kJ mol^{-1} for the monometallic reactions. In the bimetallic transition states of row (f), there are geometric changes where the breaking C-O bond length is 0.2–0.3Å shorter than in rows (a) through (e), indicating an earlier transition state along the reaction coordinate.

Long-range dispersion corrections (-D) were computed and for the transition state and pre-reactive complexes. The barrier heights change by no more than 5 kJ mol^{-1}

in either direction. These effects are on the same order or less than the expected error in our B3LYP/LANL2DZ computational methodology and thus for this reaction they do not appear to be not computationally significant.

4.4.2 Counter-ion Effects

The HKR mechanism proposed by Jacobsen in Figure 13 encompasses two pathways: one monometallic, first-order in Co-salen, examined in Figure 14 (rows (b), (c), and (e)) and one bimetallic, second-order in Co-salen, examined in Figure 14 (rows (d) and (f)). Experimentally, X=Cl^- and AcO^- are highly active (the former only initially, due to rapid counter-ion exchange with the epoxide, later depriving the reaction of the activated epoxide, species Co-salen-Cl-epoxide) but X=OH^- is far less active (based on experiments using X=Cl^- and taking measurements after the rapid induction period, when presumably all Co-salen-Cl species have been converted to Co-salen-OH.)[105] Additionally, experiments with a 50:50 mixture of X=Cl^- and SbF_6^- proceed very rapidly, the former presumably converting entirely to the X=OH^- species and the latter activating epoxide[104].

Of particular interest is examining why Co-salen-OH is unable to catalyze HKR as the sole Co-salen-X species. Based on experimental evidence as well our computations above, Co-salen-OH seems very effective as an activated nucleophile. Hence, the inactivity of Co-salen-OH by itself may indicate its inability to activate epoxide. One might suppose that Co-salen-OH is less effective in binding to epoxide due to a more covalent Co bond, making Co less effective as a Lewis acid. We investigated this possibility by computing atomic charges on cobalt in the Co-salen-X complex but did not find a revealing trend, as X=Cl^-, OAc^-, OH^-, SbF_6^- or none (cation) give similar Co charges in the range 1.04–1.22 e^-. Similarly, the gas-phase binding strengths to epoxide of the stable complexes (Cl^-: −82.8; AcO^-: −87.9 kJ/mol) differ negligibly from from the *in situ* species (OH^-: −82.0 kJ/mol). One of the clearest signs of

epoxide activation is a shift in charge distribution among the atoms forming the three-membered epoxide ring. Counter-ions considered (X=Cl^-, OAc^-, OH^-, SbF_6^-) increase the magnitude of charge: secondary epoxide carbon from −0.16 isolated to −0.16–−0.19 in complex, and tertiary epoxide carbon from +0.14 isolated to +0.21–+0.26 in complex. But it is interesting to note that for this property, and indeed essentially all binding energies, charges, and structural properties considered in Table 2, the value for Co-salen-OH is approximately equal to or between its X=Cl^- and OAc^- counterparts. Exceptions are in the binding of the counter-ion, where hydroxide is bound more than 200 kJ/mol more strongly than any other, and structurally where the epoxide in Co-salen-OH-epoxide is bound somewhat more loosely (2.09 Å) than X=Cl^- or AcO^- ($\approx$ 2.05Å). Nevertheless, our comparison of Co-salen-X and their complexes with epoxide show no clear reason why X=OH^- would be less effective at activating epoxide, indicating that the inactivity of Co-salen-OH is due to some other reason, perhaps due to a higher kinetic barrier for the bimetallic ring-opening reaction. We carried out a transition state optimization for the bimetallic reaction (Figure 14 f(right)) in which the chloride counter-ion was replaced with a hydroxide counter-ion. The barrier height for this transition state (confirmed via IRC analysis) is 48.5 kJ mol^{-1}. This barrier is higher by 11 kJ mol^{-1} or greater when compared to the other three counter-ions studied. HKR is normally run at room temperature (25°C). If we use the Arrhenius equation at this temperature, assuming that $\Delta G \approx \Delta G$ and that the pre-exponential factors are approximately the same, we see that this 11 kJ mol^{-1} difference would result in a reaction rate that is ≈1% as fast, which would be considered essentially inactive compared to the other three counter-ions.

We now move from considering the particular case of Co-salen-OH to a more general comparison of counter-ions. We examined counter-ion trends for the Co-salen-X-epoxide complex, particularly the differences between the nucleophilic anions X=Cl^- and AcO^- that vigorously catalyze the HKR reaction discussed in this work

Table 2: Effects of counter-ion identity upon electronic characteristics, ligand binding strength, charge distribution, and geometry of the Co(III)-salen-epoxide-counter-ion complex as derived from the B3LYP/LANL2DZ level of theory.

	Nucleophilic			**Non-nucleophilic**	
Property	**Cl^-**	**AcO^-**	**HO^-**	**BF_4^-**	**SbF_6^-**
multiplicity[1]	1	1	1	3	3
Interaction Energy (kJ/mol; gas-phase)					
epoxide	-82.8	-87.9	-82.0	-58.6	-64.0
counter-ion	-520.9	-557.7	-817.6	-359.0	-346.9
Charge (e)					
epoxide ligand	+0.17	+0.08	+0.08	+0.02	+0.05
Co-salen	+0.22	+0.50	+0.33	+0.75	+0.73
counter-ion	-0.39	-0.58	-0.41	-0.77	-0.78
O (epoxide)	-0.26	-0.36	-0.33	-0.37	-0.34
Co(III)	+0.52	+1.20	+0.96	+1.10	+1.07
Co(III)[2]	+1.04	+1.22	+1.18	+1.12	+1.12
Structure (Å)					
Co$\cdots$O (epoxide)	2.05	2.04	2.09	2.27	2.27
Co$\cdots$counter-ion[3]	2.29	1.89	1.85	2.19	2.18

[1] Lowest energy species, singlet or triplet, for which all subsequent quantities tabulated

[2] Charge on cobalt for species without epoxide: neutral, pentavalent, triplet multiplicity

[3] Distance between cobalt and the nearest counter-ion atom, not comparable between counter-ions

through the bimetallic route, and non-nucleophilic anions BF_4^- and SbF_6^- that catalyze asymmetric ring opening (ARO) in alcohols but are less effective (restricted to monometallic pathway) for HKR, presumably because they are unable to form the activated OH species Co-salen-OH through counter-ion addition to epoxide. Considering solely the monometallic route in ARO, experimentally the non-nucleophilic counter-ions perform well while X=Cl^- shows significantly reduced activity. Computationally, B3LYP/LANL2DZ finds Co-salen-X-epoxide species to have a triplet ground state when X is a non-nucleophilic counter-ion, whereas nucleophilic counter-ions favor a singlet state, as summarized in Table 2. Since singlet forms of a given Co-salen-X-epoxide system consistently bind both the epoxide and counter-ion more strongly than triplets, a comparison of ground state species unsurprisingly shows more loosely bound ligands for non-nucleophilic species. This is manifest both in interaction energies, which for non-nucleophilic are approximately 65–80% the value of nucleophilic complexes, and in geometry, where the epoxide ligand in non-nucleophilic species is situated ≈ 0.15Å more distant than in nucleophilic structures. Compared to the bare gas-phase data in 2, application of a -D3 dispersion correction strengthened epoxide binding energies by a nearly uniform 40 kJ/mol. Similarly, including a solvent (methanol) correction weakens binding by 20–40 kJ/mol, such that trendwise the reported gas-phase interaction energies are unchanged. The propensity for non-nucleophilic systems to maintain a measure of detachment among the Co-salen, epoxide, and counter-ion components is also reflected in the internal charge distribution. In nucleophilic complexes, the Co-salen bears a modest charge of +0.22–+0.50 magnitude, with the nominally neutral epoxide at $\approx$ +0.1–+0.2. In contrast, non-nucleophilic systems are similar to the sans counter-ion species in that Co-salen bears a substantial portion of its nominal +1 charge ($\approx$ +0.7), being fully balanced by the negative charge on the counter-ion, and leaving the epoxide ligand largely neutral (+0.02–+0.05), though with a sizable polarization toward its reactive oxygen

atom. Thus, nucleophilic counter-ions impart to a Co(III)-salen complex a tightly bound, charge blended system in comparison to non-nucleophilic that support independence among metal-salen and ligand components with regard to distance, charge, and interaction strength. Hence, the electronic structure of Co-salen-X and their binding energies to epoxide do show significant differences between nucleophilic and non-nucleophilic counter-ions, consistent with the rather different reactivity of nucleophilic vs. non-nucleophilic counter-ions for ARO. However, one might have supposed that stronger binding to epoxide would lead to more effective activation of epoxide and hence faster reactions. The binding energies of Co-salen-X show the opposite trend, indicating that in fact Co-salen-X epoxide binding energies do not correlate well with experimental reaction rates for ARO. This lack of correlation between epoxide binding energies of Co-salen-X and reaction rates is also consistent with our discussion above regarding the inactivity of Co-salen-OH when it is the sole species in HKR, even though it has very similar epoxide binding energies as X=Cl^- and X=OAc^-, which are active.

Nielsen et al.[105] reported rates for the HKR of epoxyhexanes using Co-salen-X with the counter-ions Cl^-, OAc^-, and OTs^-. The reaction profiles for the three counter-ions are diverse in shape. For chloride, the reaction rate peaks quickly, presumably due to very fast counter-ion exchange of Co-salen-Cl to produce Co-salen-OH as required for the reaction to proceed through the bimetallic transition state. Both acetate and tosylate show longer induction periods, not having peak reaction rates until 40–50% conversion of water. While the profiles show very different induction periods, the peak reaction rates are quite similar for all three counter-ions, as shown in Table 3: 18×10^4 M s^{-1}, 12×10^4 M s^{-1}, and 21×10^4 M s^{-1} for chloride, acetate and tosylate respectively. We obtain transition state barriers of 35, 38, and 34 kJ mol^{-1} for the three counter-ions using the B3LYP functional which shows good agreement with the reported peak reaction rates being very close to each other. The similarity

Table 3: Experimental Reaction Rates (Ref. [105]) vs. Computed Barrier Heights (B3LYP/LANL2DZ) for different counter-ions in the HKR of terminal epoxides. The experimental reaction rates are reported with epoxyhexane and the computational barriers are using propylene oxide.

Counter-ion	Reaction Rate (10^4 M s^{-1})	Barrier Height (kJ mol^{-1})
Chloride	18	35
Acetate	12	38
Tosylate	21	34

of the barrier heights for these three counter-ions indicates that the counter-ion has little effect on the electronic structure of the transition state, and it suggests that the experimental reaction profiles differ primarily due to differences in other steps of the reaction, such as the rate of counter-ion loss.

4.4.3 Substrate Effects

Our model system is propylene oxide reacting with water or -OH to form a diol, but more commonly HKR is run using 1-hexene oxide. We focused primarily on propylene oxide because it's smaller, and thus more computationally tractable, and because the rotationally flexible hydrocarbon tail of 1-hexene oxide introduces many degrees of freedom that may cause technical difficulties while doing transition state optimization. To ensure that eliminating the hydrocarbon tail does not affect the nature of the system significantly, we have found the lowest barrier transition states (corresponding to f(right) in 14) using both 1-hexene oxide and propylene oxide. 1-hexene oxide has a barrier height of 33.2 kJ mol^{-1}, while propylene oxide has a barrier height of 35.5 kJ mol^{-1}, a very minor change. We also investigated epichlorohydrin as a substrate. Chengjun showed that the reaction rate constants for HKR of epichlorohydrin and propylene oxide using Co-salen-OAc were 8.9×10^3 and 3.3×10^3 mol^{-1} s^{-1}, respectively[33]. Our transition state barriers for epichlorohydrin and propylene oxide were 18.8 and 35.5 kJ mol^{-1}, respectively. Comparing the computed barriers to the reaction rates quantitatively is difficult given that the full reaction from which

the effective rate constants were extracted consists of multiple fundamental steps and that the DFT barriers surely exhibit errors of at least several kJ mol^{-1}. However it is gratifying that B3LYP computations for the proposed rate-determining step are able to obtain the correct qualitative reactivity order of the different substrates.

4.5 Conclusions

We have studied the catalysis of the rate-limiting step of the HKR of terminal epoxides with Co-salen catalysts. The DFT functionals studied have given the same trends as one another, even though the absolute barrier heights differ by as much as 60 kJ mol^{-1}. The barrier heights follow the expected trend that the uncatalyzed reaction has a higher barrier than any of the monocatalyzed reactions, which in turn also have higher barriers than the bicatalyzed reactions. The bicatalyzed reactions show a non-additive cooperative catalysis effect with a greater barrier height reduction than one would expect by summing the barrier height reductions from activation of the epoxide and activation of the nucleophile. Semi-empirical dispersion corrections through the DFT-D approach showed only small effects on the barrier heights. The chloride, acetate and tosylate counter-ions do not show significantly different binding of epoxide or barrier heights, which is in good agreement with their very similar experimental peak reaction rates. Differences in overall reaction rate profiles seen experimentally therefore appear to be due to differences in rates of other steps of the reaction, especially the rate of counter-ion loss to form Co-salen-OH. The Co-salen-OH complex, which provides the activated nucleophile for the bimetallic pathway as proposed by Jacobsen, is not catalytically active when used as the sole Co-salen species in experiments. However, the catalytically active Co-salen-X (X = Cl^-, OAc^-, OTs^-) do not show significant differences when compared to Co-salen-OH when considering charge distribution among the Co-salen backbone, charges on the carbons being attacked in the epoxide ring, or the binding energy of the epoxide reactant. This suggests that

Co-salen-OH is no less effect at activating epoxide as a reactant. Co-salen-OH has a 10-15 kJ mol^{-1} higher transition state barrier compared to these other counter-ions when it is the only catalytic species present. We also studied three substrates in the transition state of the HKR of terminal epoxides. By comparing propene oxide and 1-hexene oxide, we were able to verify that studying the computationally simpler propylene oxide doesn't significantly effect the transition state barriers. We also examined epichlorohydrin in the HKR transition state and found that its barrier height was approximately half as large as those of 1-hexene oxide and propylene oxide, which is consistent with epichlorohydrin reacting faster experimentally.

CHAPTER V

CONCLUSIONS AND OUTLOOK

This work demonstrates how one can use electronic structure theory to elucidate information about a variety of types of chemical systems. Performing such computations allows us to gain new understanding about non-covalent interactions in an array of chemical environments. We have shown through comparison to benchmark quality computations that when π-π stacking occurs in systems that are curved, the stacking interactions are enhanced if the two molecules are nested like bowls stacked in the cupboard. Using symmetry-adapted perturbation theory (SAPT) we were able to discover which contributions to the non-covalent interactions are enhanced or diminished by adding curvature to the molecules. All four components of the SAPT computation (i.e., electrostatics, dispersion, induction, and exchange) are larger in magnitude as one introduces more curvature into the system. Both dispersion and exchange are affected most strongly by the simple fact that the interatomic distances between the two monomers decrease with increasing curvature. This same geometric effect also leads to enhanced electrostatic interactions due to charge penetration effects becoming important at shorter intermonomer distances. The curvature also creates a permanent dipole via a rearrangement of electron density in the molecule which otherwise does not have a dipole, and since the molecules are aligned along the axis that the dipole is created along, one gets a favorable head-to-tail alignment of the dipole. These principles of how π-π interactions change with curvature should be able to guide future studies that explore chemical systems featuring curved π-π stacking.

Another area where non-covalent interactions are of major importance is in crystal packing. We use "gold standard" level CCSD(T) computations to confirm that three-body dispersion cannot be neglected if one wants an accurate computation of the lattice energy of benzene. We show that three-body dispersion contributes 0.89 kcal mol^{-1}, which is 7.2% of our revised estimate lattice energy. We performed "gold standard" computations on trimers taken from the crystal structure of benzene. Using our benchmark quality results we were able to assess the accuracy of other approximate methods that have been used for estimation of the three-body dispersion in crystalline benzene. The methods for computing three-body dispersion that have been previously used were the many-body dispersion formula of Tkatchenko[155], geometric based C_6 and C_9 coefficients with the atom-based Axilrod-Teller-Muto term[55], and frequency-dependent polarizabilities computed by way of Casimir-Polder integration[167, 162]. These procedures must be considered with caution as some of the results overestimate the three-body dispersion by as much as a factor of 2. Based on these results, it could be necessary to include accurate computation of three-body dispersion for other aromatic hydrocarbons or π-conjugated systems.

Lastly, the hydrolytic kinetic resolution (HKR) of epoxides was studied using DFT. We computed the barrier height for many variations of the HKR transition state for epoxide ring openining, including different number of catalysts, different counter-ions, and different substrates. The reaction has been proposed to be a co-operative mechanism where one Co-salen molecule activates a nucleophile (water or hydroxide) while another Co-salen molecule activates an epoxide. We found that the catalysts do have a cooperative effect, meaning that having both the epoxide and nucleophile being activated has a greater effect on lowering the barrier height than the sum of the two individual catalysts. Three functionals for DFT were used to compute barrier heights and while the barrier heights followed the same trends with all three functionals, the absolute barrier heights were different by as much as 60 kJ mol^{-1}.

We also investigated including an empirical dispersion correction to the barrier height computations and found that it has only small effects on the barrier heights. Next we investigated the effect that different counter-ions have on the barrier height for the reaction. Experimental reaction profiles were published[105] and showed very different profiles, but very similar peak reaction rates for all three counter-ions (chloride, acetate, and tosylate.) We computed the barrier height for those three counter-ions and found barrier heights of 35, 38, and 34 kJ mol^{-1} respectively. This shows a good agreement between the experimental peak reaction rates and our computed transition state barriers. The other counter-ion studied was hydroxide, which is necessary as one component for the proposed bimetallic, cooperative mechanism, but is inactive if it is the only counter-ion available in the reaction vessel. We find that hydroxide as the only counter-ion has a barrier height of 11-14 kJ mol^{-1} higher than the other three counter-ions. HKR is normally run at room temperature (25° C) and using the Arrhenius equation assuming $\Delta E \approx \Delta G$ and the pre-exponential factors being approximately the same, we see that an 11 kJ mol^{-1} difference would result in a reaction rate that is ≈1% as fast, which would be considered inactive under the reaction conditions when compared to the other three counter-ions. We also considered the effect of substrate on the reaction rate of HKR. We find a qualitative agreement between out computed barrier heights of epichlorohydrin and propylene oxide and the overall experimental rate constants[33].

One of the remaining problems to be studied in the area of non-covalent interactions is the effect that solvent has on the interactions. Elucidating the effects of solvation on non-covalent interactions is a difficult problem to solve due to either using an empirical/implicit solvent correction or the need to sample a large configuration space of solvent molecules around the complex. These effects could play a major role in some of the projects studied in this thesis. For example, in HKR there are frequently many solvent molecules around that would compete to fill the two axial

ligand positions around the cobalt center in the salen complex and we have ignored them due to the computational cost it would take to explore that space. The algorithms and code are not developed to a point where computation of derivatives is fast enough to run dynamics on systems of the size that are of interest to this work. It is of note that the results presented in this thesis are purely gas-phase electronic interaction energies or transition state barriers, but many of the results are compared to experimental data in solution. To properly compare our results to experimental results the thermodynamic corrections from solvent, ΔH and ΔS, would need to be computed if we were to hope to have answers that were within "chemical accuracy" (i.e., $\pm$1 kcal mol^{-1}.) Eventually the methodologies will evolve and improve to a point where theorists will be able to estimate these important contributions even for large systems like the HKR transition states, and be able to compare with solution-phase experimental results on a quantitative level. While computing barrier heights or interaction energies in a solvated environment is important for comparing to experimental data, it should be noted that DFT functionals must be improved as well. The discrepancies between functionals evaluated in this work is as large as 60 kJ mol^{-1} which is substantial. This is another area where advancements in methodologies is needed to accurately describe chemical systems of interest.

APPENDIX A

ANCILLARY MATERIAL

A.1 XYZ Coordinates for Figure 2

R = 3.54 Å

C -0.70622800 0.97212500 2.4186270

C -1.14280400 -0.37137200 2.4184910

C 0.00000000 -1.20165400 2.4182740

C 1.14280400 -0.37137200 2.4184910

C 1.45779000 2.00650700 1.8958130

C -1.45779000 2.00650700 1.8958130

C -2.35873800 -0.76639200 1.8956510

C 0.00000000 -2.48003500 1.8953480

C 2.35873800 -0.76639200 1.8956510

C 0.69261800 3.17924500 1.5484640

C -0.69261800 3.17924500 1.5484640

C -2.80958100 1.64120300 1.5487510

C -3.23765700 0.32374300 1.5486410

C -2.42918200 -2.16498400 1.5486530

C -1.30841500 -2.97916300 1.5484020

C 1.30841500 -2.97916300 1.5484020

C 2.42918200 -2.16498400 1.5486530

C 3.23765700 0.32374300 1.5486410

C 2.80958100 1.64120300 1.5487510

H 1.20851300 4.06642600 1.1874910

H -1.20851300 4.06642600 1.1874910

H -3.49401500 2.40602700 1.1880070

H -4.24094400 0.10730100 1.1879390

H -3.36816400 -2.57958300 1.1881730

H -1.41248600 -4.00023700 1.1876990

H 1.41248600 -4.00023700 1.1876990

H 3.36816400 -2.57958300 1.1881730

H 4.24094400 0.10730100 1.1879390

H 3.49401500 2.40602700 1.1880070

C 0.70622800 0.97212500 5.9586270

C -0.70622800 0.97212500 5.9586270

C -1.14280400 -0.37137200 5.9584910

C 0.00000000 -1.20165400 5.9582740

C 1.14280400 -0.37137200 5.9584910

C 1.45779000 2.00650700 5.4358130

C -1.45779000 2.00650700 5.4358130

C -2.35873800 -0.76639200 5.4356510

C 0.00000000 -2.48003500 5.4353480

C 2.35873800 -0.76639200 5.4356510

C 0.69261800 3.17924500 5.0884640

C -0.69261800 3.17924500 5.0884640

C -2.80958100 1.64120300 5.0887510

C -3.23765700 0.32374300 5.0886410

C -2.42918200 -2.16498400 5.0886530

C -1.30841500 -2.97916300 5.0884020

C 1.30841500 -2.97916300 5.0884020

C 2.42918200 -2.16498400 5.0886530

C 3.23765700 0.32374300 5.0886410

C 2.80958100 1.64120300 5.0887510

H 1.20851300 4.06642600 4.7274910

H -1.20851300 4.06642600 4.7274910

H -3.49401500 2.40602700 4.7280070

H -4.24094400 0.10730100 4.7279390

H -3.36816400 -2.57958300 4.7281730

H -1.41248600 -4.00023700 4.7276990

H 1.41248600 -4.00023700 4.7276990

H 3.36816400 -2.57958300 4.7281730

H 4.24094400 0.10730100 4.7279390

H 3.49401500 2.40602700 4.7280070

R = 3.64 Å

C 0.70622800 0.97212500 2.4186270

C -0.70622800 0.97212500 2.4186270

C -1.14280400 -0.37137200 2.4184910

C 0.00000000 -1.20165400 2.4182740

C 1.14280400 -0.37137200 2.4184910

C 1.45779000 2.00650700 1.8958130

C -1.45779000 2.00650700 1.8958130

C -2.35873800 -0.76639200 1.8956510

C 0.00000000 -2.48003500 1.8953480

C 2.35873800 -0.76639200 1.8956510

C 0.69261800 3.17924500 1.5484640

C -0.69261800 3.17924500 1.5484640

C -2.80958100 1.64120300 1.5487510

C -3.23765700 0.32374300 1.5486410

C -2.42918200 -2.16498400 1.5486530

C -1.30841500 -2.97916300 1.5484020

C 1.30841500 -2.97916300 1.5484020

C 2.42918200 -2.16498400 1.5486530

C 3.23765700 0.32374300 1.5486410

C 2.80958100 1.64120300 1.5487510

H 1.20851300 4.06642600 1.1874910

H -1.20851300 4.06642600 1.1874910

H -3.49401500 2.40602700 1.1880070

H -4.24094400 0.10730100 1.1879390

H -3.36816400 -2.57958300 1.1881730

H -1.41248600 -4.00023700 1.1876990

H 1.41248600 -4.00023700 1.1876990

H 3.36816400 -2.57958300 1.1881730

H 4.24094400 0.10730100 1.1879390

H 3.49401500 2.40602700 1.1880070

C 0.70622800 0.97212500 6.0586270

C -0.70622800 0.97212500 6.0586270

C -1.14280400 -0.37137200 6.0584910

C 0.00000000 -1.20165400 6.0582740

C 1.14280400 -0.37137200 6.0584910

C 1.45779000 2.00650700 5.5358130

C -1.45779000 2.00650700 5.5358130

C -2.35873800 -0.76639200 5.5356510

C 0.00000000 -2.48003500 5.5353480

C 2.35873800 -0.76639200 5.5356510

C 0.69261800 3.17924500 5.1884640

C -0.69261800 3.17924500 5.1884640

C -2.80958100 1.64120300 5.1887510

C -3.23765700 0.32374300 5.1886410

C -2.42918200 -2.16498400 5.1886530

C -1.30841500 -2.97916300 5.1884020

C 1.30841500 -2.97916300 5.1884020

C 2.42918200 -2.16498400 5.1886530

C 3.23765700 0.32374300 5.1886410

C 2.80958100 1.64120300 5.1887510

H 1.20851300 4.06642600 4.8274910

H -1.20851300 4.06642600 4.8274910

H -3.49401500 2.40602700 4.8280070

H -4.24094400 0.10730100 4.8279390

H -3.36816400 -2.57958300 4.8281730

H -1.41248600 -4.00023700 4.8276990

H 1.41248600 -4.00023700 4.8276990

H 3.36816400 -2.57958300 4.8281730

H 4.24094400 0.10730100 4.8279390

H 3.49401500 2.40602700 4.8280070

R = 3.74 Å

C 0.70622800 0.97212500 2.4186270

C -0.70622800 0.97212500 2.4186270

C -1.14280400 -0.37137200 2.4184910

C 0.00000000 -1.20165400 2.4182740

C 1.14280400 -0.37137200 2.4184910

C 1.45779000 2.00650700 1.8958130

C -1.45779000 2.00650700 1.8958130

C -2.35873800 -0.76639200 1.8956510

C 0.00000000 -2.48003500 1.8953480

C 2.35873800 -0.76639200 1.8956510

C 0.69261800 3.17924500 1.5484640

C -0.69261800 3.17924500 1.5484640

C -2.80958100 1.64120300 1.5487510

C -3.23765700 0.32374300 1.5486410

C -2.42918200 -2.16498400 1.5486530

C -1.30841500 -2.97916300 1.5484020

C 1.30841500 -2.97916300 1.5484020

C 2.42918200 -2.16498400 1.5486530

C 3.23765700 0.32374300 1.5486410

C 2.80958100 1.64120300 1.5487510

H 1.20851300 4.06642600 1.1874910

H -1.20851300 4.06642600 1.1874910

H -3.49401500 2.40602700 1.1880070

H -4.24094400 0.10730100 1.1879390

H -3.36816400 -2.57958300 1.1881730

H -1.41248600 -4.00023700 1.1876990

H 1.41248600 -4.00023700 1.1876990

H 3.36816400 -2.57958300 1.1881730

H 4.24094400 0.10730100 1.1879390

H 3.49401500 2.40602700 1.1880070

C 0.70622800 0.97212500 6.1586270

C -0.70622800 0.97212500 6.1586270

C -1.14280400 -0.37137200 6.1584910

C 0.00000000 -1.20165400 6.1582740

C 1.14280400 -0.37137200 6.1584910

C 1.45779000 2.00650700 5.6358130

C -1.45779000 2.00650700 5.6358130

C -2.35873800 -0.76639200 5.6356510

C 0.00000000 -2.48003500 5.6353480

C 2.35873800 -0.76639200 5.6356510

C 0.69261800 3.17924500 5.2884640

C -0.69261800 3.17924500 5.2884640

C -2.80958100 1.64120300 5.2887510

C -3.23765700 0.32374300 5.2886410

C -2.42918200 -2.16498400 5.2886530

C -1.30841500 -2.97916300 5.2884020

C 1.30841500 -2.97916300 5.2884020

C 2.42918200 -2.16498400 5.2886530

C 3.23765700 0.32374300 5.2886410

C 2.80958100 1.64120300 5.2887510

H 1.20851300 4.06642600 4.9274910

H -1.20851300 4.06642600 4.9274910

H -3.49401500 2.40602700 4.9280070

H -4.24094400 0.10730100 4.9279390

H -3.36816400 -2.57958300 4.9281730

H -1.41248600 -4.00023700 4.9276990

H 1.41248600 -4.00023700 4.9276990

H 3.36816400 -2.57958300 4.9281730

H 4.24094400 0.10730100 4.9279390

H 3.49401500 2.40602700 4.9280070

R = 3.84 Å

C 0.70622800 0.97212500 2.4186270

C -0.70622800 0.97212500 2.4186270

C -1.14280400 -0.37137200 2.4184910

C 0.00000000 -1.20165400 2.4182740

C 1.14280400 -0.37137200 2.4184910

C 1.45779000 2.00650700 1.8958130

C -1.45779000 2.00650700 1.8958130

C -2.35873800 -0.76639200 1.8956510

C 0.00000000 -2.48003500 1.8953480

C 2.35873800 -0.76639200 1.8956510

C 0.69261800 3.17924500 1.5484640

C -0.69261800 3.17924500 1.5484640

C -2.80958100 1.64120300 1.5487510

C -3.23765700 0.32374300 1.5486410

C -2.42918200 -2.16498400 1.5486530

C -1.30841500 -2.97916300 1.5484020

C 1.30841500 -2.97916300 1.5484020

C 2.42918200 -2.16498400 1.5486530

C 3.23765700 0.32374300 1.5486410

C 2.80958100 1.64120300 1.5487510

H 1.20851300 4.06642600 1.1874910

H -1.20851300 4.06642600 1.1874910

H -3.49401500 2.40602700 1.1880070

H -4.24094400 0.10730100 1.1879390

H -3.36816400 -2.57958300 1.1881730

H -1.41248600 -4.00023700 1.1876990

H 1.41248600 -4.00023700 1.1876990

H 3.36816400 -2.57958300 1.1881730

H 4.24094400 0.10730100 1.1879390

H 3.49401500 2.40602700 1.1880070

C 0.70622800 0.97212500 6.2586270

C -0.70622800 0.97212500 6.2586270

C -1.14280400 -0.37137200 6.2584910

C 0.00000000 -1.20165400 6.2582740

C 1.14280400 -0.37137200 6.2584910

C 1.45779000 2.00650700 5.7358130

C -1.45779000 2.00650700 5.7358130

C -2.35873800 -0.76639200 5.7356510

C 0.00000000 -2.48003500 5.7353480

C 2.35873800 -0.76639200 5.7356510

C 0.69261800 3.17924500 5.3884640

C -0.69261800 3.17924500 5.3884640

C -2.80958100 1.64120300 5.3887510

C -3.23765700 0.32374300 5.3886410

C -2.42918200 -2.16498400 5.3886530

C -1.30841500 -2.97916300 5.3884020

C 1.30841500 -2.97916300 5.3884020

C 2.42918200 -2.16498400 5.3886530

C 3.23765700 0.32374300 5.3886410

C 2.80958100 1.64120300 5.3887510

H 1.20851300 4.06642600 5.0274910

H -1.20851300 4.06642600 5.0274910

H -3.49401500 2.40602700 5.0280070

H -4.24094400 0.10730100 5.0279390

H -3.36816400 -2.57958300 5.0281730

H -1.41248600 -4.00023700 5.0276990

H 1.41248600 -4.00023700 5.0276990

H 3.36816400 -2.57958300 5.0281730

H 4.24094400 0.10730100 5.0279390

H 3.49401500 2.40602700 5.0280070

R = 3.94 Å

C -0.70622800 0.97212500 2.4186270

C -1.14280400 -0.37137200 2.4184910

C 0.00000000 -1.20165400 2.4182740

C 1.14280400 -0.37137200 2.4184910

C 1.45779000 2.00650700 1.8958130

C -1.45779000 2.00650700 1.8958130

C -2.35873800 -0.76639200 1.8956510

C 0.00000000 -2.48003500 1.8953480

C 2.35873800 -0.76639200 1.8956510

C 0.69261800 3.17924500 1.5484640

C -0.69261800 3.17924500 1.5484640

C -2.80958100 1.64120300 1.5487510

C -3.23765700 0.32374300 1.5486410

C -2.42918200 -2.16498400 1.5486530

C -1.30841500 -2.97916300 1.5484020

C 1.30841500 -2.97916300 1.5484020

C 2.42918200 -2.16498400 1.5486530

C 3.23765700 0.32374300 1.5486410

C 2.80958100 1.64120300 1.5487510

H 1.20851300 4.06642600 1.1874910

H -1.20851300 4.06642600 1.1874910

H -3.49401500 2.40602700 1.1880070

H -4.24094400 0.10730100 1.1879390

H -3.36816400 -2.57958300 1.1881730

H -1.41248600 -4.00023700 1.1876990

H 1.41248600 -4.00023700 1.1876990

H 3.36816400 -2.57958300 1.1881730

H 4.24094400 0.10730100 1.1879390

H 3.49401500 2.40602700 1.1880070

C 0.70622800 0.97212500 6.3586270

C -0.70622800 0.97212500 6.3586270

C -1.14280400 -0.37137200 6.3584910

C 0.00000000 -1.20165400 6.3582740

C 1.14280400 -0.37137200 6.3584910

C 1.45779000 2.00650700 5.8358130

C -1.45779000 2.00650700 5.8358130

C -2.35873800 -0.76639200 5.8356510

C 0.00000000 -2.48003500 5.8353480

C 2.35873800 -0.76639200 5.8356510

C 0.69261800 3.17924500 5.4884640

C -0.69261800 3.17924500 5.4884640

C -2.80958100 1.64120300 5.4887510

C -3.23765700 0.32374300 5.4886410

C -2.42918200 -2.16498400 5.4886530

C -1.30841500 -2.97916300 5.4884020

C 1.30841500 -2.97916300 5.4884020

C 2.42918200 -2.16498400 5.4886530

C 3.23765700 0.32374300 5.4886410

C 2.80958100 1.64120300 5.4887510

H 1.20851300 4.06642600 5.1274910

H -1.20851300 4.06642600 5.1274910

H -3.49401500 2.40602700 5.1280070

H -4.24094400 0.10730100 5.1279390

H -3.36816400 -2.57958300 5.1281730

H -1.41248600 -4.00023700 5.1276990

H 1.41248600 -4.00023700 5.1276990

H 3.36816400 -2.57958300 5.1281730

H 4.24094400 0.10730100 5.1279390

H 3.49401500 2.40602700 5.1280070

A.2 Coronene Dimer Coordinates with R = 3.7Å and τ=0°

C 1.00000000 0.00000000 -0.3915000

C 1.00000000 1.20507400 0.3042500

C 1.00000000 1.20507400 1.6957500

C 1.00000000 0.00000000 2.3915000

C 1.00000000 -1.20507400 1.6957500

C 1.00000000 -1.20507400 0.3042500

C 1.00000000 0.00000000 -1.7830000

C 1.00000000 2.41014900 -0.3915000

C 1.00000000 2.41014900 2.3915000

C 1.00000000 0.00000000 3.7830000

C 1.00000000 -2.41014900 2.3915000

C 1.00000000 -2.41014900 -0.3915000

C 1.00000000 1.20507400 -2.4787500

C 1.00000000 2.41014900 -1.7830000

C 1.00000000 3.61522300 0.3042500

C 1.00000000 3.61522300 1.6957500

C 1.00000000 2.41014900 3.7830000

C 1.00000000 1.20507400 4.4787500

C 1.00000000 -1.20507400 4.4787500

C 1.00000000 -2.41014900 3.7830000

C 1.00000000 -3.61522300 1.6957500

C 1.00000000 -3.61522300 0.3042500

C 1.00000000 -2.41014900 -1.7830000

C 1.00000000 -1.20507400 -2.4787500

H 1.00000000 1.20507400 -3.5587500

H 1.00000000 3.34545600 -2.3230000

H 1.00000000 4.55053000 -0.2357500

H 1.00000000 4.55053000 2.2357500

H 1.00000000 3.34545600 4.3230000

H 1.00000000 1.20507400 5.5587500

H 1.00000000 -1.20507400 5.5587500

H 1.00000000 -3.34545600 4.3230000

H 1.00000000 -4.55053000 2.2357500

H 1.00000000 -4.55053000 -0.2357500

H 1.00000000 -3.34545600 -2.3230000

H 1.00000000 -1.20507400 -3.5587500

C -2.70000000 0.00000000 -0.3915000

C -2.70000000 1.20507400 0.3042500

C -2.70000000 1.20507400 1.6957500

C -2.70000000 0.00000000 2.3915000

C -2.70000000 -1.20507400 1.6957500

C -2.70000000 -1.20507400 0.3042500

C -2.70000000 0.00000000 -1.7830000

C -2.70000000 2.41014900 -0.3915000

C -2.70000000 2.41014900 2.3915000

C -2.70000000 0.00000000 3.7830000

C -2.70000000 -2.41014900 2.3915000

C -2.70000000 -2.41014900 -0.3915000

C -2.70000000 1.20507400 -2.4787500

C -2.70000000 2.41014900 -1.7830000

C -2.70000000 3.61522300 0.3042500

C -2.70000000 3.61522300 1.6957500

C -2.70000000 2.41014900 3.7830000

C -2.70000000 1.20507400 4.4787500

C -2.70000000 -1.20507400 4.4787500

C -2.70000000 -2.41014900 3.7830000

C -2.70000000 -3.61522300 1.6957500

C -2.70000000 -3.61522300 0.3042500

C -2.70000000 -2.41014900 -1.7830000

C -2.70000000 -1.20507400 -2.4787500

H -2.70000000 1.20507400 -3.5587500

H -2.70000000 3.34545600 -2.3230000

H -2.70000000 4.55053000 -0.2357500

H -2.70000000 4.55053000 2.2357500

H -2.70000000 3.34545600 4.3230000

H -2.70000000 1.20507400 5.5587500

H -2.70000000 -1.20507400 5.5587500

H -2.70000000 -3.34545600 4.3230000

H -2.70000000 -4.55053000 2.2357500

H -2.70000000 -4.55053000 -0.2357500

H -2.70000000 -3.34545600 -2.3230000

H -2.70000000 -1.20507400 -3.5587500

A.3 Corannulene Dimer Coordinates with R = 3.7Å and τ=50°

C 1.00000000 0.00000000 -0.2061040

C 1.00000000 1.14707300 0.6272930

C 1.00000000 0.70893000 1.9757580

C 1.00000000 0.00000000 -0.2061040

C 1.00000000 1.14707300 0.6272930

C 1.00000000 0.70893000 1.9757580

C 1.00000000 -0.70893000 1.9757580

C 1.00000000 -1.14707300 0.6272930

C 0.50884400 0.00000000 -1.5080400

C 0.50884400 2.38528800 0.2249730

C 0.50884400 1.47418900 3.0290470

C 0.50884400 -1.47418900 3.0290470

C 0.50884400 -2.38528800 0.2249730

C 0.02140000 1.24419700 -1.8961710

C 0.02140000 2.36994400 -1.0782680

C 0.02140000 3.13890000 1.2883360

C 0.02140000 2.70890300 2.6117310

C 0.02140000 0.69575000 4.0743720

C 0.02140000 -0.69575000 4.0743720

C 0.02140000 -2.70890300 2.6117310

C 0.02140000 -3.13890000 1.2883360

C 0.02140000 -2.36994400 -1.0782680

C 0.02140000 -1.24419700 -1.8961710

H -0.38163100 1.34213400 -2.8933540

H -0.38163100 3.28805700 -1.4795580

H -0.38163100 4.11754200 1.0733330

H -0.38163100 3.37426500 3.3609020

H -0.38163100 1.20264600 4.9386760

H -0.38163100 -1.20264600 4.9386760

H -0.38163100 -3.37426500 3.3609020

H -0.38163100 -4.11754200 1.0733330

H -0.38163100 -3.28805700 -1.4795580

H -0.38163100 -1.34213400 -2.8933540

C -2.70000000 0.00000000 -0.2061040

C -2.70000000 1.14707300 0.6272930

C -2.70000000 0.70893000 1.9757580

C -2.70000000 -0.70893000 1.9757580

C -2.70000000 -1.14707300 0.6272930

C -3.19115600 0.00000000 -1.5080400

C -3.19115600 2.38528800 0.2249730

C -3.19115600 1.47418900 3.0290470

C -3.19115600 -1.47418900 3.0290470

C -3.19115600 -2.38528800 0.2249730

C -3.67860000 1.24419700 -1.8961710

C -3.67860000 2.36994400 -1.0782680

C -3.67860000 3.13890000 1.2883360

C -3.67860000 2.70890300 2.6117310

C -3.67860000 0.69575000 4.0743720

C -3.67860000 -0.69575000 4.0743720

C -3.67860000 -2.70890300 2.6117310

C -3.67860000 -3.13890000 1.2883360

C -3.67860000 -2.36994400 -1.0782680

C -3.67860000 -1.24419700 -1.8961710

H -4.08163100 1.34213400 -2.8933540

H -4.08163100 3.28805700 -1.4795580

H -4.08163100 4.11754200 1.0733330

H -4.08163100 3.37426500 3.3609020

H -4.08163100 1.20264600 4.9386760

H -4.08163100 -1.20264600 4.9386760

H -4.08163100 -3.37426500 3.3609020

H -4.08163100 -4.11754200 1.0733330

H -4.08163100 -3.28805700 -1.4795580

H -4.08163100 -1.34213400 -2.8933540

A.4 Z-Matrix and Variables for Model Systems

Coronene

X

X 1 XX

X 2 XX 1 A0

C 3 CX 2 A0 1 0.0

C 3 CX 2 A0 1 60.0

C 3 CX 2 A0 1 120.0

C 3 CX 2 A0 1 180.0

C 3 CX 2 A0 1 240.0

C 3 CX 2 A0 1 300.0

C 4 CC 5 A1 6 D1

C 5 CC 6 A1 7 D1

C 6 CC 7 A1 8 D1

C 7 CC 8 A1 9 D1

C 8 CC 9 A1 4 D1

C 9 CC 4 A1 5 D1

C 10 CC 11 A2 5 D2

C 11 CC 10 A2 4 D2n

C 11 CC 12 A2 6 D2

C 12 CC 11 A2 5 D2n

C 12 CC 13 A2 7 D2

C 13 CC 12 A2 6 D2n

C 13 CC 14 A2 8 D2

C 14 CC 13 A2 7 D2n

C 14 CC 15 A2 9 D2

C 15 CC 14 A2 8 D2n

C 15 CC 10 A2 4 D2

C 10 CC 15 A2 9 D2n

H 16 CH 17 A3 11 D2

H 17 CH 16 A3 10 D2n

H 18 CH 19 A3 12 D2

H 19 CH 18 A3 11 D2n

H 20 CH 21 A3 13 D2

H 21 CH 20 A3 12 D2n

H 22 CH 23 A3 14 D2

H 23 CH 22 A3 13 D2n

H 24 CH 25 A3 15 D2

H 25 CH 24 A3 14 D2n

H 26 CH 27 A3 10 D2

H 27 CH 26 A3 15 D2n

X 1 R 2 A0 3 180.0

X 40 XX 1 A0 2 0.0

X 41 XX 40 A0 1 0.0

C 42 CX 41 A0 40 0.0

C 42 CX 41 A0 40 60.0

C 42 CX 41 A0 40 120.0

C 42 CX 41 A0 40 180.0

C 42 CX 41 A0 40 240.0

C 42 CX 41 A0 40 300.0

C 43 CC 44 A1 45 D1

C 44 CC 45 A1 46 D1

C 45 CC 46 A1 47 D1

C 46 CC 47 A1 48 D1

C 47 CC 48 A1 43 D1

C 48 CC 43 A1 44 D1

C 49 CC 50 A2 44 D2

C 50 CC 49 A2 43 D2n

C 50 CC 51 A2 45 D2

C 51 CC 50 A2 44 D2n

C 51 CC 52 A2 46 D2

C 52 CC 51 A2 45 D2n

C 52 CC 53 A2 47 D2

C 53 CC 52 A2 46 D2n

C 53 CC 54 A2 48 D2

C 54 CC 53 A2 47 D2n

C 54 CC 49 A2 43 D2

C 49 CC 54 A2 48 D2n

H 55 CH 56 A3 50 D2

H 56 CH 55 A3 49 D2n

H 57 CH 58 A3 51 D2

H 58 CH 57 A3 50 D2n

H 59 CH 60 A3 52 D2

H 60 CH 59 A3 51 D2n

H 61 CH 62 A3 53 D2

H 62 CH 61 A3 52 D2n

H 63 CH 64 A3 54 D2

H 64 CH 63 A3 53 D2n

H 65 CH 66 A3 49 D2

H 66 CH 65 A3 54 D2n

Variables for the Z-matrix variable equations below are R (the interatomic distance), τ (the curvature), and τ' (the dihedral angle) are defined in 1.

Bond Lengths

$$XX = 1.0 \tag{41}$$

$$CC = 1.3915 \tag{42}$$

$$CX = \frac{CC}{2 * \cos(\frac{1}{2} * 120^\circ)} \tag{43}$$

$$CH = 1.08 \tag{44}$$

$$\tag{45}$$

Dihedral Angles

$$D1 = \tau' = 180.0^\circ - 0.5 * \tau \tag{46}$$

$$D2 = 180.0^\circ \tag{47}$$

$$D2n = -1 * D2 \tag{48}$$

Bond Angles

$$A0 = 90.0^\circ \tag{49}$$

$$A1 = 180.0^\circ - \cos^{-1}(\cos(60^\circ) * \sqrt{1 + (\sin(60^\circ)\tan(D1))^2}) \tag{50}$$

$$A2 = 180.0^\circ - A1 \tag{51}$$

$$A3 = 180.0^\circ - \cos^{-1}(\cos(\frac{1}{2}(180^\circ - A2)) * (1 + (\sin(\frac{1}{2}(180^\circ - A2))\tan(D2))^2)^{-\frac{1}{2}}) \tag{52}$$

Corannulene

X

X 1 XX

X 2 XX 1 A0

C 3 CX 2 A0 1 0.0

C 3 CX 2 A0 1 72.0

C 3 CX 2 A0 1 144.0

C 3 CX 2 A0 1 216.0

C 3 CX 2 A0 1 288.0

C 4 CC 5 A1 6 D1

C 5 CC 6 A1 7 D1

C 6 CC 7 A1 8 D1

C 7 CC 8 A1 4 D1

C 8 CC 4 A1 5 D1

C 9 CC 10 A2 5 D2

C 10 CC 9 A2 4 D2n

C 10 CC 11 A2 6 D2

C 11 CC 10 A2 5 D2n

C 11 CC 12 A2 7 D2

C 12 CC 11 A2 6 D2n

C 12 CC 13 A2 8 D2

C 13 CC 12 A2 7 D2n

C 13 CC 9 A2 4 D2

C 9 CC 13 A2 8 D2n

H 14 CH 15 A3 10 D2

H 15 CH 14 A3 9 D2n

H 16 CH 17 A3 11 D2

H 17 CH 16 A3 10 D2n

H 18 CH 19 A3 12 D2

H 19 CH 18 A3 11 D2n

H 20 CH 21 A3 13 D2

H 21 CH 20 A3 12 D2n

H 22 CH 23 A3 9 D2

H 23 CH 22 A3 13 D2n

X 1 R 2 A0 3 180.0

X 34 XX 1 A0 2 0.0

X 35 XX 34 A0 1 0.0

C 36 CX 35 A0 34 0.0

C 36 CX 35 A0 34 72.0

C 36 CX 35 A0 34 144.0

C 36 CX 35 A0 34 216.0

C 36 CX 35 A0 34 288.0

C 37 CC 38 A1 39 D1

C 38 CC 39 A1 40 D1

C 39 CC 40 A1 41 D1

C 40 CC 41 A1 37 D1

C 41 CC 37 A1 38 D1

C 42 CC 43 A2 38 D2

C 43 CC 42 A2 37 D2n

C 43 CC 44 A2 39 D2

C 44 CC 43 A2 38 D2n

C 44 CC 45 A2 40 D2

C 45 CC 44 A2 39 D2n

C 45 CC 46 A2 41 D2

C 46 CC 45 A2 40 D2n

C 46 CC 42 A2 37 D2

C 42 CC 46 A2 41 D2n

H 47 CH 48 A3 43 D2

H 48 CH 47 A3 42 D2n

H 49 CH 50 A3 44 D2

H 50 CH 49 A3 43 D2n

H 51 CH 52 A3 45 D2

H 52 CH 51 A3 44 D2n

H 53 CH 54 A3 46 D2

H 54 CH 53 A3 45 D2n

H 55 CH 56 A3 42 D2

H 56 CH 55 A3 46 D2n

Bond Lengths

$$XX = 1.0 \tag{53}$$

$$CC = 1.3915 \tag{54}$$

$$CX = \frac{CC}{2 * \cos(\frac{1}{2} * 108^\circ)} \tag{55}$$

$$CH = 1.08 \tag{56}$$

$$\tag{57}$$

Dihedral Angles

$$D1 = \tau' = 180.0^\circ - 0.5 * \tau \tag{58}$$

$$D2 = 180.0^\circ \tag{59}$$

$$D2n = -1 * D2 \tag{60}$$

Bond Angles

$$A0 = 90.0^\circ \tag{61}$$

$$A1 = 180.0^\circ - \cos^{-1}(\cos(54^\circ) * \sqrt{1 + (\sin(54^\circ)\tan(D1))^2}) \tag{62}$$

$$A2 = 180.0^\circ - \cos^{-1}(\frac{1}{2} * (1 - \frac{108^\circ}{120^\circ}) + \cos(A1)) \tag{63}$$

$$A3 = 180.0^\circ - \cos^{-1}(\cos(\frac{1}{2}(180^\circ - A2)) * (1 + (\sin(\frac{1}{2}(180^\circ - A2))\tan(D2))^2)^{-\frac{1}{2}}) \tag{64}$$

A.5 Basis Set Convergence of Three-Body Interaction

Geometry from the -55 degree used to compute the three-body interaction with both the aug-cc-pVDZ and aug-cc-pVTZ basis sets.

C -0.4486 10.7322 -0.0470

C -1.0176 9.8411 0.8581

C 0.5690 10.3224 -0.9023

H -0.7730 11.7769 -0.0838

H -1.8165 10.1557 1.5261

H 1.0132 11.0035 -1.6072

C -0.5690 8.5176 0.9023

C 1.0176 8.9989 -0.8581

C 0.4486 8.1078 0.0470

H -1.0132 7.8365 1.6072

H 1.8165 8.6843 -1.5261

H 0.7730 7.0631 0.0838

C -0.4486 10.7322 6.7630

C -1.0176 9.8411 7.6681

C 0.5690 10.3224 5.9077

H -0.7730 11.7769 6.7262

H -1.8165 10.1557 8.3361

H 1.0132 11.0035 5.2028

C -0.5690 8.5176 7.7123

C 1.0176 8.9989 5.9519

C 0.4486 8.1078 6.8570

H -1.0132 7.8365 8.4172

H 1.8165 8.6843 5.2839

H 0.7730 7.0631 6.8938

C -0.4486 3.3978 3.3580

C -1.0176 4.2889 4.2631

C 0.5690 3.8076 2.5027

H -0.7730 2.3531 3.3212

H -1.8165 3.9743 4.9311

H 1.0132 3.1265 1.7978

C -0.5690 5.6124 4.3073

C 1.0176 5.1311 2.5469

C 0.4486 6.0222 3.4520

H -1.0132 6.2935 5.0122

H 1.8165 5.4457 1.8789

H 0.7730 7.0669 3.4888

Three-body interaction is 0.027353166 kcal mol^{-1} for the aug-cc-pVTZ basis set and 0.027768656^{-1} for the aug-cc-pVDZ basis set.

Table 4: Interaction Energies for Figure 2 reported in kcal mol^{-1}

	3.54Å	3.64Å	3.74Å	3.84Å	3.94Å
B3LYP-D2	-14.70	-14.65	-14.11	-13.31	-12.37
B3LYP-D3	-11.61	-12.76	-13.10	-12.93	-12.45
B3LYP-D3(BJ)	-15.47	-16.05	-15.90	-15.30	-14.42
B3LYP-XDM	-12.31	-13.11	-13.20	-12.86	-12.19
B97-D2	-16.09	-16.18	-15.77	-15.12	-14.32
B97-D3	-12.23	-12.88	-12.85	-12.45	-11.84
B97-D3(BJ)	-17.18	-17.54	-17.25	-16.59	-15.70
M05-2X	-6.96	-7.74	-8.27	-8.15	-7.74
M06-2X	-13.79	-14.22	-13.80	-12.87	-11.62

Figure 15: Investigation of parallel displaced corannulene dimer at three different slipped distances compared with the nested configuration. The parallel displaced configuration has a weaker interaction than the nested configuration, so the nested configuration was used for this study

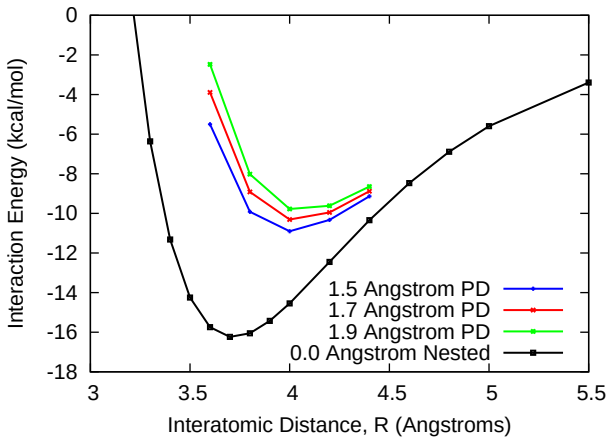

REFERENCES

[1] Spartan '08, Wavefunction, Inc., Irvine CA.

[2] Turney, J. M.; Simmonett, A. C.; Parrish, R. M.; Hohenstein, E. G.; Evangelista, F. A.; Fermann, J. T.; Mintz, B. J.; Burns, L. A.; Wilke, J. J.; Abrams, M. L.; Russ, N. J.; Leininger, M. L.; Janssen, C. L.; Seidl, E. T.; Allen, W. D.; Schaefer, H. F.; King, R. A.; Valeev, E. F.; Sherrill, C. D.; Crawford, T. D. *WIREs Comput. Mol. Sci.* **2**, 556-565 (2012).

[3] MOLPRO, version 2010.1, a package of ab initio programs, H.-J. Werner, P. J. Knowles, F. R. Manby, M. Schütz, P. Celani, G. Knizia, T. Korona, R. Lindh, A. Mitrushenkov, G. Rauhut, T. B. Adler, R. D. Amos, A. Bernhardsson, A. Berning, D. L. Cooper, M. J. O. Deegan, A. J. Dobbyn, F. Eckert, E. Goll, C. Hampel, A. Hesselmann, G. Hetzer, T. Hrenar, G. Jansen, C. Köppl, Y. Liu, A. W. Lloyd, R. A. Mata, A. J. May, R. Tarroni, T. Thorsteinsson, M. Wang, and A. Wolf, see http://www.molpro.net.

[4] For an online compilation of sublimation energies, see the NIST webbook at http://webbook.nist.gov/cgi/cbook.cgi?ID=C71432&Units=SI&Mask=4 and references given there.

[5] Angyan, J. G., "On the exchange-hole model of london dispersion forces," *J. Chem. Phys.*, vol. 127, p. 024108, 2007.

[6] Antony, J. and Grimme, S., "Density functional theory including dispersion corrections for intermolecular interactions in a large benchmark set of biologically relevant molecules," *Phys. Chem. Chem. Phys.*, vol. 8, pp. 5287–5293, 2006.

[7] Aquilante, F., Gagliardi, L., Pedersen, T. B., and Lindh, R., "Atomic cholesky decompositions: A route to unbiased auxiliary basis sets for density fitting approximation with tunable accuracy and efficiency," *J. Chem. Phys.*, vol. 130, p. 154107, 2009.

[8] Aquilante, F., Pedersen, T. B., and Lindh, R., "Low-cost evaluation of the exchange fock matrix from cholesky and density fitting representations of the electron repulsion integrals," *J. Chem. Phys.*, vol. 126, p. 194106, 2007.

[9] Aquilante, F., Vico, L. D., Ferre, N., Ghigo, G., Malmqvist, P., Neogrady, P., Pedersen, T. B., Pitonak, M., Reiher, M., Roos, B. O., Serrano-Andres, L., Urban, M., Veryazov, V., and Lindh, R., "Software news and update MOLCAS 7: The next generation," *J. Comput. Chem.*, vol. 31, pp. 224–247, 2010.

[10] Axilrod, B. M. and Teller, E., "Interaction of the van der Waals type between three atoms," *J. Chem. Phys.*, vol. 11, pp. 299–300, 1943.

[11] Bacon, G. E., Curry, N. A., and Wilson, S. A., "Crystallographic study of solid benzene by neutron diffraction," *Proc. R. Soc. London Ser. A*, vol. 279, pp. 98–100, 1964.

[12] Bartlett, R. J., Sekino, H., and Purvis, G. D., "Comparison of MBPT and coupled-cluster methods with full CI. importance of triplet excitations and infinite summations," *Chem. Phys. Lett.*, vol. 98, pp. 66–71, 1983.

[13] Becke, A. D., "Density-functional exchange-energy approximations with correct asymptotic behavior," *Phys. Rev. A*, vol. 38, pp. 3098–3100, 1988.

[14] Becke, A. D., "Density-functional thermochemistry. iii. the role of exact exchange," *J. Chem. Phys.*, vol. 98, pp. 5648–5652, 1993.

[15] Becke, A. D. and Johnson, E. R., "Exchange-hole dipole moment and the dispersion interaction," *J. Chem. Phys.*, vol. 122, p. 154104, 2005.

[16] Becke, A. D. and Johnson, E. R., "Exchange-hole dipole moment and the dispersion interaction: High-order dispersion coefficients," *J. Chem. Phys.*, vol. 124, p. 014104, 2006.

[17] Becke, A. D. and Johnson, E. R., "Exchange-hole dipole moment and the dispersion interaction revisited," *J. Chem. Phys.*, vol. 127, p. 154108, 2007.

[18] Becke, A. D. and Roussel, M. R., "Exchange holes in inhomogeneous systems - a coordinate-space model," *Phys. Rev. A*, vol. 39, p. 3761, 1989.

[19] Beebe, N. H. F. and Linderberg, J., "Simplifications in the generation and transformation of two-electron integrals in molecular calculations," *Int. J. Quantum Chem.*, vol. 12, pp. 683–705, 1977.

[20] Behn, A., Zimmerman, P. M., Bell, A. T., and Head-Gordon, M., "Efficient exploration of reaction paths via a freezing string method," *J. Chem. Phys.*, vol. 135, p. 224108, 2011.

[21] Beran, G. J. O. and Nanda, K., "Predicting organic crystal lattice energies with chemical accuracy," *J. Phys. Chem. Lett.*, vol. 1, pp. 3480–3487, 2010.

[22] Bernholdt, D. E. and Harrison, R. J., "Large-scale correlated electronic structure calculations: The ri-mp2 method on parallel computers," *Chem. Phys. Lett.*, vol. 250, pp. 477–484, 1996.

[23] Bochevarov, A. D., Harder, E., Hughes, T. F., Greenwood, J. R., Braden, D. A., Philipp, D. M., Rinaldo, D., Halls, M. D., Zhang, J., and Friesner, R. A., "Jaguar: A high-performance quantum chemistry software program with strengths in life and materials sciences," *Int. J. Quantum Chem.*, vol. 113, pp. 2110–2142, 2013.

[24] Boström, J., Aquilante, F., Pedersen, T. B., and Lindh, R., "Ab initio density fitting: Accuracy assessment of auxiliary basis sets from cholesky decompositions," *J. Chem. Theory Comput.*, vol. 5, pp. 1545–1553, 2009.

[25] Boström, J., Delcey, M. G., Aquilante, F., Serrano-Andrés, L., Pedersen, T. B., and Lindh, R., "Calibration of cholesky auxiliary basis sets for multiconfigurational perturbation theory calculations of excitation energies," *J. Chem. Theory Comput.*, vol. 6, pp. 747–754, 2010.

[26] Boström, J., Pitoňák, M., Aquilante, F., Neogrády, P., Pedersen, T. B., and Lindh, R., "Coupled cluster and Møller-Plesset perturbation theory calculations of noncovalent intermolecular interactions using density fitting with auxiliary basis sets from Cholesky decompositions," *J. Chem. Theory Comput.*, vol. 8, pp. 1921–1928, 2012.

[27] Boys, S. F. and Bernardi, F., "The calculation of small molecular interactions by the differences of separate total energies. Some procedures with reduced errors," *Mol. Phys.*, vol. 19, no. 4, pp. 553–566, 1970.

[28] Burns, L., Thanthiriwatte, K., Kong, J., and Sherrill, C. D., "Improved performance for the exchange-dipole moment method. a reparameterization and assessment.," unpublished.

[29] Burns, L. A., Vázquez-Mayagoitia, Á., Sumpter, B. G., and Sherrill, C. D., "Density-functional approaches to noncovalent interactions: A comparison of dispersion corrections (DFT-D), exchange-hole dipole moment (XDM) theory, and specialized functionals," *J. Chem. Phys.*, vol. 134, p. 084107, 2011.

[30] Bylaska, E. J., de Jong, W. A., Govind, N., Kowalski, K., Straatsma, T. P., Valiev, M., Wang, D., Apra, E., Windus, T. L., Hammond, J., Nichols, P., Hirata, S., Hackler, M. T., Zhao, Y., Fan, P.-D., Harrison, R. J., Dupuis, M., Smith, D. M. A., Nieplocha, J., Tipparaju, V., Krishnan, M., Wu, Q., Voorhis, T. V., Auer, A. A., Nooijen, M., Brown, E., Cisneros, G., Fann, G. I., Fruchtl, H., Garza, J., Hirao, K., Kendall, R., Nichols, J. A., Tsemekhman, K., Wolinski, K., Anchell, J., Bernholdt, D., Borowski, P., Clark, T., Clerc, D., Dachsel, H., Deegan, M., Dyall, K., Elwood, D., Glendening, E., Gutowski, M., Hess, A., Jaffe, J., Johnson, B., Ju, J., Kobayashi, R., Kutteh, R., Lin, Z., Littlefield, R., Long, X., Meng, B., Nakajima, T., Niu, S., Pollack, L., Rosing, M., Sandrone, G., Stave, M., Taylor, H., Thomas, G., van Lenthe, J., Wong, A., and Zhang, Z., "NWChem, A Computational Chemistry Package for Parallel Computers, version 5.1 (2007), Pacific Northwest National Laboratory, Richland, Washington, 99352-0999, USA.."

[31] Casella, G. and Saielli, G., "Dft study of the interaction free energy of π-π complexes of fullerenes with buckybowls and viologen dimers," *New J. Chem.*, vol. 35, pp. 1453–1459, 2011.

[32] Černý, J., Kabeláč, M., and Hobza, P., "Double-helical → ladder structural transition in the B-DNA is induced by a loss of dispersion energy," *J. Am. Chem. Soc.*, vol. 130, pp. 16055–16059, 2008.

[33] Chengjun, J., "Asymmetric ring opening of terminal epoxides via kinetic resolution catalyzed by chiral (salen)co mixture," *Kinet. Catal.*, vol. 52, pp. 691–696, 2011.

[34] Chickos, W. E. and Jr., W. E. A. *J. Phys. Chem. Ref. Data*, vol. 31, pp. 537–698, 2002.

[35] Chirlian, L. E. and Francl, M. M., "Atomic charges derived from electrostatic potentials: A detailed study," *J. Comput. Chem.*, vol. 8, pp. 894–905, 1987.

[36] Chwee, T. S. and Carter, E. A., "Cholesky decomposition within local multireference singles and doubles configuration interaction," *J. Chem. Phys.*, vol. 132, p. 074104, 2010.

[37] Cozzi, P. G., "Metal-salen schiff base complexes in catalysis: Practical aspects," *Chem. Soc. Rev.*, vol. 33, pp. 410–421, 2004.

[38] Das, A., Sood, A. K., Maiti, P. K., Das, M., Varadarajan, R., and Rao, C. N. R., "Binding of nucleobases with single-walled carbon nanotubes: Theory and experiment," *Chem. Phys. Lett.*, vol. 453, pp. 266–273, 2008.

[39] de-la Roza, A. O. and Johnson, E. R., "Van der waals interactions in solids using the exchange-hole dipole moment model," *J. Chem. Phys.*, vol. 136, p. 174109, 2012.

[40] Delgado, M. C. R., Kim, E., da Silva Filho, D. A., and Brédas, J., "Tuning the charge-transport parameters of perylene diimide single crystals via end and/or core functionalization: A density functional theory investigation," *J. Am. Chem. Soc.*, vol. 132, pp. 3375–3387, 2010.

[41] Denis, P. A., "Theoretical investigation of the stacking interactions between curved conjugated systems and their interaction with fullerenes," *Chem. Phys. Lett.*, vol. 516, pp. 82–87, 2011.

[42] DePrince, A. E., Kennedy, M. R., Sumpter, B. G., and Sherrill, C. D., "Density-fitted singles and doubles coupled cluster on graphics processing units," *Mol. Phys.*, vol. 112, pp. 844–852, 2014.

[43] DePrince, A. E. and Sherrill, C. D., "Accuracy and efficiency of coupled-cluster theory using density fitting/cholesky decomposition, frozen natural orbitals, and a t_1-transformed hamiltonian," *J. Chem. Theory Comput.*, vol. 9, pp. 2687–2696, 2013.

[44] DePrince, A. E. and Sherrill, C. D., "Accurate noncovalent interaction energies using truncated basis sets based on frozen natural orbitals," *J. Chem. Theory Comput.*, vol. 9, pp. 293–299, 2013.

[45] Dunlap, B. I., Connolly, J. W. D., and Sabin, J. R., "Applicability of LCAO-X-alpha methods to molecules containing transition-metal atoms - nickel atom and nickel hydride," *Int. J. Quantum Chem. Symp.*, vol. 11, p. 81, 1977.

[46] Dunlap, B. I., Connolly, J. W. D., and Sabin, J. R., "On some approximations in applications of $X\alpha$ theory," *J. Chem. Phys.*, vol. 71, pp. 3396–3402, 1979.

[47] Dunning, T. H., "Gaussian basis sets for use in correlated molecular calculations. I. The atoms boron through neon and hydrogen," *J. Chem. Phys.*, vol. 90, pp. 1007–1023, 1989.

[48] Feyereisen, M., Fitzgerald, G., and Komornicki, A., "Use of approximate integrals in ab initio theory. an application in mp2 calculations," *Chem. Phys. Lett.*, vol. 208, pp. 359–363, 1993.

[49] Filatov, A. S., Scott, L. T., and Petrukhina, M. A., "Pi-pi interactions and solid state packing trends of polycyclic aromatic bowls in the indenocorannulene family: Predicting potentially useful bulk properties," *Cryst. Growth Des.*, vol. 10, pp. 4607–4621, 2010.

[50] Friesner, R. A., Murphy, R. B., Beachy, M. D., Ringnalda, M. N., Pollard, W. T., Dunietz, B. D., and Cao, Y., "Correlated ab initio electronic structure calculations for large molecules," *J. Phys. Chem. A*, vol. 103, pp. 1913–1928, 1999.

[51] Fukui, K., "The path of chemical reactions: The IRC approach," *Acc. Chem. Res.*, vol. 14, pp. 363–368, 1981.

[52] Gora, U., Podeszwa, R., Cencek, W., and Szalewicz, K., "Interaction energies of large clusters from many-body expansion," *J. Chem. Phys.*, vol. 135, p. 224102, 2011.

[53] Grimme, S., "Accurate description of van der waals complexes by density functional theory including empirical corrections," *J. Comput. Chem.*, vol. 25, pp. 1463–1473, 2004.

[54] Grimme, S., "Semiempirical GGA-type density functional constructed with a long-range dispersion correction," *J. Comput. Chem.*, vol. 27, no. 15, pp. 1787–1799, 2006.

[55] Grimme, S., Antony, J., Ehrlich, S., and Krieg, H., "A consistent and accurate ab initio parametrization of density functional dispersion correction (DFT-D) for the 94 elements H-Pu," *J. Chem. Phys.*, vol. 132, p. 154104, 2010.

[56] Grimme, S., Ehrlich, S., and Goerigk, L., "Effect of the damping function in dispersion corrected density functional theory," *J. Comput. Chem.*, vol. 32, pp. 1456–1465, 2011.

[57] Haak, R. M., Wezenberg, S. J., and Kleij, A. W., "Cooperative multimetallic catalysis using metallosalens," *Chem. Comm.*, vol. 46, pp. 2713–2723, 2010.

[58] Hankins, D., Moskowitz, J. W., and Stillinger, F. H., "Water molecule interactions," *J. Chem. Phys.*, vol. 53, pp. 4544–4554, 1970.

[59] Hansen, K. B., Leighton, J. L., and Jacobsen, E. N., "On the mechanism of asymmetric nucleophilic ring-opening of epoxides catalyzed by (salen)cr-iii complexes," *J. Am. Chem. Soc.*, vol. 118, pp. 10924–10925, 1996.

[60] Hay, P. J. and Wadt, W. R., "Ab initio effective core potentials for molecular calculations. Potentials for K to Au including the outermost core orbitals," *J. Chem. Phys.*, vol. 82, pp. 299–310, 1985.

[61] Hehre, W. J., Ditchfield, R., and Pople, J. A., "Self-consistent molecular orbital methods. XII. further extensions of gaussian-type basis sets for use in molecular orbital studies of organic molecules," *J. Chem. Phys.*, vol. 56, pp. 2257–2261, 1972.

[62] Hesselmann, A., "Derivation of the dispersion energy as an explicit density- and exchange-hole functional," *J. Chem. Phys.*, vol. 130, p. 084104, 2009.

[63] Hesselmann, A. and Jansen, G., "First-order intermolecular interaction energies from kohn-sham orbitals," *Chem. Phys. Lett.*, vol. 357, pp. 464–470, 2002.

[64] Hesselmann, A., Jansen, G., and Schütz, M., "Density-functional theory-symmetry-adapted intermolecular perturbation theory with density fitting: A new efficient method to study intermolecular interaction energies," *J. Chem. Phys.*, vol. 122, p. 014103, 2005.

[65] Hohenberg, P. and Kohn, W., "Inhomogeneous electron gas," *Phys. Rev. B*, vol. 136, p. B864, 1964.

[66] Hohenberg, P. and Kohn, W., "Inhomogeneous electron gas," *Phys. Rev. B*, vol. 136, pp. B864–+, 1964.

[67] Hohenstein, E. G., Duan, J., and Sherrill, C. D., "Origin of the surprising enhancement of electrostatic energies by electron-donating substituents in substituted sandwich benzene dimers," *J. Am. Chem. Soc.*, vol. 133, pp. 13244–13247, 2011.

[68] Hohenstein, E. G., Parrish, R. M., Sherrill, C. D., Turney, J. M., and Schaefer, H. F., "Large-scale symmetry-adapted perturbation theory computations via density fitting and Laplace transformation techniques: Investigating the fundamental forces of DNA-intercalator interactions," *J. Chem. Phys.*, vol. 135, p. 174107, 2011.

[69] Hohenstein, E. G. and Sherrill, C. D., "Density fitting and Cholesky decomposition approximations in symmetry-adapted perturbation theory: Implementation and application to probe the nature of π-π interactions in linear acenes," *J. Chem. Phys.*, vol. 132, p. 184111, 2010.

[70] Hohenstein, E. G. and Sherrill, C. D., "Density fitting of intramonomer correlation effects in symmetry-adapted perturbation theory," *J. Chem. Phys.*, vol. 133, p. 014101, 2010.

[71] Jain, S., Venkatasubbaiah, K., Jones, C. W., and Davis, R. J., "Factors influencing recyclability of co(iii)-salen catalysts in the hydrolytic kinetic resolution of epichlorohydrin," *J. Mol. Catal. A-Chem.*, vol. 316, pp. 8–15, 2010.

[72] Jain, S., Zheng, X., Jones, C. W., Weck, M., and Davis, R. J., "Importance of counterion reactivity on the deactivation of co-salen catalysts in the hydrolytic kinetic resolution of epichlorohydrin," *Inorg. Chem.*, vol. 46, pp. 8887–8896, 2007.

[73] Janowski, T., Ford, A. R., and Pulay, P., "Accurate correlated calculation of the intermolecular potential surface in the coronene dimer," *Mol. Phys.*, vol. 108, pp. 249–257, 2010.

[74] Janowski, T. and Pulay, P., "High accuracy benchmark calculations on the benzene dimer potential energy surface," *Chem. Phys. Lett.*, vol. 447, pp. 27–32, 2007.

[75] Janowski, T. and Pulay, P., "A benchmark quantum chemical study of the stacking interaction between larger polycondensed aromatic hydrocarbons," *Theor. Chem. Acc.*, vol. 130, pp. 419–427, 2011.

[76] Janowski, T., Pulay, P., Karunarathna, A. A. S., Sygula, A., and Saebo, S., "Convex-concave stacking of curved conjugated networks: Benchmark calculations on the corannulene dimer," *Chem. Phys. Lett.*, vol. 512, pp. 155–160, 2011.

[77] Jansen, G. and Hesselmann, A., "Comment on using kohnsham orbitals in symmetry-adapted perturbation theory to investigate intermolecular interactions," *J. Phys. Chem. A*, vol. 105, pp. 11156–11157, 2001.

[78] Jeziorski, B., Moszynski, R., and Szalewicz, K., "Perturbation theory approach to intermolecular potential energy surfaces of van der Waals complexes," *Chem. Rev.*, vol. 94, pp. 1887–1930, 1994.

[79] Johnson, E. R., "Dependence of dispersion coefficients on atomic environment," *J. Chem. Phys.*, vol. 135, p. 234109, 2011.

[80] Johnson, E. R. and Becke, A. D., "A post-hartree-fock model of intermolecular interactions," *J. Chem. Phys.*, vol. 123, p. 024101, 2005.

[81] Johnson, E. R. and Becke, A. D., "A post-hartree-fock model of intermolecular interactions: Inclusion of higher-order corrections," *J. Chem. Phys.*, vol. 124, p. 174104, 2006.

[82] Josa, D., Rodriguez, O. J., and Cabaleiro, L. E. M., "A dft study of substituent effects in corannulene dimers," *Phys. Chem. Chem. Phys.*, vol. 13, pp. 21139–21145, 2011.

[83] Kendall, R. A., Apra, E., Bernholdt, D. E., Bylaska, E. J., Dupuis, M., Fann, G. I., Harrison, R. J., Ju, J. L., Nichols, J. A., Nieplocha, J., Straatsma, T. P., Windus, T. L., and Wong, A. T., "High performance computational chemistry: An overview of nwchem a distributed parallel application," *Comput. Phys. Commun.*, vol. 128, pp. 260–283, 2000.

[84] Kendall, R. A., Dunning, T. H., and Harrison, R. J., "Electron affinities of the first-row atoms revisited. systematic basis sets and wave functions," *J. Chem. Phys.*, vol. 96, pp. 6796–6806, 1992.

[85] Kendall, R. A. and Fruchtl, H. A., "The impact of the resolution of the identity approximate integral method on modern ab initio algorithm development," *Theor. Chem. Acc.*, vol. 97, pp. 158–163, 1997.

[86] Kim, G. J. and Shin, J. H., "Application of new unsymmetrical chiral mn(iii), co(ii,iii) and ti(iv) salen complexes in enantioselective catalytic reactions," *Catal. Lett.*, vol. 63, pp. 83–90, 1999.

[87] Klopper, W., Noga, J., Koch, H., and Helgaker, T., "Multiple basis sets in calculations of triples corrections in coupled-cluster theory," *Theor. Chem. Acc.*, vol. 97, pp. 164–176, 1997.

[88] Koch, H., de Meras, A. S., and Pedersen, T. B., "Reduced scaling in electronic structure calculations using cholesky decompositions," *J. Chem. Phys.*, vol. 118, pp. 9481–9484, 2003.

[89] Kohn, W., Becke, A. D., and Parr, R. G., "Density functional theory of electronic structure," *J. Phys. Chem.*, vol. 100, pp. 12974–12980, 1996.

[90] Kohn, W. and Sham, L. J., "Self-consistent equations including exchange and correlation effects," *Phys. Rev.*, vol. 140, p. 1133, 1965.

[91] Kumar, P., Naidu, V., and Gupta, P., "Application of hydrolytic kinetic resolution (hkr) in the synthesis of bioactive compounds," *Tetrahedron*, vol. 63, pp. 2745–2785, 2007.

[92] Kureshy, R. I., Das, A., Khan, N. H., Abdi, S. H. R., and Bajaj, H. C., "Cu(ii)-macrocylic [h-4]salen catalyzed asymmetric nitroaldol reaction and its application in the synthesis of alpha 1-adrenergic receptor agonist (r)-phenylephrine," *ACS Catal.*, vol. 1, pp. 1529–1535, 2011.

[93] Landau, A., Khistyaev, K., Dolgikh, S., and Krylov, A. I., "Frozen natural orbitals for ionized states within equation-of-motion coupled-cluster formalism," *J. Chem. Phys.*, vol. 132, p. 014109, 2010.

[94] Lee, T. J. and Scuseria, G. E., *Quantum Mechanical Electronic Structure Calculations with Chemical Accuracy*. Dordrecht: Springer, 1995.

[95] Leininger, M. L., Allen, W. D., Schaefer, H. F., and Sherrill, C. D., "Is Møller-plesset perturbation theory a convergent *ab initio* method?," *J. Chem. Phys.*, vol. 112, pp. 9213–9222, 2000.

[96] Madhavan, N., Takatani, T., Sherrill, C. D., and Weck, M., "Macrocyclic cyclooctene-supported salen(alcl) catalysts for conjugated addition reactions: Effect of linker and support-structure on catalysis," *Chem. Eur. J.*, vol. 15, pp. 1186–1194, 2009.

[97] Martinez, T. J. and Carter, E. A., "Pseudospectral methods applied to the electron correlation problem," in *Modern Electronic Structure Theory* (Yarkony, D. R., ed.), vol. 2 of *Advanced Series in Physical Chemistry*, pp. 1132–1165, Singapore: World Scientific, 1995.

[98] Martinez, T. J., Mehta, A., and Carter, E. A., "Pseudospectral full configuration interaction," *J. Chem. Phys.*, vol. 97, pp. 1876–1880, 1992.

[99] Matsunaga, S. and Shibasaki, M., "Multimetallic schiff base complexes as cooperative asymmetric catalysts," *Synthesis*, vol. 45, pp. 421–437, 2013.

[100] Meyer, E. A., Castellano, R. K., and Diederich, F., "Interactions with aromatic rings in chemical and biological recognition," *Angew. Chem., Int. Ed. Engl.*, vol. 42, no. 11, pp. 1210–1250, 2003.

[101] Misquitta, A. J., Podeszwa, R., Jeziorski, B., and Szalewicz, K., "Intermolecular potentials based on symmetry-adapted perturbation theory with dispersion energies from time-dependent density-functional calculations," *J. Chem. Phys.*, vol. 123, p. 214103, 2005.

[102] Müller, C. and Paulus, B., "Wavefunction-based electron correlation methods for solids," *Phys. Chem. Chem. Phys.*, vol. 14, pp. 7605–7614, 2012.

[103] Muto, Y., "?," *J. Phys.-Math. Soc. Japan*, vol. 17, p. 629, 1943.

[104] Nielsen, L. P. C., Stevenson, C. P., Blackmond, D. G., and Jacobsen, E. N., "Mechanistic investigation leads to a synthetic improvement in the hydrolytic kinetic resolution of terminal epoxides," *J. Am. Chem. Soc.*, vol. 126, pp. 1360–1362, 2004.

[105] Nielsen, L. P. C., Zuend, S. J., Ford, D. D., and Jacobsen, E. N., "Mechanistic basis for high reactivity of (salen)co-ots in the hydrolytic kinetic resolution of terminal epoxides," *J. Org. Chem.*, vol. 77, pp. 2486–2495, 2012.

[106] Papajak, E., Zheng, J., Xu, X., Leverentz, H. R., and Truhlar, D. G., "Perspectives on basis sets beautiful: Seasonal plantings of diffuse basis functions," *J. Chem. Theory Comput.*, vol. 7, pp. 3027–3034, 2011.

[107] Pedersen, T. B., Sánchez de Merás, A. M. J., and Koch, H., "Polarizability and optical rotation calculated from the approximate coupled cluster singles and doubles CC2 linear response theory using Cholesky decompositions," *J. Chem. Phys.*, vol. 120, pp. 8887–8897, 2004.

[108] Peng, C. Y. and Schlegel, H. B., "Combining synchronous transit and quasi-newton methods to find transition states," *Isr. J. Chem.*, vol. 33, pp. 449–454, 1993.

[109] Perdew, J. P., "Density-functional approximation for the correlation energy of the inhomogeneous electron gas," *Phys. Rev. B*, vol. 33, pp. 8822–8824, 1986.

[110] Perdew, J. P., Burke, K., and Ernzerhof, M., "Generalized gradient approximation made simple," *Phys. Rev. Lett.*, vol. 77, pp. 3865–3868, 1996.

[111] Petrukhina, M. A., Andreini, K. W., Mack, J., and Scott, L. T., "X-ray quality geometries of geodesic polyarenes from theoretical calculations: What levels of theory are reliable?," *J. Org. Chem.*, vol. 70, pp. 5713–5716, 2005.

[112] Pitonak, M., Aquilante, F., Hobza, P., Neogrady, P., Noga, J., and Urban, M., "Parallelized implementation of the CCSD(T) method in MOLCAS using optimized virtual orbitals space and Cholesky decomposed two-electron integrals," *Collect. Czech. Chem. Commun.*, vol. 76, pp. 713–742, 2011.

[113] Pitoňák, M., Neogrády, P., Řezáč, J., Jurečka, P., Urban, M., and Hobza, P., "Benzene dimer: High-level wave function and density functional theory calculations," *J. Chem. Theory Comput.*, vol. 4, pp. 1829–1834, 2008.

[114] Pitoňák, M., Řezác, J., and Hobza, P., "Spin-component scaled coupled-clusters singles and doubles optimized towards calculation of noncovalent interactions," *Phys. Chem. Chem. Phys.*, vol. 12, pp. 9611–9614, 2010.

[115] Podeszwa, R., "Comment on "Beyond the Benzene Dimer: An Investigation of the Additivity of π-π Interactions"," *J. Phys. Chem. A*, vol. 112, pp. 8884–8885, 2008.

[116] Podeszwa, R., Bukowski, R., and Szalewicz, K., "Density-fitting method in symmetry-adapted perturbation theory based on Kohn-Sham description of monomers," *J. Chem. Theory Comput.*, vol. 2, pp. 400–412, 2006.

[117] Podeszwa, R., Rice, B. M., and Szalewicz, K., "Predicting structure of molecular crystals from first principles," *Phys. Rev. Lett.*, vol. 101, p. 115503, 2008.

[118] Podeszwa, R., Rice, B. M., and Szalewicz, K., "Crystal structure prediction for cyclotrimethylene trinitramine (rdx) from first principles.," *Phys. Chem. Chem. Phys.*, vol. 11, pp. 5512–5518, 2009.

[119] Podeszwa, R. and Szalewicz, K., "Accurate interaction energies for argon, krypton, and benzene dimers from perturbation theory based on the kohn-sham model," *Chem. Phys. Lett.*, vol. 412, pp. 488–493, 2005.

[120] Podeszwa, R. and Szalewicz, K., "Three-body symmetry-adapted perturbation theory based on kohn-sham description of the monomers," *J. Chem. Phys.*, vol. 126, p. 194101, 2007.

[121] Purvis, G. D. and Bartlett, R. J., "A full coupled-cluster singles and doubles model: The inclusion of disconnected triples," *J. Chem. Phys.*, vol. 76, pp. 1910–1918, 1982.

[122] Raghavachari, K., Trucks, G. W., Pople, J. A., and Head-Gordon, M., "A 5th-order perturbation comparison of electron correlation theories," *Chem. Phys. Lett.*, vol. 157, pp. 479–483, 1989.

[123] Raju, R. K., Bloom, J. W. G., An, Y., and Wheeler, S. E., "Substituent effects on non-covalent interactions with aromatic rings: Insights from computational chemistry," *ChemPhysChem*, vol. 12, pp. 3116–3130, 2011.

[124] Rendell, A. P. and Lee, T. J., "Coupled-cluster theory employing approximate integrals: An approach to avoid the input/output and storage bottlenecks," *J. Chem. Phys.*, vol. 101, pp. 400–408, 1994.

[125] Ringer, A. L. and Sherrill, C. D., "First principles computation of lattice energies of organic solids: The benzene crystal," *Chem. Eur. J.*, vol. 14, pp. 2542–2547, 2008.

[126] Ringer, A. L., Sinnokrot, M. O., Lively, R. P., and Sherrill, C. D., "The effect of multiple substituents on sandwich and t-shaped π-π interactions," *Chem. Eur. J.*, vol. 12, pp. 3821–3828, 2006.

[127] Rittby, M. and Bartlett, R. J., "An open-shell spin-restricted coupled cluster method: Application to ionization potentials in N_2," *J. Phys. Chem.*, vol. 92, p. 3033, 1988.

[128] Roeggen, I. and Wisloff-Nilssen, E., "On the beebe-linderberg 2-electron integral approximation," *Chem. Phys. Lett.*, vol. 132, pp. 154–160, 1986.

[129] Sadhukhan, A., Khan, N. H., Roy, T., Kureshy, R. I., Abdi, S. H. R., and Bajaj, H. C., "Asymmetric hydrolytic kinetic resolution with recyclable macrocyclic coiii-salen complexes: A practical strategy in the preparation of (r)-mexiletine and (s)-propranolol," *Chem. Eur. J.*, vol. 18, pp. 5256–5260, 2012.

[130] Salonen, L. M., Ellermann, M., and Diederich, F., "Aromatic rings in chemical and biological recognition: Energetics and structures," *Angew. Chem., Int. Ed. Engl.*, vol. 50, pp. 4808–4842, 2011.

[131] Schaus, S. E., Brandes, B. D., Larrow, J. F., Tokunaga, M., Hansen, K. B., Gould, A. E., Furrow, M. E., and Jacobsen, E. N., "Highly selective hydrolytic kinetic resolution of terminal epoxides catalyzed by chiral (salen)co-iii complexes. practical synthesis of enantioenriched terminal epoxides and 1,2-diols," *J. Am. Chem. Soc.*, vol. 124, pp. 1307–1315, 2002.

[132] Scuseria, G. E., Janssen, C. L., and Schaefer, H. F., "An efficient reformulation of the closed-shell coupled cluster single and double excitation (CCSD) equations," *J. Chem. Phys.*, vol. 89, p. 7382, 1988.

[133] Scuseria, G. E. and Lee, T. J., "Comparison of coupled-cluster methods which include the effects of connected triple excitations," *J. Chem. Phys.*, vol. 93, p. 5851, 1990.

[134] Scuseria, G. E., Scheiner, A. C., Lee, T. J., Rice, J. E., and Schaefer, H. F., "The closed-shell coupled sluster single and double excitation (CCSD) model for the description of electron correlation. a comparison with configuration interaction (CISD) results," *J. Chem. Phys.*, vol. 86, pp. 2881–2890, 1987.

[135] Sears, J. S. and Sherrill, C. D., "Assessing the performance of density functional theory for the electronic structure of metal-salens: The $3d^0$-metals," *J. Phys. Chem. A*, vol. 112, no. 15, pp. 3466–3477, 2008.

[136] Sears, J. S. and Sherrill, C. D., "Assessing the performance of density functional theory for the electronic structure of metal-salens: The d^2-metals," *J. Phys. Chem. A*, vol. 112, pp. 6741–6752, 2008.

[137] Shao, Y., Molnar, L. F., Jung, Y., Kussmann, J., Ochsenfeld, C., Brown, S. T., Gilbert, A. T. B., Slipchenko, L. V., Levchenko, S. V., O'Neill, D. P., Jr., R. A. D., Lochan, R. C., Wang, T., Beran, G. J. O., Besley, N. A., Herbert, J. M., Lin, C. Y., Voorhis, T. V., Chien, S. H., Sodt, A., Steele, R. P., Rassolov, V. A., Maslen, P. E., Korambath, P. P., Adamson, R. D., Austin, B., Baker, J., Byrd, E. F. C., Dachsel, H., Doerksen, R. J., Dreuw, A., Dunietz, B. D., Dutoi, A. D., Furlani, T. R., Gwaltney, S. R., Heyden, A., Hirata, S., Hsu, C.-P., Kedziora, G., Khalliulin, R. Z., Klunzinger, P., Lee, A. M., Lee, M. S., Liang, W., Lotan, I., Nair, N., Peters, B., Proynov, E. I., Pieniazek, P. A., Rhee, Y. M., Ritchie, J., Rosta,

E., Sherrill, C. D., Simmonett, A. C., Subotnik, J. E., Woodcock, H. L., Zhang, W., Bell, A. T., Chakraborty, A. K., Chipman, D. M., Keil, F. J., Warshel, A., Hehre, W. J., Schaefer, H. F., Kong, J., Krylov, A. I., Gill, P. M. W., and Head-Gordon, M., "Advances in methods and algorithms in a modern quantum chemistry program package," *Phys. Chem. Chem. Phys.*, vol. 8, pp. 3172–3191, 2006.

[138] Sharada, S. M., Zimmerman, P. M., Bell, A. T., and Head-Gordon, M., "Automated transition state searches without evaluating the hessian," *J. Chem. Theory Comput.*, vol. 8, pp. 5166–5174, 2012.

[139] Sherrill, C. D., Takatani, T., and Hohenstein, E. G., "An assessment of theoretical methods for nonbonded interactions: Comparison to complete basis set limit coupled-cluster potential energy curves for the benzene dimer, the methane dimer, benzene-methane, and benzene-H_2S," *J. Phys. Chem. A*, vol. 113, pp. 10146–10159, 2009.

[140] Shibasaki, K., Fujii, A., Mikami, N., and Tsuzuki, S., "Magnitude of the ch/pi interaction in the gas phase: Experimental and theoretical determination of the accurate interaction energy in benzene-methane," *J. Phys. Chem. A*, vol. 110, pp. 4397–4404, 2006.

[141] Sinnokrot, M. O. and Sherrill, C. D., "High-accuracy quantum mechanical studies of π-π interactions in benzene dimers," *J. Phys. Chem. A*, vol. 110, pp. 10656–10668, 2006.

[142] Sinnokrot, M. O., Valeev, E. F., and Sherrill, C. D., "Estimates of the ab initio limit for π-π interactions: The benzene dimer," *J. Am. Chem. Soc.*, vol. 124, pp. 10887–10893, 2002.

[143] Sodt, A., Subotnik, J. E., and Head-Gordon, M., "Linear scaling density fitting," *J. Chem. Phys.*, vol. 125, p. 194109, 2006.

[144] Sosa, C., Geersten, J., Trucks, G. W., Barlett, R. J., and Franz, J. A., "Selection of the reduced virtual space for correlated calculations - an application to the energy and dipole-moment of H_2O," *Chem. Phys. Lett.*, vol. 159, pp. 148–154, 1989.

[145] Stone, A. J., "Distributed multipole analysis, or how to describe a molecular charge-distribution," *Chem. Phys. Lett.*, vol. 83, pp. 233–239, 1981.

[146] Sun, K., Li, W., Feng, Z., and Li, C., "Cooperative activation in ring-opening hydrolysis of epoxides by co-salen complexes: A first principle study," *Chem. Phys. Lett.*, vol. 470, pp. 259–263, 2009.

[147] Szabo, A. and Ostlund, N. S., *Modern Quantum Chemistry: Introduction to Advanced Electronic Structure Theory.* New York: McGraw-Hill, 1989.

[148] Szalewicz, K., "Symmetry-adapted perturbation theory of intermolecular forces," *WIREs Comput. Mol. Sci.*, vol. 2, pp. 254–272, 2012.

[149] Takatani, T., Hohenstein, E. G., and Sherrill, C. D., "Improvement of the coupled-cluster singles and doubles method via scaling same- and opposite-spin components of the double excitation correlation energy," *J. Chem. Phys.*, vol. 128, p. 124111, 2008.

[150] Takatani, T., Sears, J. S., and Sherrill, C. D., "Assessing the performance of density functional theory for the electronic structure of metal-salens: The d^6-metals," *J. Phys. Chem. A*, vol. 113, pp. 9231–9236, 2009.

[151] Takatani, T., Sears, J. S., and Sherrill, C. D., "Assessing the performance of density functional theory for the electronic structure of metal-salens: The m06 suite of functionals and the d^4-metals," *J. Phys. Chem. A*, vol. 114, pp. 11714–11718, 2010.

[152] Taube, A. G. and Bartlett, R. J., "Frozen natural orbitals: Systematic basis set truncation for coupled-cluster theory," *Collect. Czech. Chem. Commun.*, vol. 70, pp. 837–850, 2005.

[153] Taube, A. G. and Bartlett, R. J., "Frozen natural orbital coupled-cluster theory: Forces and application to decomposition of nitroethane," *J. Chem. Phys.*, vol. 128, p. 164101, 2008.

[154] Tauer, T. P. and Sherrill, C. D., "Beyond the benzene dimer: An investigation of the additivity of π-π interactions," *J. Phys. Chem. A*, vol. 109, pp. 10475–10478, 2005.

[155] Tkatchenko, A., DiStasio, J. R. A., Car, R., and Scheffler, M., "Accurate and efficient method for many-body van der waals interactions," *Phys. Rev. Lett.*, vol. 108, p. 236402, 2012.

[156] Tokunaga, M., Larrow, J. F., Kakiuchi, F., and Jacobsen, E. N., "Asymmetric catalysis with water: Efficient kinetic resolution of terminal epoxides by means of catalytic hydrolysis," *Science*, vol. 277, pp. 936–938, 1997.

[157] Tsuzuki, S., Honda, K., Uchimaru, T., Mikami, M., and Tanabe, K., "Origin of attraction and directionality of the π-π interaction: Model chemistry calculations of benzene dimer interaction," *J. Am. Chem. Soc.*, vol. 124, no. 1, pp. 104–112, 2002.

[158] Turney, J. M., Simmonett, A. C., Parrish, R. M., Hohenstein, E. G., Evangelista, F. A., Fermann, J. T., Mintz, B. J., Burns, L. A., Wilke, J. J., Abrams, M. L., Russ, N. J., Leininger, M. L., Janssen, C. L., Seidl, E. T., Allen, W. D., Schaefer, H. F., King, R. A., Valeev, E. F., Sherrill, C. D., and Crawford, T. D., "Psi4: An open-source *ab initio* electronic structure program," *WIREs Comput. Mol. Sci.*, vol. 2, pp. 556–565, 2012.

[159] Vahtras, O., Almlöf, J., and Feyereisen, M. W., "Integral approximations for lcao-scf calculations," *Chem. Phys. Lett.*, vol. 213, pp. 514–518, 1993.

[160] Valiev, M., Bylaska, E. J., Govind, N., Kowalski, K., Straatsma, T. P., Dam, H. J. J. V., Wang, D., Nieplocha, J., Apra, E., Windus, T. L., and de Jong, W., "Nwchem: A comprehensive and scalable open-source solution for large scale molecular simulations," *Comput. Phys. Commun.*, vol. 181, pp. 1477–1489, 2010.

[161] Venkatasubbaiah, K., Zhu, X., Kays, E., Hardcastle, K. I., and Jones, C. W., "Co(iii)-porphyrin-mediated highly regioselective ring-opening of terminal epoxides with alcohols and phenols," *ACS Catal.*, vol. 1, pp. 489–492, 2011.

[162] von Lilienfeld, O. A. and Tkatchenko, A., "Two- and three-body interatomic dispersion energy contributions to binding in molecules and solids," *J. Chem. Phys.*, vol. 132, p. 234109, 2010.

[163] Weigend, F., "A fully direct ri-hf algorithm: Implementation, optimized auxiliary basis sets, demonstration of accuracy and efficiency," *Phys. Chem. Chem. Phys.*, vol. 4, pp. 4285–4291, 2002.

[164] Weigend, F., Kattannek, M., and Ahlrichs, R., "Approximated electron repulsion integrals: Cholesky decomposition versus resolution of the identity methods," *J. Chem. Phys.*, vol. 130, p. 164106, 2009.

[165] Weigend, F., Köhn, A., and Hättig, C., "Efficient use of the correlation consistent basis sets in resolution of the identity mp2 calculations," *J. Chem. Phys.*, vol. 116, pp. 3175–3183, 2002.

[166] Weinan, E., Ren, W. Q., and Vanden-Eijnden, E., "String method for the study of rare events," *Phys. Rev. B*, vol. 66, p. 052301, 2002.

[167] Wen, S. and Beran, G. J. O., "Accurate molecular crystal lattice energies from a fragment qm/mm approach with on-the-fly ab initio force field parametrization," *J. Chem. Theory Comput.*, vol. 7, pp. 3733–3742, 2011.

[168] Werner, H.-J. and Manby, F. *J. Chem. Phys.*, vol. 124, p. 054114, 2006.

[169] Werner, H.-J., Manby, F. R., and Knowles, P. J., "Fast linear scaling second-order Møller-Plesset perturbation theory (MP2) using local and density fitting approximations," *J. Chem. Phys.*, vol. 118, no. 18, pp. 8149–8160, 2003.

[170] Wheeler, S. E. and Houk, K. N., "Substituent effects in cation/π interactions and electrostatic potentials above the centers of substituted benzenes are due primarily to through-space effects of the substituents," *J. Am. Chem. Soc.*, vol. 131, p. 3126, 2009.

[171] Whitten, J. L., "Coulombic potential-energy integrals and approximations," *J. Chem. Phys.*, vol. 58, pp. 4496–4501, 1973.

[172] Williams, H. L. and Chabalowski, C. F., "Using kohn-sham orbitals in symmetry-adapted perturbation theory to investigate intermolecular interactions," *J. Phys. Chem. A*, vol. 105, pp. 646–659, 2001.

[173] Woods, R. J., Khalil, M., Pell, W., Moffat, S. H., and Smith, V. H., "Derivation of net atomic charges from molecular electrostatic potentials," *J. Comput. Chem.*, vol. 11, pp. 297–310, 1990.

[174] Wu, Q. and Yang, W., "Empirical correction to density functional theory for van der waals interactions," *J. Chem. Phys.*, vol. 116, pp. 515–524, 2002.

[175] Zhang, X., Jia, Y., Lu, X., Li, B., Wang, H., and Sun, L., "Intramolecularly two-centered cooperation catalysis for the synthesis of cyclic carbonates from co2 and epoxides," *Tetrahedron Lett.*, vol. 49, pp. 6589–6592, 2008.

[176] Zhao, Y., Schultz, N. E., and Truhlar, D. G., "Design of density functionals by combining the method of constraint satisfaction with parametrization for thermochemistry, thermochemical kinetics, and noncovalent interactions," *J. Chem. Theory Comput.*, vol. 2, pp. 364–382, 2006.

[177] Zhao, Y. and Truhlar, D. G., "The m06 suite of density functionals for main group thermochemistry, thermochemical kinetics, noncovalent interactions, excited states, and transition elements: Two new functionals and systematic testing of four m06-class functionals and 12 other functionals," *Theor. Chem. Acc.*, vol. 120, pp. 215–241, 2008.

[178] Zienau, J., Clin, L., Doser, B., and Ochsenfeld, C., "Cholesky-decomposed densities in Laplace-based second-order Møller-Plesset perturbation theory," *J. Chem. Phys.*, vol. 130, p. 204112, 2009.

VITA

Matthew R. Kennedy was born in 1986 in Alexandria, Virginia to William B. Kennedy and Lynn G. Kennedy. He graduated high-school in 2004 from Hayfield Secondary School in Alexandria, Virginia. He then attended the University of Tennessee at Knoxville, where he worked with Dr. Robert Hinde and Dr. Robert Harrison, graduating *cum laude* with degrees in Chemistry and Computer Science. He then spent five years studying computational chemistry under the guidance of Dr. C. David Sherrill.